Development of a Holistic Model of the Carleton Supercritical Water Loop (SCWL)

by

Alexey Zakharchenko

A thesis submitted to

The Faculty of Graduate Studies and Research

in partial fulfilment of

the degree requirements of

M.A.Sc. in Mechanical Engineering

Ottawa-Carleton Institute for

Mechanical and Aerospace Engineering

Department of Mechanical and Aerospace Engineering

Carleton University

Ottawa, Ontario, Canada

November, 2012

Your file Votre référence
ISBN: 978-0-494-94269-7

Our file Notre référence
ISBN: 978-0-494-94269-7

Abstract

In contrast to classical design of piping systems such as the Super Critical Water Loop (SCWL), i.e., design by rule or handbook equations, the goal of this thesis is to demonstrate a capability to do design by analysis, i.e., design based on a 3D transient nonlinear coupled holistic macroscopic model of the piping system of the Carleton SCWL.

This work focuses on the development of time-efficient and reasonably precise thermal/stress nonlinear analysis of the SCWL piping system, resolving 3D transient fields of interest in the solid and fluid domains of the loop.

The analysis makes use of the Dittus-Boelter correlation for computing heat transfer at the fluid-to-solid interface and proposes a simplified methodology for approximation of radial heat transport for turbulent flow in pipes.

Using the described analysis methodology, this work provides thermal-mechanical stress analysis of the SCWL, making conclusions about the existing design, providing an example of appropriate operation parameters, and suggesting possible ways to improve the design.

To my wife and parents

Acknowledgements

I would like to thank my advisor Distinguished Research Professor J. Goldak for his patience, motivation, enthusiasm, and immense knowledge. I want to thank Prof. Goldak for his contribution into this work and financial support.

I would also like to thank Prof. M. Yaras, whose support and motivation played important role for this research, and Dr. M. Yetisir (AECL) for his valuable comments and suggestions.

This thesis would not have been possible without technical support from Stanislav Tchernov, Jianguo Zhou, and Dan Downey.

I owe a debt of gratitude to my labmates Komeil Kazemi and Ahmed Nasser for their time and support.

Finally, I would like to thank Masih Balouch, Alex Pickard, Anne Mason, and some other students from the team of Prof. Yaras, who supported this work on many occasions.

Contents

List of Figures

List of Tables

List of Abbreviations

AC	Alternating current
$AECL$	Atomic Energy of Canada Limited
$ASME$	American Society of Mechanical Engineers
BC/BCs	Boundary condition/Boundary conditions
CAD	Computer Assisted Design
CAE	Computer Assisted Engineering
$CANDU$	Canada Deuterium Uranium reactor
FEA	Finite Element Analysis
FEM	Finite Element Methods
GIF	Generation IV International Forum
$NIST$	National Institute of Standards and Technology (USA)

NPS	Nominal Pipe Size
$SCWL$	Supercritical Water Loop

Nomenclature

b	Body force, $[\frac{N}{m^3}]$
C_p	Specific heat at constant pressure, $\left[\frac{J}{kg*K}\right]$
$\bar{C}_p$	Averaged over cross-section specific heat at constant pressure $\left(\frac{H_w-H_b}{T_w-T_b}\right)$, $\left[\frac{J}{kg*K}\right]$
D	Thermal diffusivity, $\left[\frac{m^2}{sec}\right]$
E	Young's modulus, $[Pa]$
g	Acceleration due to gravity $[\frac{m}{sec^2}]$
H	Volumetric specific enthalpy, $\left[\frac{J}{m^3}\right]$
h	Convection coefficient, $\left[\frac{W}{m^2*K}\right]$
j	Current density, $\left[\frac{A}{m^2}\right]$
k	Thermal conductivity, $\left[\frac{W}{m*K}\right]$
L	Length of interest, $[m]$
P	Pressure, $[Pa]$
p_c	Pressure at elasto-plastic interface
Q	Heat generation, $\left[\frac{W}{m^3}\right]$
q_s	Surface heat flux, $\left[\frac{W}{m^2}\right]$

r_c	Radius of elasto-plastic interface
T	Temperature field, $[°K]$
T_i	Initial temperature, $[°K]$
T_s	Surface temperature, $[°K]$
t	Characteristic time scale of interest, $[sec]$
u	Displacement field, $[m]$
V	Voltage field, $[V]$
v	Velocity field, $\left[\frac{m}{sec}\right]$

Greek Symbols

β	Thermal expansion coefficient.
ε	Green-Lagrange strain tensor, $(\nabla u + (\nabla u)^T + (\nabla u)^T \nabla u)/2$
θ^*	Dimensionless temperature, $\frac{T-T_\infty}{T_i-T_\infty}$
μ	Dynamic viscosity, $\left[\frac{kg}{m*sec}\right]$
ν	Poisson's ratio
ρ	Density, $\left[\frac{kg}{m^3}\right]$
σ	Cauchy stress tensor, $[Pa]$
σ_e	Electrical conductivity, $\left[\frac{1}{ohm*m}\right]$
σ_y	Yield stress, $[Pa]$
σ_{rr}, $\sigma_{\theta\theta}$, and σ_{zz}	Radial, hoop, and axial stress components in cylindrical

coordinates, $[Pa]$

Dimensionless Numbers

C	Courant number $\left(\frac{u\Delta t}{\Delta x}\right)$
Fo	Fourier number $\left(\frac{Dt}{L^2}\right)$
Nu/Nu_D	Nusselt number for a cylinder of diameter "D" $\left(\frac{hD}{k}\right)$
Pr	Pandtl number $\left(\frac{\mu C_p}{k}\right)$
$\overline{Pr}$	Modified Prandtl number $\left(\frac{(H_w - H_b)}{(T_w - T_b)(\mu_b/k_b)}\right)$
$\overline{Pr}_b$	Cross-sectional averaged Prandtl number
Ra_D	Rayleigh numbers for a cylinder of diameter "D" $\left(\frac{g\beta(T_s - T_a)D^3}{D\nu}\right)$
Re	Reynolds number $\left(\frac{\rho v L}{\mu}\right)$
Re_b	Reynolds number based on the flow bulk parameters

Chapter 1: Introduction

1.1 Background

Water at near-critical conditions has been used as coolant in various applications for decades.

One of the first research activities devoted to the problem of heat transfer at supercritical conditions started in the 1930s. Those investigations related to the free convection heat transfer of fluids at the near-critical point with the application to a new effective turbine blades cooling system of gas turbine engines. By the end of the 1940s and until1970s, the idea of achieving thermal efficiency of 40 – 45%, decreasing reactor coolant pumping power and environment impact during Loss of Coolant Accident (LOCA) and achieving some other advantages using near-critical water in the power generation plants, became very attractive [17]. However, due to the technological limitations and geopolitical circumstances in the 1980s, the interest to the problem was noticeably downscaled for about two decades.

During the last years the interest in the advantages offered by supercritical water cooled reactors is regaining support once again. By the late 1990s, a significant number of research projects directed to the improvement of understanding of near-critical thermo-hydraulic water properties have been initiated around the globe. In 2001 the Generation IV International Forum (GIF) was established to undertake the research and development of next-generation nuclear reactor designs.

As a part of worldwide activities directed to the development of the next generation nuclear reactors, Carleton University is building a Supercritical Water Loop (SCWL) test facility. This effort, sponsored by Atomic Energy of Canada Ltd. and the National Science and Engineering Research Council, aims to study thermal-hydraulic water properties at near-critical region.

However, along with the numerous advantages of the use of supercritical water for cooling nuclear reactors, there are certain challenges related to the development of such technologies. Some of them are high pressures and temperatures required to bring water to supercritical state. It raises questions about the structural integrity and reliability of supercritical water test facilities and, therefore, about the ability to analyze thermo-structural behaviour of the involved test equipment.

It is important to realize that selection of appropriate analysis methods play a crucial role for the optimal trade-off between the cost, time, and quality of the analysis results. For instance, one may have to choose between traditional analysis approaches (i.e. design by rule) and analysis based on a 3D FE model. Even though the design by rule incorporates years of experience and well-established design practices, they have certain limitations. For example, bolted joints are widely used for pipe-to-pipe connections in many industries; the methods used for design of such connections are usually based on the codes developed for a range of typical bolted joints; such bolted connections are bolted flange joints that usually consist of two flanges clamped with bolts and a sealing gasket between the flanges. The sealing performance of gaskets depends on

how the gasket compressed and, therefore, how the bolt clamping force is transferred to a corresponding gasket and how the gasket behaves under particular loading rule. Due to the wide variety of working conditions, highly non-linear properties of gasket materials and gasket assemblies, manufacturing allowances for joint components and many other factors, the codes accepted for such joints in many cases do not predict the real behaviour of such connections. In addition, to compensate for the inaccuracy of this "standardized" approach, the resulted design is often overweighed and requires more material, space, and other costly resources.

Therefore, the design of the joints would greatly benefit from the analysis methods that allow quick adjustment of the input parameters, such as flange geometry and gasket properties, and obtaining prompt results based on specific working conditions of the joints. Such designs can be optimized, and optimal experiments can be designed to further optimize the design. Furthermore, in most cases, this approach proves to be much faster and cheaper.

This work is an attempt to develop and demonstrate a new methodology for the analysis and optimization of piping systems. This methodology is supposed to be able to account for the multyphysics nature of the problem represented by the supercritical water test facilities, at the same time producing reasonably accurate and time- and cost-efficient solution.

This analysis approach is used to perform the analysis and optimization of a 3D transient nonlinear coupled holistic macroscopic model of the piping system of

the Carleton SCWL. The model is also used for the preliminary development of the loop test program.

1.2 Scope and organization of the thesis

Chapter 2 deals with the verification of the FEM software used for the analysis of the loop structure. Due to the lack of the available experimental data or literature related to the FEA of mechanical systems similar to the Carleton SCWL or loop components, the main analysis tool in the presented work was the VrSuite software. Therefore, the pronounced amount of the efforts was focused on ensuring the software capability to analyze the problems typical for this research. Chapter 3 presents the key concepts used in the analysis of the Carleton SCWL. The chapter provides a general outline of the work done in this thesis with respect to the SCWL development and analysis. It describes the analysis goals, mentioning the improvements of the software used for the analysis and briefly comparing this analysis with the similar one done by another graduate student [18] who utilized the same FEM software package. The chapter details the approach used for the analysis, provides details of additional hand calculations, mentions the assumptions and simplifications, elaborates on the step-by-step solution sequence for resolving the multiphysics problem represented by the SCWL, states essential analysis parameters, such as mesh parameters, BCs and governing equations, and provides analysis of the obtained results. Chapter 4 describes and analyses the potential deficiencies of the current design and proposes possible improvements of the SCWL design, which are backed up by the included thermal-stress analysis of the proposed design.

Chapter 5 provides the summary of the work done with respect to the main goal of the work, which is the development of a methodology for the design and optimization of piping systems, and with respect to the thermal-mechanical analysis of the SCWL, giving the overall conclusions about the effectiveness of the developed methodology and proposing possible future research activities and ways for improvement of the presented numerical model and the existing SCWL mechanical design.

Chapter 2: VrSuite software verification

Large number of problems, from basic and robust single element problems to multiphysics problems involving complicated domain geometry, has been solved using the VrSuite software and verified against exact analytic solutions or/and validated using available experimental data, confirming the usefulness of the software.

As was shown by R.G. Alena (2011) [18], the VrSuite software demonstrates very good agreement between numerical and classical analytic solutions related to the SCWL design and processes. For example, R.G. Alena found excellent agreement between the VrSuite solution and corresponding analytic solutions for the problems concerned with the stress and temperature fields in the pipe subjected to pure mechanical stress (inner pressure) or two different Dirichlet temperature boundary conditions applied at the inner and outer diameters of the pipe.

To consolidate the existing set of verification problems, resembling the typical geometry of the SCWL, the additional analytic solutions for transient temperature distribution in various domains are considered.

The SCWL piping system in general and SCWL test section in particular are subjects to the effects of thermal shock and convection boundary conditions that take place between the ambient air, working fluid (water) and piping system of the SCWL. In order to verify VrSuite from this angle, classical analytic solutions are compared with corresponding FEM solutions obtained using the VrSuite software for the following problems:

- Classical problems for a semi-infinite solid with Dirichlet temperature, or Convection, or Constant flux BCs applied to the surface of the semi-infinite solid [2];
- One-dimensional transient temperature distribution in an infinite cylinder with the uniform initial temperature and convective boundary condition [33];
- One-dimensional transient temperature distribution in a solid sphere with the uniform initial temperature and Dirichlet thermal boundary condition at the sphere surface [9];
- Elastic-plastic stress distribution in an internally pressurized thick-walled cylinder of elastic-strain-hardening plastic material [5].

The comparison of the analytic and FEM solutions, obtained by means of the VrSuite for the test cases listed above, demonstrates a reasonable agreement. The detailed description and discussion of the problems mentioned above can be found in Appendix 1.

Chapter 3: Analysis of the Supercritical Water Loop (SCWL)

3.1 SCWL analysis overview

A number of graduate students at Carleton University have already put significant efforts into the research and evaluation of the SCWL design and its structural soundness. M. Balouch [26] provided the electro-mechanical design of the SCWL including sizing and structural verification of the loop components against ASME codes. The 3D CAD model used in the presented analysis was also provided by M. Balouch. A. Mason and D. McGuire developed 1D thermal and thermal-hydraulic models of the SCWL. D. McGuire also did preliminary design of the SCWL test sections. The transient SCWL temperature field obtained by A. Mason was used as an input data for the 3D thermal stress analysis done by R. G. Alena who used the VrSuite FEA software package. All mentioned authors supported the conclusion about the structural soundness of the SCWL design. The presented analysis intends to refine the work done by R. G. Alena using significant improvements of the VrSuite software package as well as employing the existing software capabilities in a more extensive manner.

The additional tools/features added into the VrSuite software and used in the presented analysis include:

- Meshers for meshing the SCWL components such as reducers, tee joints, flanges and Grayloc connections. The fore-mentioned elements are meshed with 8-node hexahedral mesh.

- Voltage-Current solver that computes power density due to the voltage BCs. The power density allows computing the heat generated from the resistive Joule heating (i.e., computing domain temperature). The solver allows the direct and realistic 3D transient simulation of the test section heating process.
- Coupling capability that supports coupling of several solvers to simulate different interdependent physical processes. For example, if a problem is represented by a pipe, which is being heated by resistive Joule heating, and if one wants to analyse the domain temperature as a function of time, the Voltage-Current and energy equations have to be solved for the solid domain. Since the temperature of the pipe is different at each time step, the temperature-dependent material properties, such as electrical conductivity, are different as well. Even if the applied electrical current or voltage heating is constant, the rate of heating is changing according to the change of the corresponding material properties. Therefore, the resulted pipe temperature would differ from the temperature obtained for the same problem with the temperature-independent material properties.
- Ability to use the Dittus-Boelter heat-transfer correlation to compute local heat-transfer convection coefficients as a function of the local pipe diameter and local averaged properties of the working fluid.
- Existing "Sub-model" feature was modified to be used in a coupled set of various problems, what allowed cutting out a part of the global domain, refining the sub-domain mesh, and using the transient coarse-mesh solution from the parent problem as BCs for this sub-model.

- The existing contact element capability that allows simulation of two distinct parts, which are in thermal and/or stress contact with each other, was debugged and modified to be used in a coupled set.
- Due to the limitation for time steps size used in the Advection-Diffusion and Fluid Flow problems the simulations for one hour of physical time may require up to 100,000 time steps, depending on the details of the model and mass flow rate used in the analysis. Since the data computed for each time step is being written on a hard drive, it may result in significant usage of the hard drive space, while the most part of the written data is not employed in the analysis. To mitigate this problem, a special feature, which allows recording the computed data with user defined stride, was developed. For example, in the presented analysis, the data computed by the Advection-Diffusion solver was recorded only for every 20^{th} time step.
- The "Boundary Condition" module was enhanced with the tools reducing the amount of routine manual work while managing big assemblies. For example, in the case of the SCWL piping system, all involved pipes have the same inside Neumann pressure boundary conditions. One can define the pressure boundary condition for one of the pipes and using the tool "Apply to all" apply the same pressure boundary condition to the rest of the pipes with one button click. This tool also allows defining and applying distinct boundary conditions to any number of distinct groups within the same type of BCs.
- Ability to solve for power density resulted from the volumetric Joule heating in the test section and preheaters in the subdomain, involving only the test

section and preheaters, and to use the obtained power density data in the energy solver, which has the domain involving all loop components.

The geometry of the SCWL model components (flow meter, filter, valves and flanges) was simplified in order to reduce the total number of the model mesh elements. Some crucial loop components, such as the heat exchanger and pump, were replaced by thermodynamic models. The number of model elements was decreased from over 130,000 elements in the solid domain of the model done by R. G. Alena to less than 12,000 elements in the solid domain for the same analysis configuration (section 3.11.4 "Solid and Fluid Domains"). This dramatically decreased the analysis CPU (wall clock) time. Depending on the mass flow rate of the working fluid, about 1.5...12 hours of CPU time is required to perform simulation for one hour physical time (Intel® Xeon® Processor X5470), computing coupled solutions for the Navier-Stokes, voltage-current, energy, advection-diffusion, and quasi-static thermal-elasto-plastic stress analysis computing local convection heat-transfer coefficients according to the Dittus-Boelter correlation. The presented analysis is done for the minimum designed mass flow rate (0.126 kg/sec), for which about 1.5 hours of CPU time is required to compute one hour physical time.

3.2 SCWL overview

The Carleton Supercritical Water Loop is designed to study thermohydraulic properties of near-critical water. The water temperature is brought to the near-critical conditions in the loop test section equipped with a data acquisition system that is able to capture targeted water parameters.

The SCWL design allows various configurations of the loop where the used test section can be installed vertically or horizontally. The direction of the working fluid flow for the vertically installed test section can be upward or downward. Due to the time limitations, only the vertical configuration of the tubular test section with upward working fluid flow is considered in the presented analysis.

The short description of the loop operation, as pertains to the presented analysis, is as follows:

A centrifugal pump Figure 3.1, Position1 provides necessary head rise for the initially pressurized (25 MPa) working fluid. Two valves Position 2 and 3 are used for the adjustment of the working fluid mass flow rate through the test section. The heat generated in the test section Position 8 and preheaters, installed on the outside surfaces of the pipe sections Position 5 and 7, is imparted to the working fluid to bring the water into near-critical state in a test section where the water parameters are measured. The heat exchanger Position 10 is used to decrease the temperature of the water to the acceptable range, allowing normal operation of all SCWL components between the heat exchanger outlet and flow meter outlet.

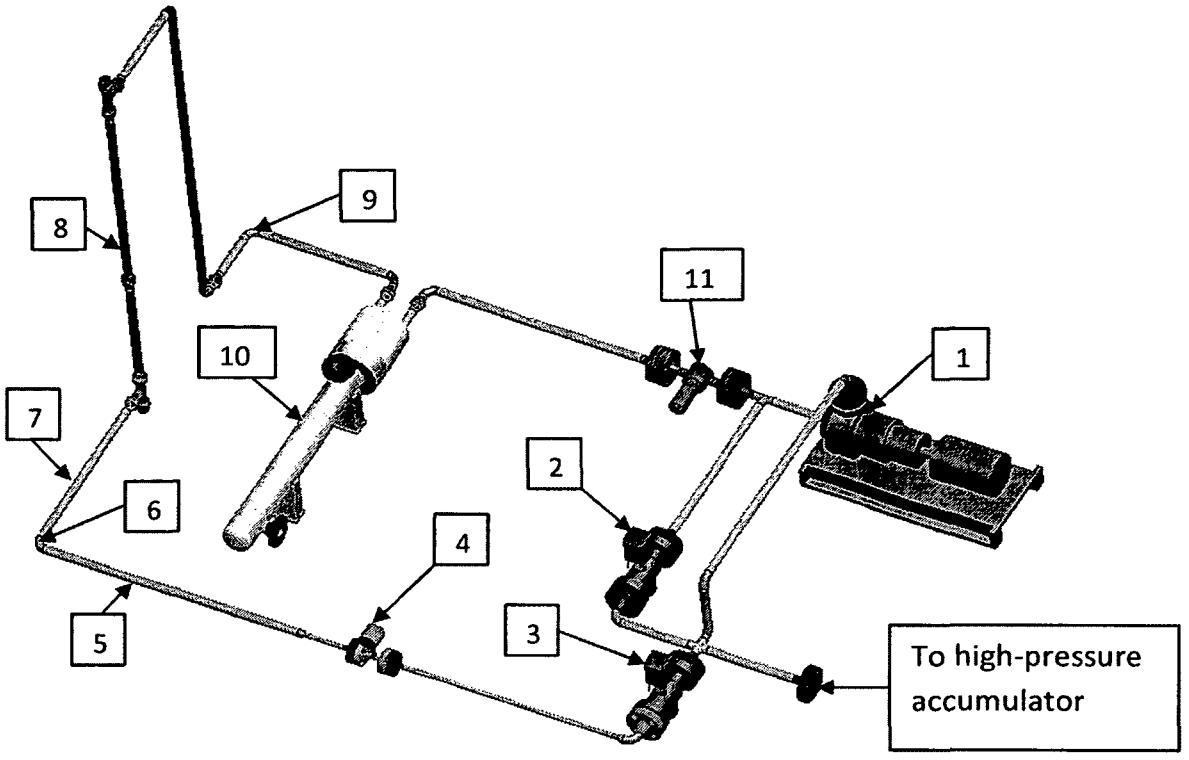

Figure 3.1 SCWL detailed CAD model

The SCW loop is designed to operate at pressures as high as 28 MPa, temperatures up to 600C and mass fluxes of up to 3000 kg/s*m^2. 300 kW of electrical DC power at 150 V and 2000 A is available for heating the SCWL test section, preheating system, and for actuating all related test equipment. According to M. Balouch [20], the maximum power dissipated in the tubular test section, based on the test section resistance, is from 51.5 to 61.2 kW, depending on the test section temperature. The maximum power dissipated in the preheaters is about 170 kW. The preheaters (further related to as Preheater 1 and Preheater 2) installed on the pipe sections Position 5 and 7.

The loop is pressurized using a high-pressure accumulator, allowing independent pressure control. The accumulator is connected with the SCWL by using

"flexible" U-shaped piping sections that prevent any noticeable influence of the accumulator in the SCWL stress or thermal fields.

All versions of the SCWL model used in the presented analysis were done using the CAD model of the loop provided by M. Balouch.

3.3 SCWL components geometry simplification considerations

The Carleton SCWL is a complex electro-mechanical system. However, many commercial components of the loop, such as a pump Position 1 (Figure 3.1), valves Position 2 and 3, flow meter Position 4, heat exchanger Position 10, and filter Position 11, are designed to work under the expected pressures and temperatures. Therefore, they are not analyzed in detail. Such components are replaced by cylindrical pipe pieces or reducer-like shapes, which have approximately the same mass (i.e., the same heat capacity) as the original components, Figure 3.2.

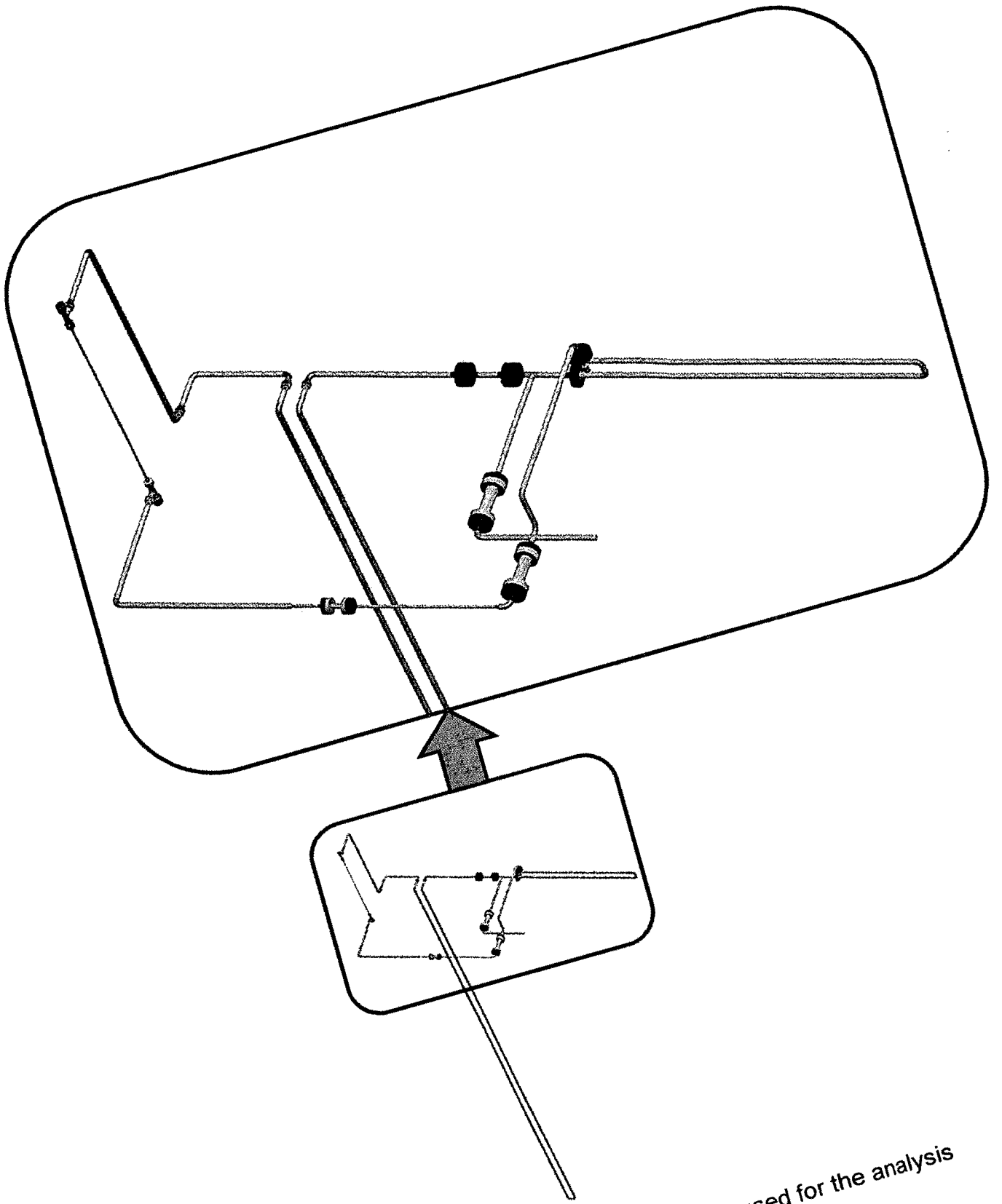

Figure 3.2 SCWL simplified CAD geometry used for the analysis

3.4 Heat exchanger and pump thermodynamics models

Since the mentioned simplification approach for the geometry of components of the pump, Figure 3.1, Position 1, and heat exchanger, Position 10 is rather rough, it was decided to use the more precise thermodynamic models of these components.

3.4.1 Heat exchanger model

The heat exchanger is replaced by a model based on the manufacturer's specification of the real SCWL heat exchanger [24]. The heat exchanger model, Figure 3.3 and Figure 3.4, is represented by a U-shaped piece of pipe with the length and outside and inside diameters equal to the corresponding parameters of the pressure pipe (i.e., pipe containing working fluid) in the real heat exchanger. The geometry of the model-to-SCWL interface corresponds to the interface of the real heat exchanger-to-SCWL.

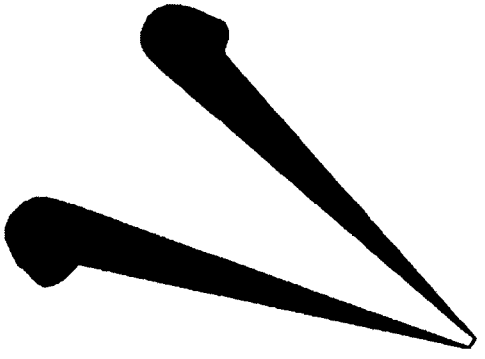

Figure 3.3 Heat Exchanger model

Convection boundary conditions are applied between the heat exchanger solid pipe, working fluid, and cooling fluid (i.e., at the outside and inside surfaces of the

pipe). Constant values of convection coefficients were selected empirically to match the available thermodynamic characteristics of the real heat exchanger at the steady state.

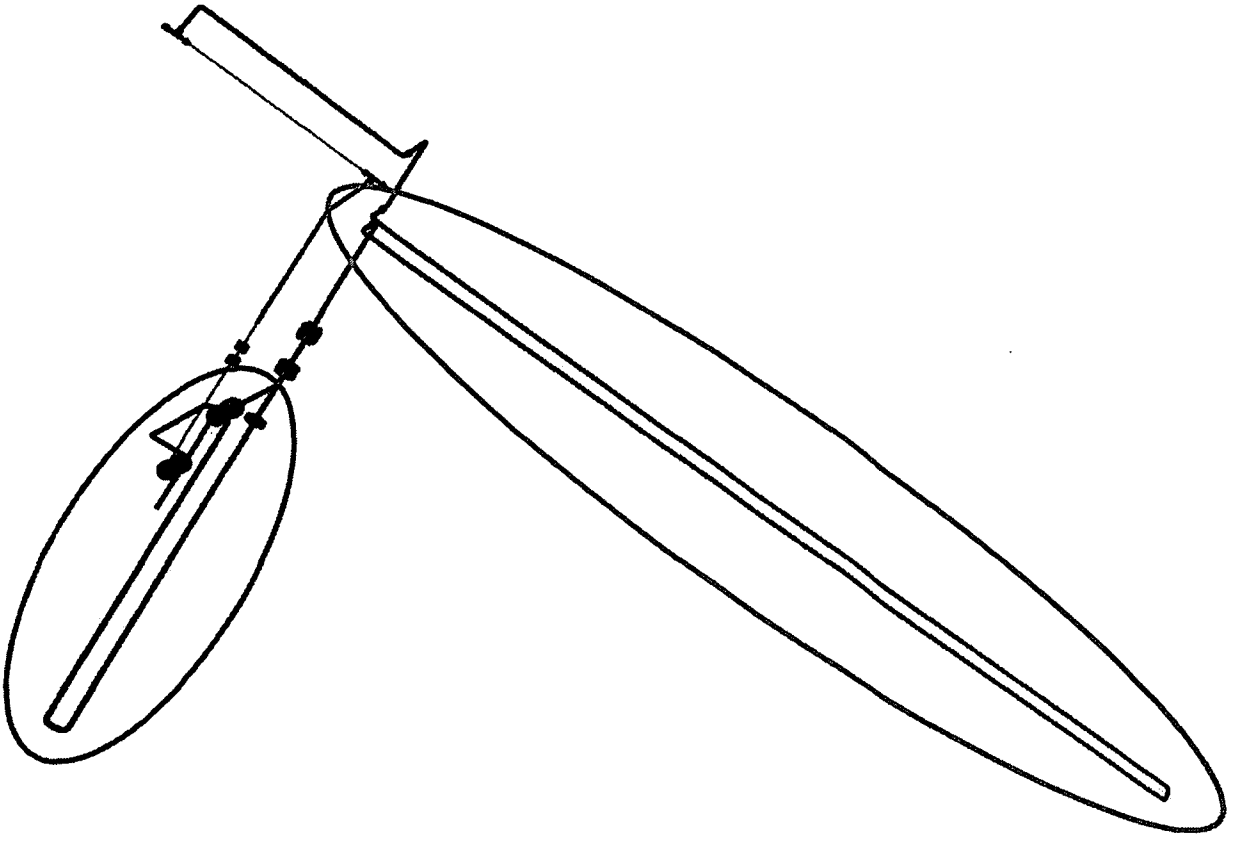

Figure 3.4 Heat Exchanger (highlighted in green) and Pump (highlighted in blue) models

Provided that the working fluid temperature at the inlet is 873K and at the outlet is 533K at a steady state (quoted characteristics of the real heat exchanger), the heat exchanger model reaches a steady state in about 1800 seconds with convection coefficients between the working fluid and heat exchanger pipe h=190 W/(m^{2}K), and between the cooling fluid and the pipe 83.4 W/(m^{2}K), Figure 3.5.

The temperature of the cooling fluid is assumed to be constant and equal to T=303K (the average temperature of the cooling fluid according to the heat exchanger specification).

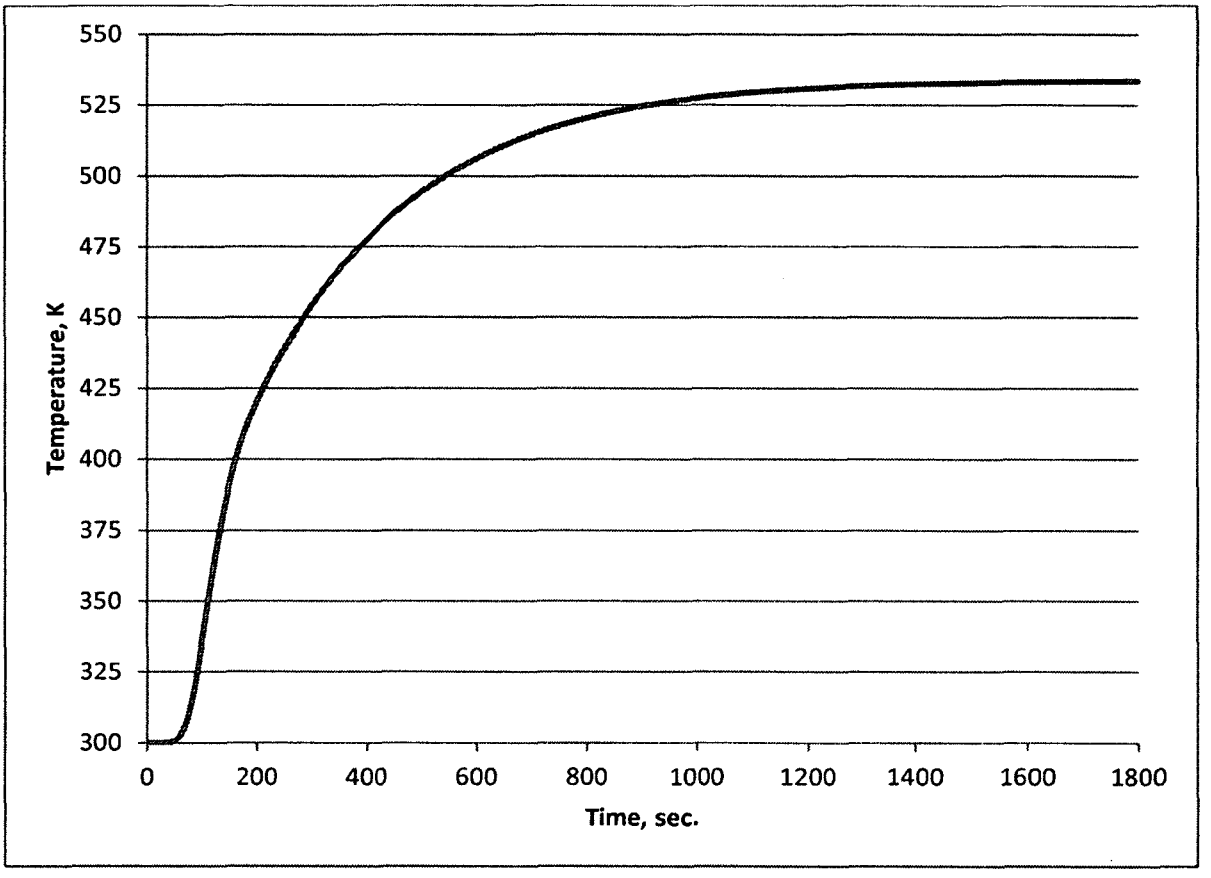

Figure 3.5 Fluid temperature at the outlet of the heat exchanger model

3.4.2 Pump model

The thermal inertia of the pump is modelled using an approach similar to the one used for the heat exchanger model. In other words, the pump is replaced by a pipe with convection boundary conditions at the pipe outside and inside diameters (i.e., between the pipe, working fluid, and ambient air) Figure 3.4.

Since the pump adds the heat into the working fluid through the viscous dissipation in the fluid, the additional amount of heat can be added as a volumetric heat source in the fluid domain of the pump model*.

The rate of heat extraction from the working fluid to the pump "cold" termal mass can be adjusted by changing the specific heat capacity of the model material and/or corresponding convection coefficients, as well as the temperature of ambient air.

Since, unlike the heat exchanger properties, there is very scarce information about the pump thermodynamic properties. The justification of the pump model size and properties is based on:

- The part of thermal mass of the real pump that significantly affects the heat exchange between the pump and fluid;
- The outside surface area of the parts included in the thermal mass that affects the fluid temperature;
- The estimated surface area of the real pump-to-fluid interface.

* After the analyses had been done, Dr. M.Yetisir (AECL) suggested that the energy from the pump be included in the model.

The model could be improved by adding the maximum amount of power that can be added to the water by the pump (pump power - 1.12 kW). This power can be added as a distributed power density to the water contained in the pump.

Selection of the pump model parameters

The total pump mass, including the pump base, is 350 kg, Figure 3.6.

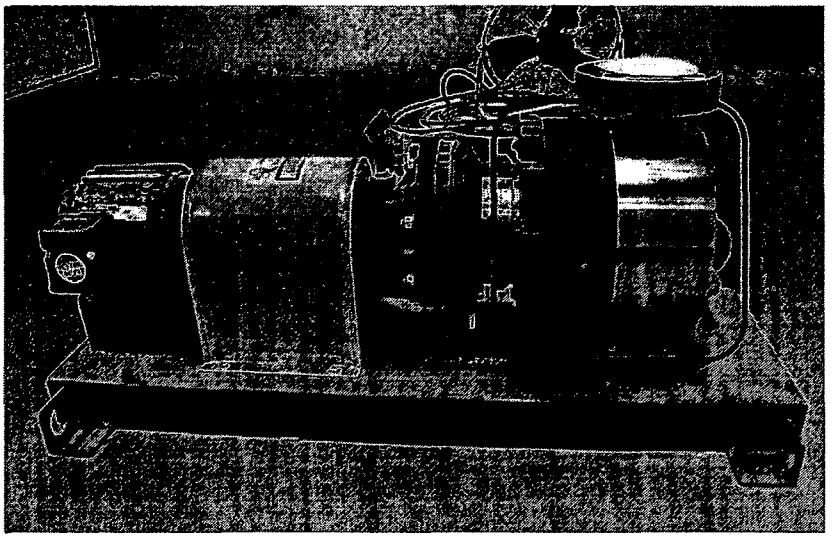

Figure 3.6 Pump

It is assumed that 150 kg (approx.) of the pump thermal mass can be considered as the pump thermal mass that significantly affects the temperature of the water flowing through the pump (the pump part highlighted in red).

Using the estimated mass (150 kg) and pipe schedule 1.5"NPS, the corresponding pipe length for 316 stainless steel is 3.88 m.

The outside surface area of the pump parts included in the selected thermal mass is 0.38 m^2. Taking into account the pump parts and other massive loop components, which are in direct contact with the selected pump part (i.e. selected thermal mass of the pump), the equivalent model outside surface area, subjected to free convection in still air, can be increased to 0.58 m^2. The corresponding length of the model pipe 1.5"NPS is 3.83 m.

The surface area of pump-to-fluid interface can be roughly estimated using available diameter of the pump impeller (Ø160 mm) and typical impeller configuration for industrial pumps, Figure 3.7.

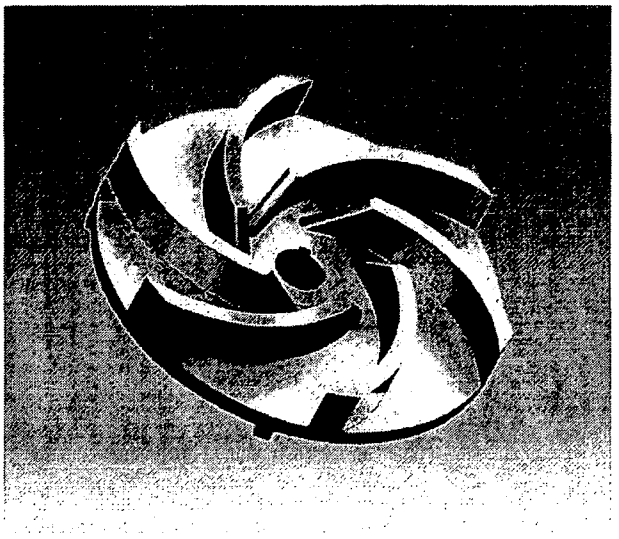

Figure 3.7 Pump impeller design example

Using the given impeller diameter, the length and width of each blade can be estimated as l=100 mm and w=20 mm. The surface area of the pump-to-fluid interface in this case is estimated to be $S \approx 3 \cdot \pi \cdot R^2 = 0.06\ \text{m}^2$. The corresponding length of the model pipe 1.5"NPS is 0.72 m.

The typical value of the convection coefficient in case of free convection in still air is about h=10 W/(m^{2}K). The typical value of the convection coefficient between liquid water and a steel pipe h=1000...3000 W/(m^{2}K). Since the surface area of the fluid-to-solid interface for the model based on the selected thermal mass is much bigger than the surface area defined using the diameter of the pump impeller, the convection coefficient can be modified proportionally.

The parameters selected for the thermodynamic pump model are shown in Table 3.1.

Table 3.1: Pump model parameters

Pipe length	Outside convection coefficient	Inside convection coefficient	Temperature of ambient air
3.9 m	10 W/(m^{2}K)	200 W/(m^{2}K)	303K

3.5 Computation of convection coefficients

One of the biggest challenges in solving convection heat-transfer problems is the computation of the corresponding convection heat-transfer coefficients. Unfortunately, there are no satisfactory analytical methods describing behaviour of thermophysical properties for the turbulent flow of supercritical fluids. Therefore, the related design solutions must rely on empirical correlations based on experimental data. Typically, convection heat-transfer coefficients are defined using non-dimensional numbers. The Nusselt number, Reynolds number, and Prandtl number is the typical dimensionless group used for the computation of turbulent heat transfer coefficient in tubes. In some cases, the empirical correlations derived for computation of the coefficients have additional parameters, which are functions of the properties of the involved fluids, such as the fluid temperature or/and wall temperature.

3.5.1 "Inside loop convection" (piping system-to-fluid)

At the early stage of working on the thesis, it was proposed to implement the capability of computing local heat-transfer convection coefficients in the VrSuite code. A number of available empirical correlations were coded in MATLAB in order to facilitate the implementation of the convection coefficient computation in the VrSuite code. The list of coded convection coefficient correlations for water flowing upward inside circular tubes, along with general descriptions of the correlations, can be found in Appendix 2.

It was decided to start with the implementation of the Dittus-Boelter correlation for the forced convection heat transfer in turbulent flow. Although the Dittus-

Boelter correlation is not very accurate in problems where phase changes take place, this well established correlation is typically used as the first approximation in many convection problems. For a flow in circular pipes the Dittus-Boelter correlation is applicable for $0.7 < Pr < 120$ and $10{,}000 < Re_D < 120{,}000$, where the Reynolds number is based on the pipe diameter.

The Dittus-Boelter convection coefficient solver

Currently, the Dittus-Boelter convection coefficient solver is implemented in the VrSuite software for problems with domains represented by either cylindrical pipe pieces or reducer-like shapes, which can be meshed using the "Pipe System" mesher, which is available in the VrSuite package.

It should be noted that the Dittus-Boelter convection coefficient correlation computes convection coefficients using the fluid bulk temperature (i.e. assuming that the temperature of the fluid is constant). It is a 1D model that is only a function of distance along the pipe axis. This correlation is derived experimentally The computation of convection coefficients using the Dittus-Boelter correlation is executed as follows:

- The Navier-Stokes equation solver solves for the velocity and pressure. Advection-diffusion solver solves for the specific enthalpy and temperature fields in the fluid, and for the flow of heat between the fluid and solid
- The Dittus-Boelter solver in the VrSuite software computes convection coefficients for each axial mesh slice along the axis of a piping system of interest. The parameters used in the computation of the convection coefficients are based on the local pipe diameter, used as a characteristic

length for computation of the Reynolds number, and on averaged 3D thermal and velocity fields computed in the Navier-Stokes and advection-diffusion

- The advection-diffusion solver computes the thermal flux between the fluid and the pipe using the pipe wall temperature and the mean fluid temperature in each slice. However, the temperature and velocity in the fluid are 3D. To compute the Dittus-Boelter convection coefficient correlation, the code computes the mean temperature and the corresponding temperature-dependent properties in each slice. This is done for each time step of the advection-diffusion solver.

The values of the time dependent computed convection coefficients can be extracted and/or visualized.

3.5.2 "Outside loop convection" (loop insulator-to-ambient air)

The typical temperature of the loop piping system is expected to be in the range 300...900K (metallic components of the piping system). The piping system insulation was developed by A. Mason [28]. The parameters of the insulation system are shown in Table 3.2.

To assess the heat flux between the loop and ambient air, the free convection at the outside surface of the insulator and insulator thermal resistance are to be taken into account.

Table 3.2: Summary of the SCWL insulation [28]

Section	Insulation material	Insulation thickness, [m]	Insulator surface temperature, [C]	Material thermal conductivity at 600K, [W/(mK]
Tubular test section	Alumina Silica Fibre	0.35	42.7	0.09
Hot section vertical	Mineral Wool Fibre	0.165	56.2	0.1
Hot section horizontal	Mineral Wool Fibre	0.165	59.6	0.1
Cold section*	Mineral Wool Fibre	0.06	55.8	0.1

*the cold section of the loop is the loop section from the heat exchanger outlet to the flow meter outlet; the rest part of the loop is considered as the hot section.

External free convection

The average convective heat transfer coefficient of a cylinder is determined by the relation:

$$\overline{h_{cyl}} = \frac{\overline{Nu}_D k}{D}$$

$\overline{Nu}_D$ is the average Nusselt number, k is the thermal conductivity of the fluid [W/(mK)], and D is the diameter of the cylinder [m].

The average Nusselt number for a long horizontal cylinder undergoing free convection is determined using the empirical correlation of Churchill & Chu [35]:

$$\overline{Nu_D} = \left[0.60 + \frac{0.387Ra_D^{1/6}}{\left(1 + \left[\frac{0.599}{Pr}\right]^{9/16}\right)^{8/27}}\right]^2$$

Prandtl and Rayleigh numbers for a cylinder, given by:

$$Pr = \frac{\nu}{D}$$

$$Ra_D = \frac{g\beta(T_s - T_a)D^3}{D\nu}$$

ν is the kinematic viscosity [m^2/s], D is the thermal diffusivity [m^2/s], g is the acceleration due to gravity [m/s^2], β is the thermal expansion coefficient, T_s is the surface temperature, and T_a is the temperature of ambient air.

For the free convection of a vertical cylinder, an alternative Nusselt number correlation is provided by Churchill & Chu [35]

$$\overline{Nu_D} = \left[0.825 + \frac{0.387Ra_D^{1/6}}{\left(1 + \left[\frac{0.492}{Pr}\right]^{9/16}\right)^{8/27}}\right]^2$$

Insulator thermal resistance

The heat transfer coefficient based on the insulator thermal resistance can be computed as follows:

$$h_{wall} = \frac{2k}{d_{in}ln(d_{out}/d_{in})}$$

k is the insulator thermal conductivity, d_i and d_o are the inner and outer diameters of the pipe, respectively.

Overall equivalent heat transfer coefficient

$$U = \frac{1}{\frac{1}{\bar{h}} + \frac{1}{h_{wall}}}$$

The equivalent convection coefficients found for the different loop sections are shown in Table 3.3.

Table 3.3: Equivalent convection coefficients

Section	Tubular test section	Hot section vertical pipes	Hot section horizontal pipes	Cold section
Convection coefficient, [W/(m^{2}K)]	0.301	0.392	0.390	0.706

3.6 Accounting for the effects of turbulence in the SCWL fluid domain

Since no turbulence models are implemented in the VrSuite software, it was decided to increase the value of thermal conductivity of the working fluid in order to account for the effects of turbulence, which facilitate the radial heat flux in the fluid domain of the loop model.

The thermal conductivity scaling coefficient "1000" was chosen from the comparative analysis of the test problems done in ANSYS CFX and computed using "laminar flow" option and "k-epsilon" and "sst" turbulence models.

In order to make sure that such significant increase in thermal conductivity is not going to cause any inacceptable increase of axial diffusion, leading to an incorrect temperature field in the fluid domain, the additional tests were done using the VrSuite software.

The detail description of the mentioned test problems and the corresponding results are included in Appendix 3.

3.7 The design of pipe hanger layouts (mechanical constraint layouts)

As will be explained later, the presented analysis consists of analysis of the SCWL with three different pipe hanger layouts. The pipe hanger layouts will be later referred to as 'first', 'second', and 'third' pipe hanger layouts.

Tables 3.4a and 3.4b explain the used mechanical constraints for each constraining spot of the used pipe hanger designs. Tables 3.4a and 3.4b correspond to Figures 3.8a and 3.8b. Both tables specify the directions in which each of the constraining spots is constrained (i.e., x, y, and z).

The first hanger layout was developed by R. G. Alena and members of the Carleton SCWL group who worked on the design and installation of the loop.

Table 3.4a: First and Second pipe hanger layouts (Figure 3.8a)

Constraining spot	1	2	3	4	5	6	7	8	9	10	11	12
First layout	x, y, z	x, y, z	y	y	y	y	-	-	y	x, y, z	x, y, z	y
Second layout	x, y, z	x, y, z	y, z	y, z	x, y	x, y	z	x, z	x, y	x, y, z	x, y, z	x, y

Table 3.4b: Third pipe hanger layout (Figure 3.8b)

Constraining spot	1	2	3	4	5	6	7	8	9	10	11
Third layout	x, y, z	y, z	y, z	x, y	x, y	z	x, z	x, y	x, y, z	x, y, z	x, y

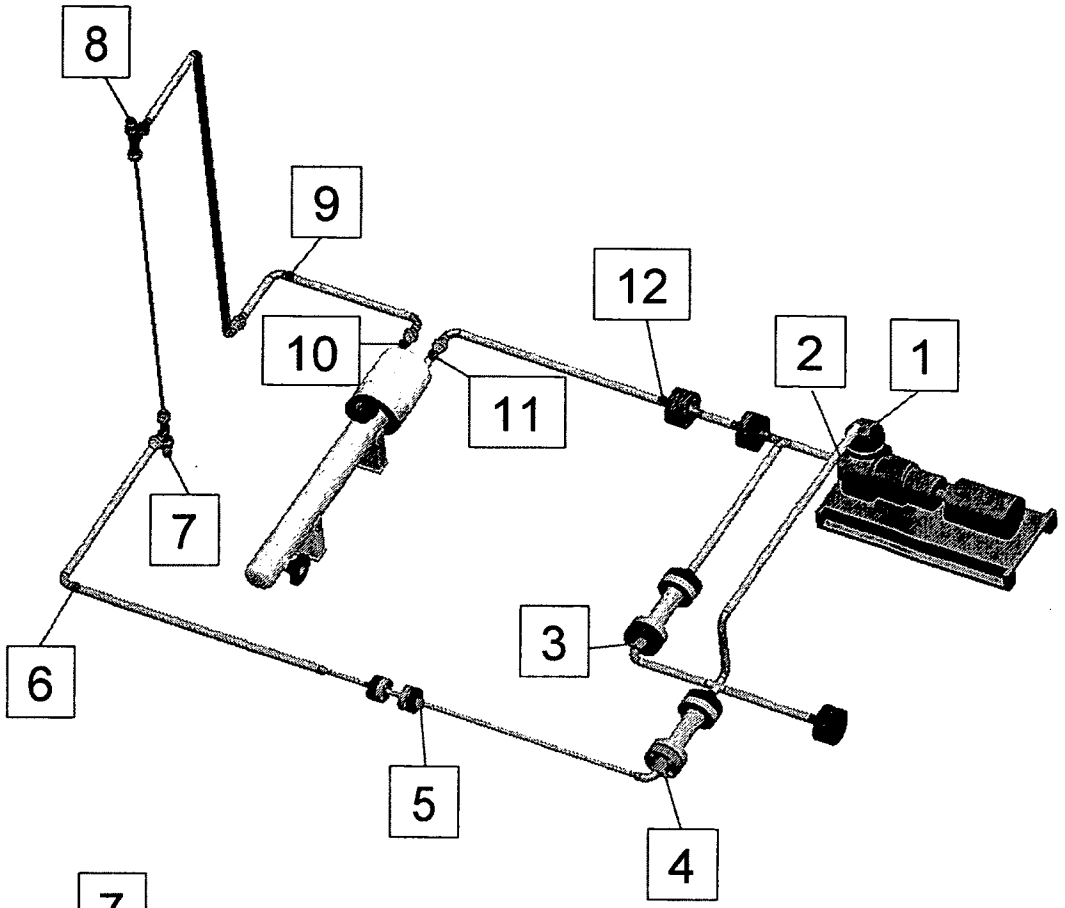

Figure 3.8a

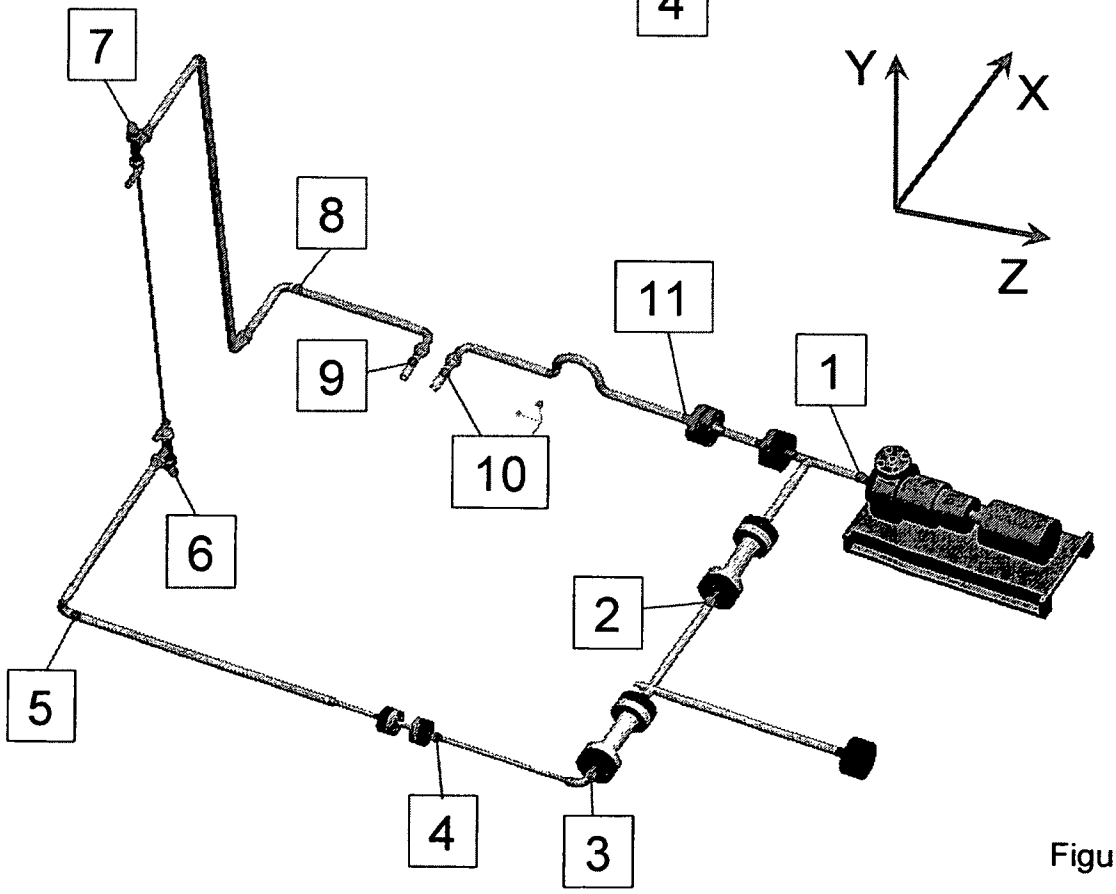

Figure 3.8b

In the constraint layouts described above, for constraining pipes in shear directions (i.e. in directions perpendicular to pipe axes) one of the possible design solutions is a split bushing shown in Figure 3.9.

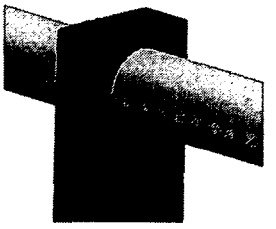

Figure 3.9 Split bushing

3.8 Research objectives

1. Perform verification of the VrSuite software package against exact analytic solutions that include physics and/or geometry specific to the SCWL piping system;
2. Develop a numerical model of the SCWL that can accurately capture/or can be easily adjusted to accurately capture the temperature, stress, and strain fields of the real loop;
3. Develop an appropriate virtual test program to contribute to the development of the test program for the real SCWL;
4. Attempt to reduce the stress levels via modification of the existing SCWL pipe hanger layout or/and design of the SCWL;
5. Perform the transient thermal and structural analyses of the SCWL models with existing and modified pipe hanger layouts or/and design and interpret the results to make sure that the model thermal parameters correspond to

the SCWL operational ranges and the stress levels do not exceed acceptable stress for the safe operation of the loop;

6. Propose possible model modifications and future research work activities to improve the ability to analyze the Carleton SCW test facility in the most efficient and accurate way.

3.9 SCWL model assumptions and simplifications

1. The working fluid is incompressible and laminar;
2. Working fluid pressure is 25 MPa;
3. Slip boundary condition is used at the working fluid-to-piping system interface;
4. Some SCWL components are replaced by components with simplified geometry or by corresponding boundary conditions;
5. The Dittus-Boelter correlation is used for computation of convection heat transfer coefficients for the convection boundary condition at the working fluid-to-the loop structure interface;
6. The Global Valve installed in the by-pass branch of the loop is assumed to be fully closed. In other words, there is no working fluid flow across the valve (i.e. no heat is convected across the valve), while the heat conduction across the "body" of the valve still takes place;
7. The material of all components of the SCWL in the presented model, except the test section, test section hubs, and preheating elements, is assumed to have properties of AISI 316L stainless steel, available in the VrSuite material library. As per SCWL design specifications, the test

section and test section hubs [25] have properties of INCONEL 617 [20]. The preheaters have properties of INCONEL 625. The corresponding material properties are taken from the on-line sources [31, 30];

8. All loop components are treated in the model as rigidly connected between each other;
9. No turbulence models are used; the increased heat flux, which takes place in a turbulent flow, is modelled by the increased thermal conductivity of the working fluid (chapter 3.6).

3.10 The analysis description

Due to the nature of physics involved in the SCWL, the model can be subdivided into solid and fluid domains. The solid domain represents the loop structure, and fluid domain represents the working fluid. The heat transportation in the fluid domain, which is a result of the forced convection, is solved by means of the Navier-Stokes and advection-diffusion solvers. The temperature field in the solid domain, resulted from the Joule heating of the test section and preheaters and convection boundary condition between the solid and fluid domains, is resolved by voltage-current and energy solvers. The displacement, strain, and stress fields in the solid domain introduced by the thermal gradient, pressurization, and applied mechanical constraints, are resolved by the stress solver.

Since the SCWL with the first and third pipe hanger layouts were analyzed only for comparative purposes, the analyses for these layouts were done for 300 sec. power ramp up scenario only. The analysis of the loop with the second layout was done for three different scenarios corresponding to the linear heating power

ramp up rules that were supposed to bring the working fluid to the near-critical state in 300, 1800, and 3600 seconds physical time.

The power input rules, controlled by corresponding voltage boundary conditions and applied to the test section and preheaters, were developed to provide linear power ramp up with respect to time. The magnitudes of the power input were selected to satisfy the maximum available power input for the test section and preheaters [26] and to obtain the water temperature that is possibly close to the near-critical temperature (i.e. around 658K at 25 MPa) at the last time step of each power ramp up scenario.

3.11 Computational sequence

To solve the transient temperature and stress fields in both solid and fluid domains, the voltage-current, energy, Navier-Stokes, advection-diffusion, stress, and Dittus-Boelter correlation solvers are employed in a coupled manner in each time step.

The description of computational sequence for one time step is provided below and the process is shown schematically in Figure 3.10:

0. The temperature field of the fluid domain is imported from the advection-diffusion solver (uniform initial temperature) to the fluid-flow solver; the temperature field of the solid domain is imported from the Thermal solver (uniform initial temperature) to the voltage-current solver. The Dittus-Boelter convection coefficient correlation, based on averaged fluid parameters for

each mesh slice along the SCWL pipe system axis, is used to compute convection coefficients for the convection BCs in the energy solver;

1. The fluid-flow solver solves for velocity and pressure in the fluid domain; the voltage-current solver solves for power density in the solid domain;
2. The solved velocity field from the fluid-flow solver is sent to the advection-diffusion solver; the solved power density field from the voltage-current solver is sent to the energy solver; ambient temperature for the convection BC in the energy solver, which is corresponding current temperature of the fluid domain in the advection-diffusion solver, is imported to the energy solver. The convection coefficients for the corresponding mesh slices computed in the step "0" are used as coefficients for the corresponding convection BC in the energy solver;
3. The energy solver solves for the temperature field in the solid domain;
4. The solved temperature field from the energy solver is sent to the advection-diffusion and stress solvers;
5. The advection-diffusion solver solves for temperature and enthalpy in the fluid domain using convection coefficients, for the corresponding mesh slices, computed in step "0" and ambient temperature obtained in step "4"; The stress solver solves for stress and strain in the solid domain.

The described computational sequence is repeated for all following time steps

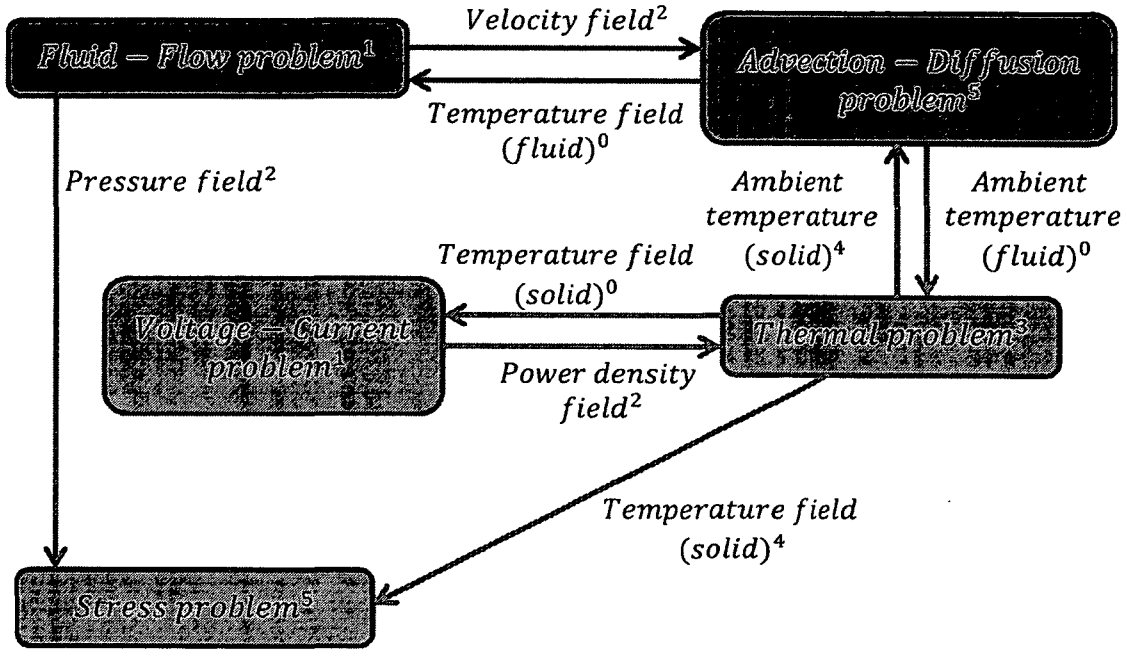

Figure 3.10 Computational sequence diagram (the superscripts in the diagram represent the order of the computation and correspond to the sequence steps (0...5) described above).

3.12 Mesh

The solid domain shown in Figure 3.11 is used in the Voltage-Current, Thermal, and Stress problems. The domain is discretized with 11,632 8-node hexahedron elements.

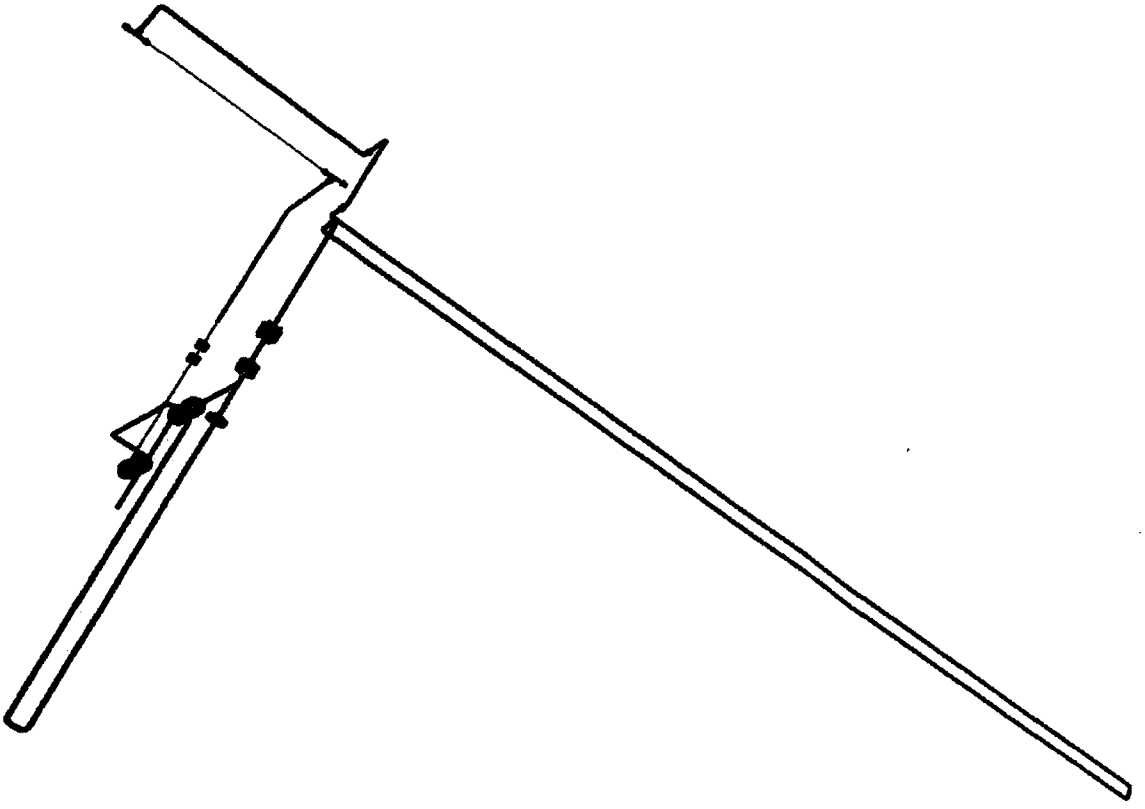

Figure 3.11 SCWL model, Schematic of the solid domain

The fluid domain shown in Figure 3.12, is used in the Fluid Flow and Advection-Diffusion problems. The domain is meshed with 14,784 8-node hexahedron elements.

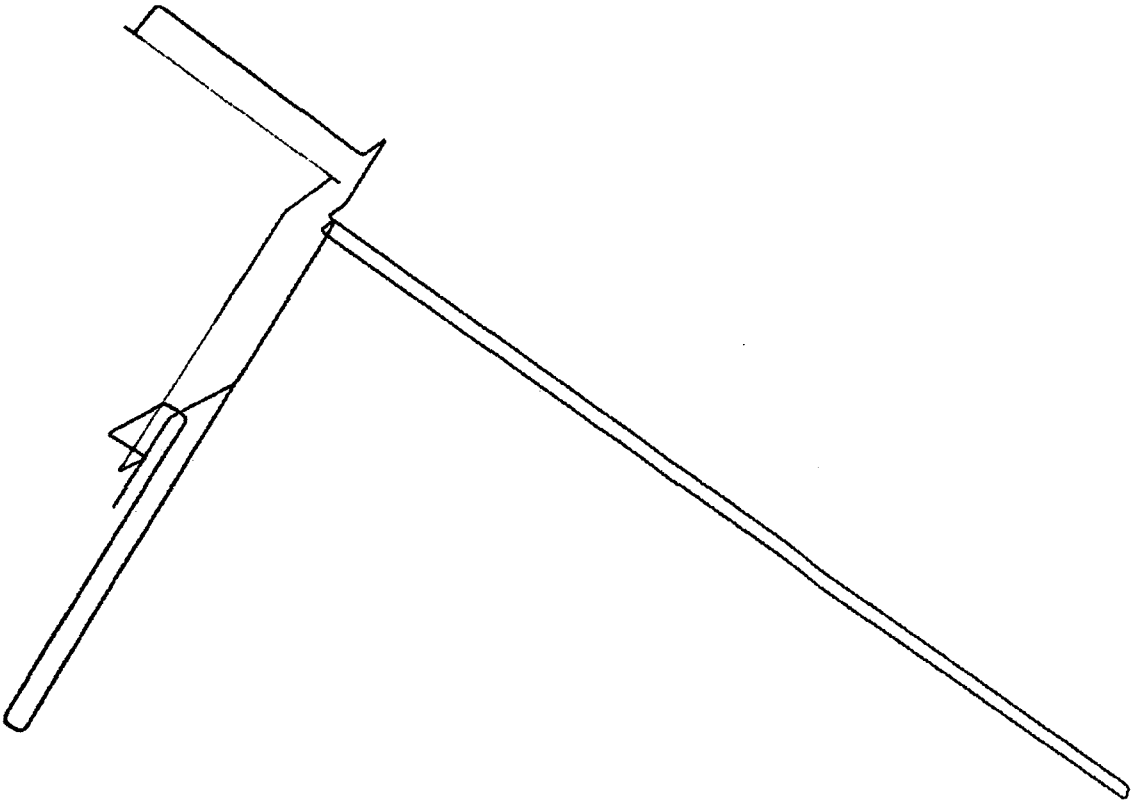

Figure 3.12 SCWL model, Schematic of the fluid domain

The detail description of the discretization used for loop components, as well as the meshing strategies used in the VrSuite software, are laid down in Appendix 4.

3.13 Description of the parameters of the Involved solvers for the first and second constraint layouts

3.13.1 Voltage-current solver

1. Mesh

Solid domain described in section 3.11.4 is used for this problem.

2. Governing equation

$$j = \sigma_e(\mathrm{T})\nabla V;\ \ \nabla \cdot \mathrm{j} = 0;$$

V is the voltage [V], j is the current density [A/m^2], and $\sigma_e(T)$ is the electrical conductivity as a function of temperature [1/(ohm*m)].

3. Material properties

Temperature dependent properties of INCONEL 617 (test section), INCONEL 625 (reducers installed between the test section and loop components), and AISI316L Steel (loop components) from the VrSuite material library are used (Appendix 6).

4. Boundary conditions

Time dependent potentials are applied to the ends of the test section and preheating elements.

Table 3.5: Boundary conditions: Voltage-Current problem

	Analysis scenario		
	300 sec.	1800 sec.	3600 sec.
Test section	0 and $5.5 * \sqrt{(t/3)}$ [V]	0 and $3.3 * \sqrt{(t/18)}$ [V]	0 and $3.7 * \sqrt{(t/36)}$ [V]
Preheater 1	0 and $7.3 * \sqrt{(t/3)}$ [V]	0 and $4.0 * \sqrt{(t/18)}$ [V]	0 and $4.4 * \sqrt{(t/36)}$ [V]
Preheater 2	0 and $5.2 * \sqrt{(t/3)}$ [V]	0 and $3.7 * \sqrt{(t/18)}$ [V]	0 and $3.6 * \sqrt{(t/36)}$ [V]

The thermal data flow is taken from the corresponding energy solver.

The time step size is taken to be equal to the time step size of the thermal problem: $\Delta t = 10.0\ sec$*

*Although the governing equations for the voltage-current solver are not time dependent, the material electrical conductivity is a function of temperature. Since the temperature field is time dependent, it indirectly makes the governing equation time dependent too.

3.13.2 Energy solver

1. Mesh

Solid domain is described in section 3.12.4 is used for this problem.

2. Governing equation

$$C_p \frac{DT}{Dt} - \nabla \cdot q + Q = 0;\ \ q = -k\nabla T$$

H is the volumetric specific enthalpy [J/m^3], t is the time [sec], q is the heat flux [W/m^2], Q is the heat generation [W/m^3], k is the thermal conductivity [W/(mK)], and T is the temperature [K]. The source term Q [W/(m^3)] is taken as a data flow from the voltage-current solver.

3. Material properties

Temperature dependent properties of INCONEL 617 (test section), INCONEL 625 (reducers installed between the test section and loop components), and AISI316L Steel (loop components) from the VrSuite material library are used (Appendix 6).

4. Boundary conditions

The problem time step is chosen from the condition:

$$Fo = \frac{D\Delta t}{l^2} \geq 1 \;\rightarrow\; \Delta t \geq \frac{l^2}{D}$$

Fo if the Fourier number, l is the characteristic length (mesh size in radial direction) and D is the thermal diffusivity. For the INCONEL 617, INCONEL 625, and AISI316L Steel, material properties at temperature T=573K (approx. average analysis temperature), the corresponding values of thermal diffusivity are $D_{\text{INCONEL\_617}}$ =3.885e-6 [m^2/J] $D_{\text{INCONEL\_625}}$ =3.87e-6 [m^2/J] and $D_{\text{AISI316L\_Steel}}$ =3.86e-6 [m^2/J]. Thermal diffusivity used in the analysis D=3.90e-6 [m^2/J].

Since the temperature field in the piping system is of primary interest of the analysis, the typical characteristic mesh size $l \approx 0.0051\ [m]$, corresponding to the

typical radial size of the piping elements, is used in the analysis. For the chosen mesh size the corresponding time steps size is: $\Delta t = 6.67\, sec$. The chosen time step size is $\Delta t = 10.0\, sec$

Convection BCs with local convection coefficients are applied to the piping system-to-working fluid interface. To simulate the reasonable insulation of the SCWL, the convection boundary conditions with convection coefficients are applied to all outside surfaces of the model in accordance with Table 3.3.

Table 3.6: Boundary conditions: Thermal problem

	Convection coefficient
The piping system-to–working fluid interface	
Convection coefficient	The Dittus-Boelter correlation
Ambient temperature	From the Advection-Diffusion solver
Outside loop surfaces	
Convection coefficients	Table 3.3
Ambient temperature	300K

5. Initial conditions

Initial temperature of the domain is 300K.

3.13.3 Navier-Stockes solver

1. Domain

Fluid domain described in section 3.11.4 is used for this problem.

2. Governing equation

For incompressible fluid the continuity and momentum equations in Eulerian frame govern the behaviour of fluid domain:

$$\nabla \cdot V = 0;\ \ \rho\left(\frac{\partial V}{\partial t} + V \cdot \nabla V\right) = -\nabla p + \mu \nabla^2 V$$

V is the velocity [m/sec], t is the time [sec], ρ is the density [kg/m^3], p is the pressure [Pa], and μ is the dynamic viscosity [kg/(m*sec)].

(Note: it would have been more realistic to use a compressible flow solver, but it is not yet available)

3. Material properties

Temperature dependent water properties from the NIST website are used for the problem (Appendix 6).

4. Boundary conditions

The time step size is chosen from the condition:

$$Co = \frac{V \Delta t}{\Delta x} \approx 5$$

$Co, V, \Delta t$ and Δx are the Courant number, velocity [m/sec], time step size [sec], and mesh element size [m] in axial direction, correspondingly. Since the

maximum Courant number corresponds to the minimum element size in the axial direction, the minimum element size is used for the time step estimation.

For $V = 0.014\ m/sec$ and $\Delta x = 0.02\ m$, the resulting time step size is $\Delta t = 7.14\ sec$. The chosen time step size is $\Delta t = 5\ sec$.

Inlet velocity is applied to the pump outlet-piping system inlet interface. Outlet pressure is applied to the loop piping system outlet – pump inlet interface.

Table 3.7: Boundary conditions: Fluid –flow problem

Inlet velocity	0.014 m/sec
Outlet pressure	25.0 MPa

5. Initial conditions

Initial temperature of the domain is 300K.

3.13.4 Advection-diffusion solver

1. Mesh

Fluid domain described in section 3.11.4 is used for this problem.

2. Governing equation

$$\frac{\partial T}{\partial t} = \nabla \cdot D\nabla T - \vec{V} \cdot \nabla T; \quad D = \frac{k}{\rho C_p}$$

T is the temperature [K], t is the time [sec], D is the thermal diffusivity [m^2/sec], V is the velocity [m/sec], k is the thermal conductivity [W/(mK)], ρ is the density [kg/m^3], and C_p is the specific heat [J/(kg*K)].

3. Material properties

Temperature dependent water properties from the NIST website are used for the problem (Appendix 6).

4. Boundary conditions

Convection BCs are applied to the piping system-to-working fluid interface.

Table 3.8: Boundary conditions: Advection-diffusion problem

Convection coefficient:	The Dittus-Boelter correlation
Ambient temperature	From the energy solver

The time step size $\Delta t = 5\,sec$ is equal to the time step size used in the Navier-Stokes solver.

5. Initial conditions

Initial temperature is 300K.

3.13.5 Stress solver

1. Domain

Solid domain described in section 3.11.4 is used for this problem.

2. Governing equation

$$\nabla \cdot \sigma + b = 0; \;\; \sigma = E\varepsilon; \;\; \varepsilon = (\nabla u + (\nabla u)^T + (\nabla u)^T \nabla u)/2$$

The first equation above is the conservation of momentum equation, where inertial term "$\rho(\frac{\partial v}{\partial t} + v \cdot \nabla v)$", with the density field ρ and the velocity field v, is ignored. The second and third equations are the stress-strain constitutive relation and relation between displacement and strain.

In the above governing equations, σ is the Cauchy stress tensor, E is the 6x6 elasticity tensor, ε is the Green-Lagrange strain tensor, and b is the body force.

3. Material properties

Temperature dependent properties of INCONEL 617 (test section), INCONEL 625 (reducers installed between the test section and loop components), and AISI316L Steel (loop components) from the VrSuite material library are used (Appendix 6).

4. Boundary conditions

Neumann pressure boundary condition is applied to the inside surfaces of the loop piping system.

Table 3.9: Boundary conditions: Stress problem

Pressure BCs	From the Navier-Stokes solver
Thermal data flow	From the energy solver

All rigid body modes are restrained

The time step size $\Delta t = 20\ sec$ is chosen to satisfy the condition of maximum temperature change $\Delta T = 50$ degrees for any of the two consequent time steps.

5. Initial conditions

Initial temperature of the domain is 300K.

3.14 Results

3.14.1 Temperature fields in the solid and fluid domains

Although the primary goal of this analysis is to verify if the stress levels in the loop piping system stay within the acceptable range, the temperatures of the test section, preheaters, and other components of the loop are to be maintained below the appropriate level (i.e. below 900K for both fluid and solid domains). In addition, the temperature of the working fluid in a test section of the real loop is supposed to correspond to the water pseudo-critical temperature at P=25 MPa (i.e. about 658K). Therefore, in order to make sure that the simulations correspond to the expected ranges of the mass flow rate and temperature field (approx.) of the real loop, it is essential to check the mentioned thermal operational parameters.

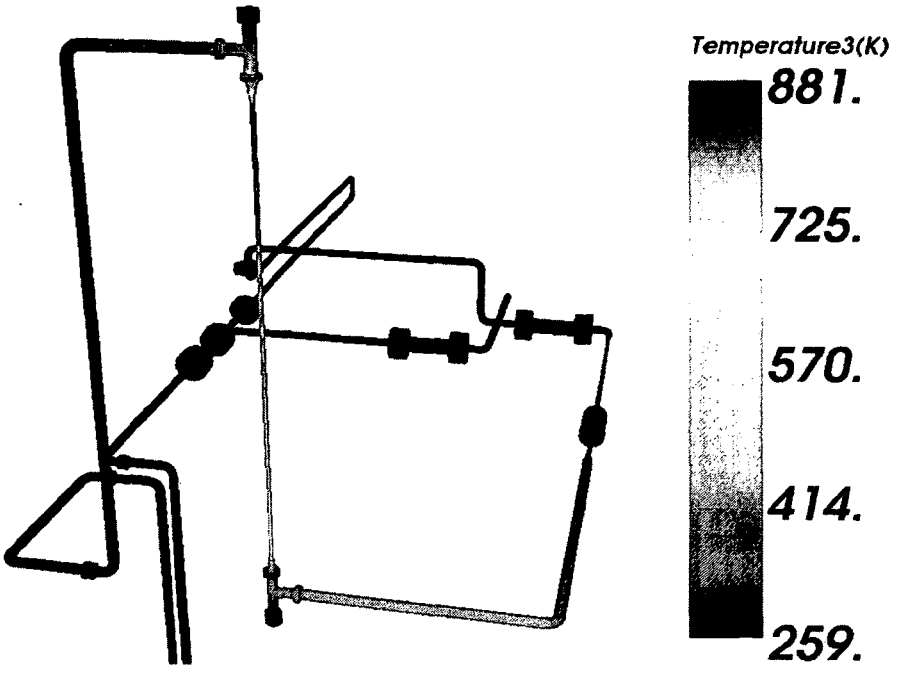

Figure 3.13 Solid domain temperature for the 300 sec. power ramp up scenario at the last time step

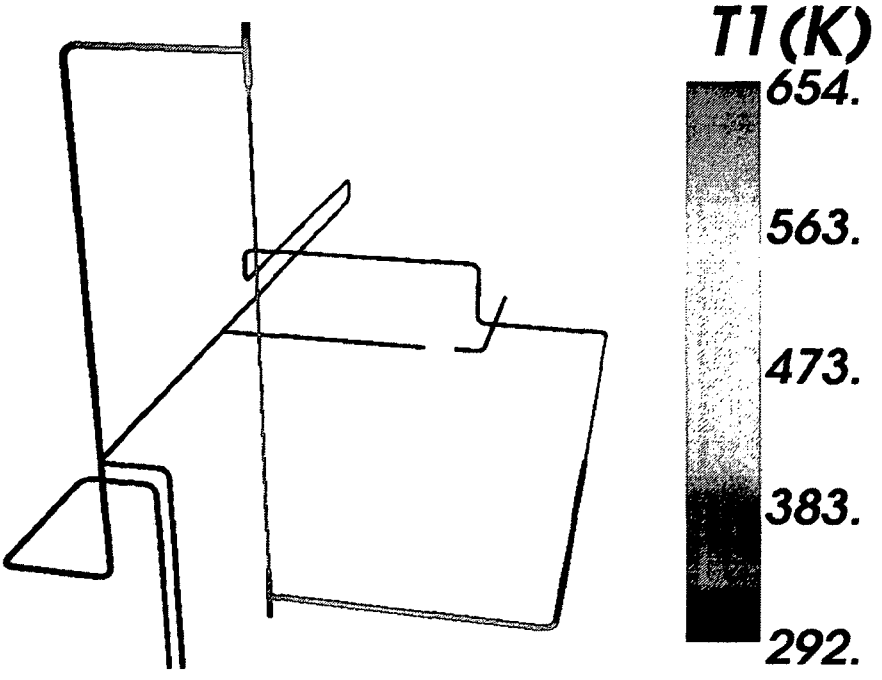

Figure 3.14 Fluid domain temperature for the 300 sec. power ramp up scenario at the last time step

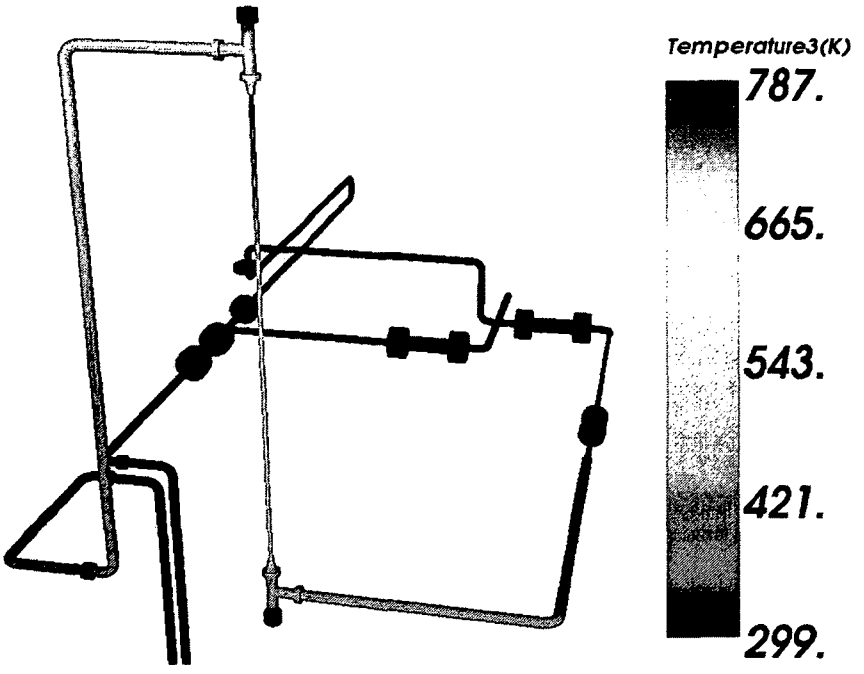

Figure 3.15 Solid domain temperature for the 1800 sec. power ramp up scenario at the last time step

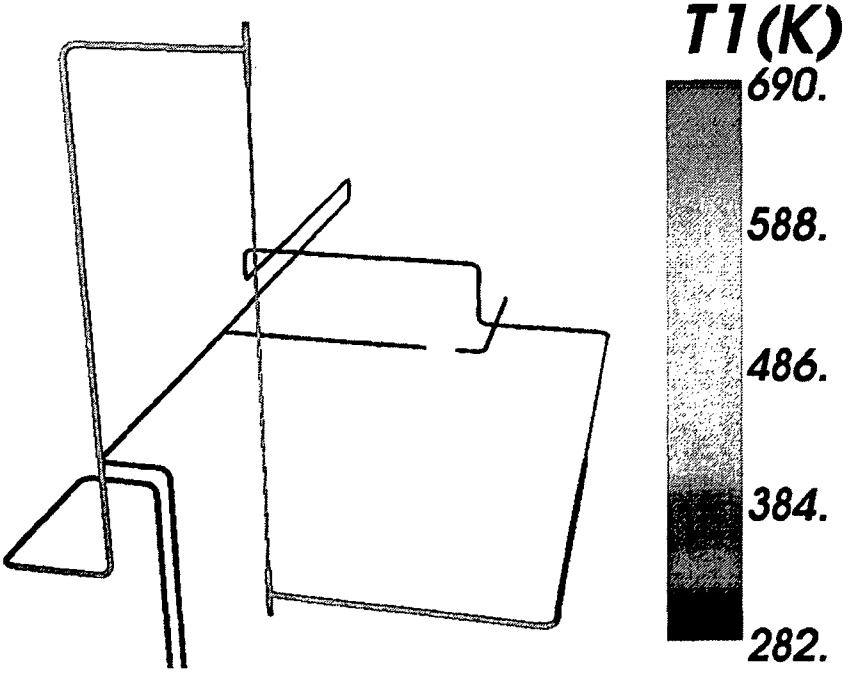

Figure 3.16 Fluid domain temperature for the 1800 sec. power ramp up scenario at the last time step

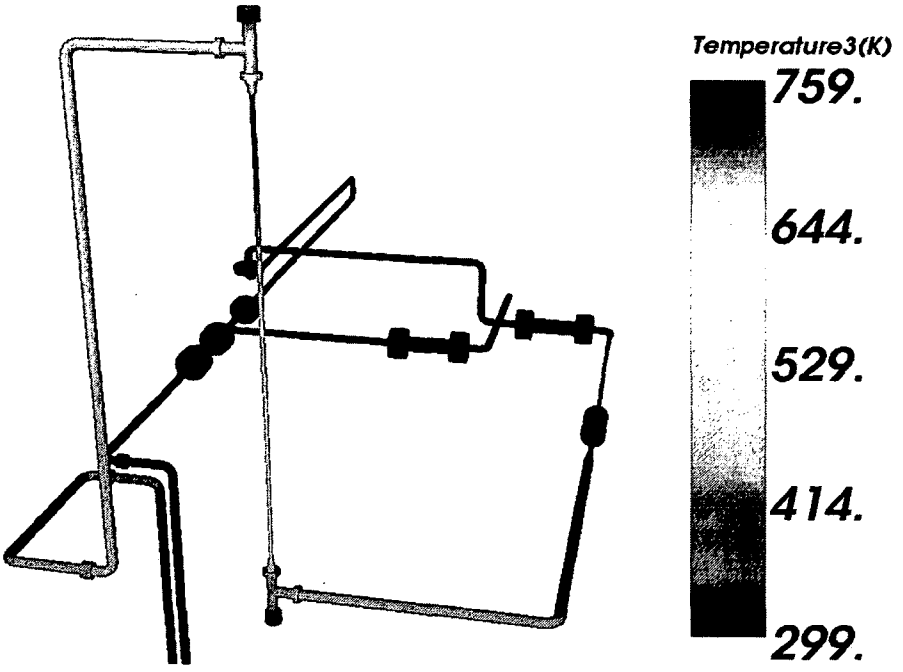

Figure 3.17 Solid domain temperature for the 3600 sec. power ramp up scenario at the last time step

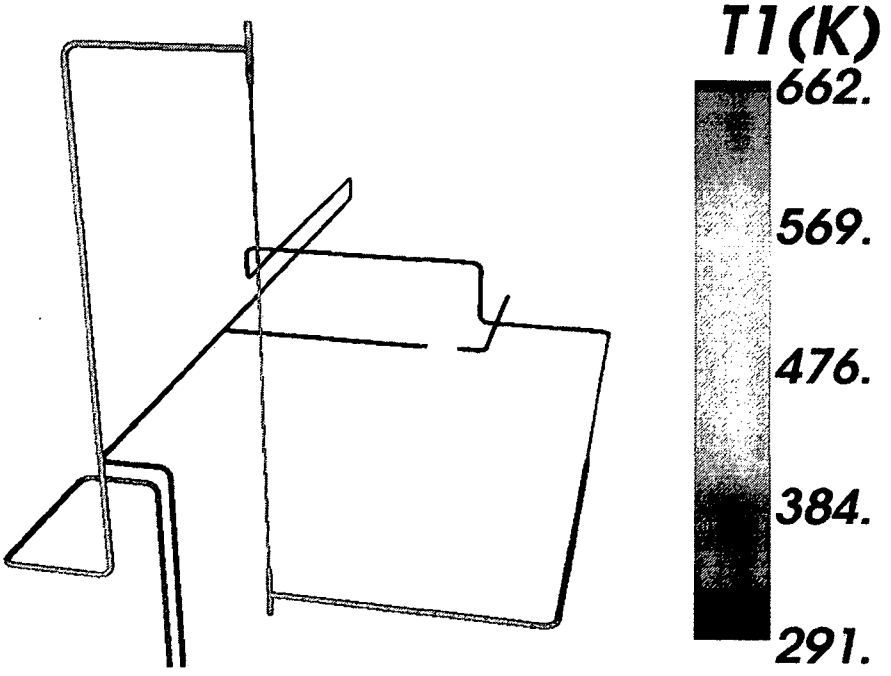

Figure 3.18 Fluid domain temperature for the 3600 sec. power ramp up scenario at the last time step

As can be seen in Figs. 3.13...3.18, the temperatures of the solid loop components do not exceed 900K, the working fluid temperature range in the test section includes pseudo-critical region, and the fluid domain does not exceed 900K for all three scenarios.

3.14.2 Stress

The stress results are subdivided into groups according to the pipe hanger layouts described above (3.7 The design of pipe hanger layouts). Since the maximum effective stresses are relatively constant for all time steps in each of the analysis cases for the first and second pipe hanger layouts (149.5...149.6 MPa for the first layout; 438.3...439.7 MPa for the second layout), it was assumed that the stress levels were mostly constant during the analyses, and it was decided to detail only the last time step for each case, where slight increase in the maximum effective stress (149.6 MPa for the first layout; 439.7 MPa for the second layout) takes place.

3.14.2.1 First pipe hanger layout; 300 sec power ramp up

Although the maximum effective stress obtained for the first constraint layout is about 440 MPa (Figure3.19), it should be said that such high effective stress is not realistic even if the material allows such high stress levels. This high stress level resulted from the simplified geometry of some parts of the SCWL. For example, the stress peaks (above 300 MPa) take place at the sharp corners of the tee shown in Figure 3.19. The actual cast or cold formed piping components usually have technological fillets or finite radiuses instead of perfectly sharp corners. Finite radiuses would prevent such high stress levels.

In Figure 3.20 it is seen that there are several zones where effective stress level exceeds the yield stress (red spots) of the loop piping system material (180...190 MPa) at the typical estimated SCWL operating temperatures for the given parameters. The most part of the regions with stress exceeding yield limit

corresponds to the bending stress in the upper region of the plot (highlighted in red). The bending stress is a result of the significant deformation of the loop structure (Figs. 3.20, 3.21).

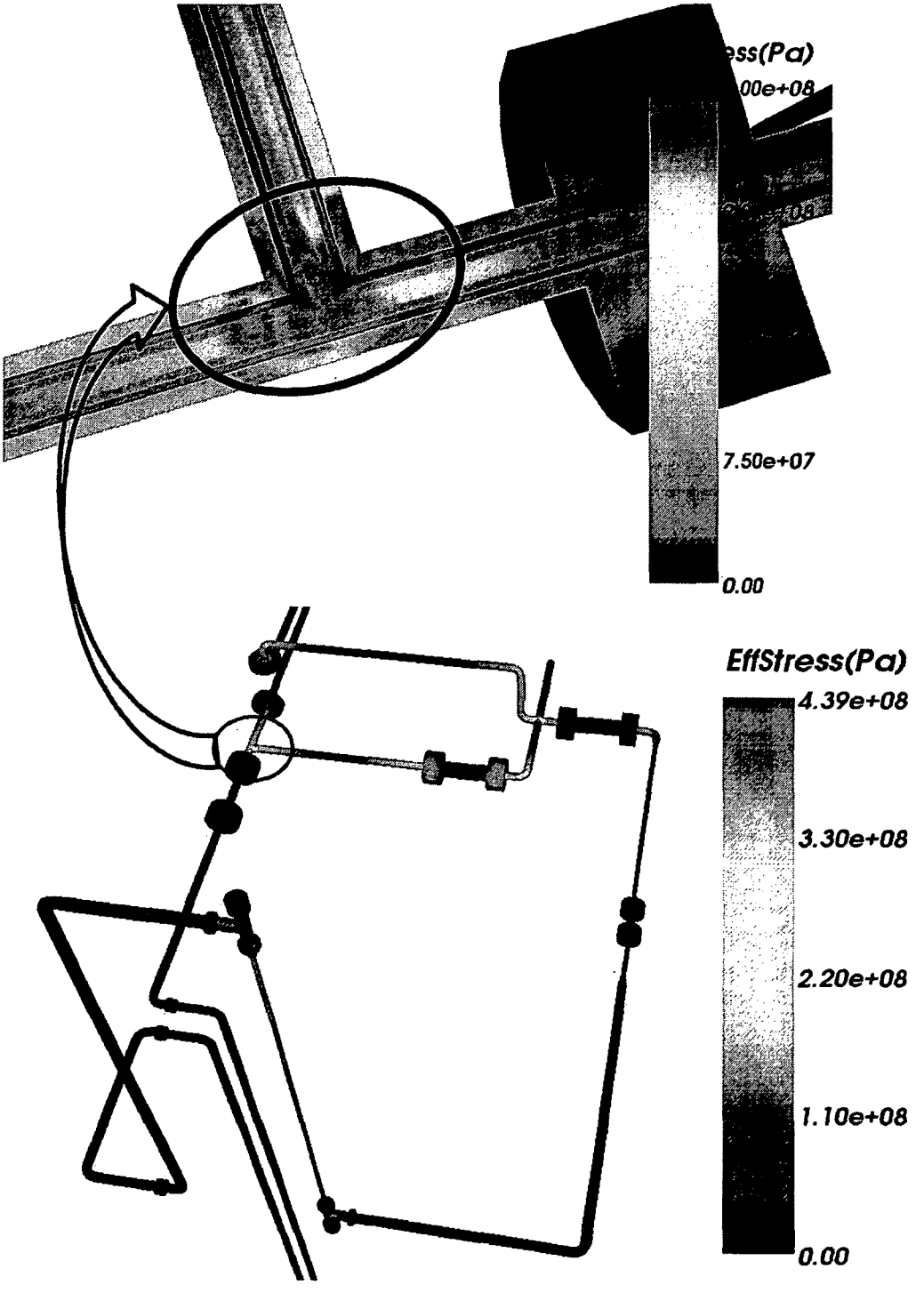

Figure 3.19 Sharp corners resulted from the geometry simplification

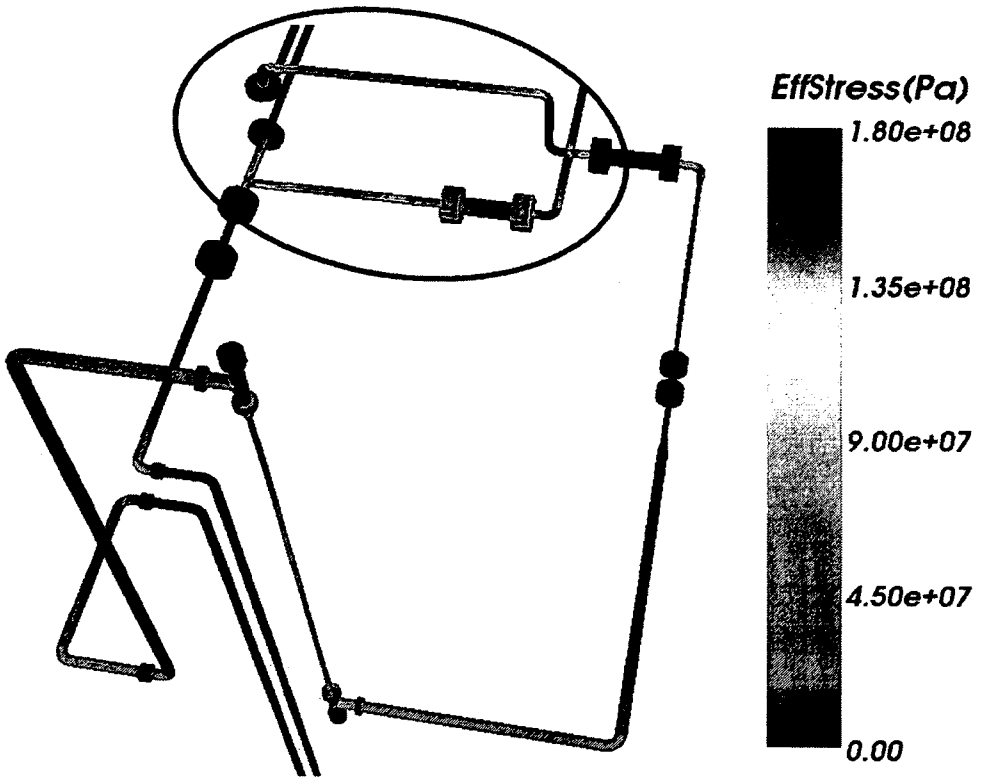

Figure 3.20 First pipe hanger layout; Effective stress above 180 MPa

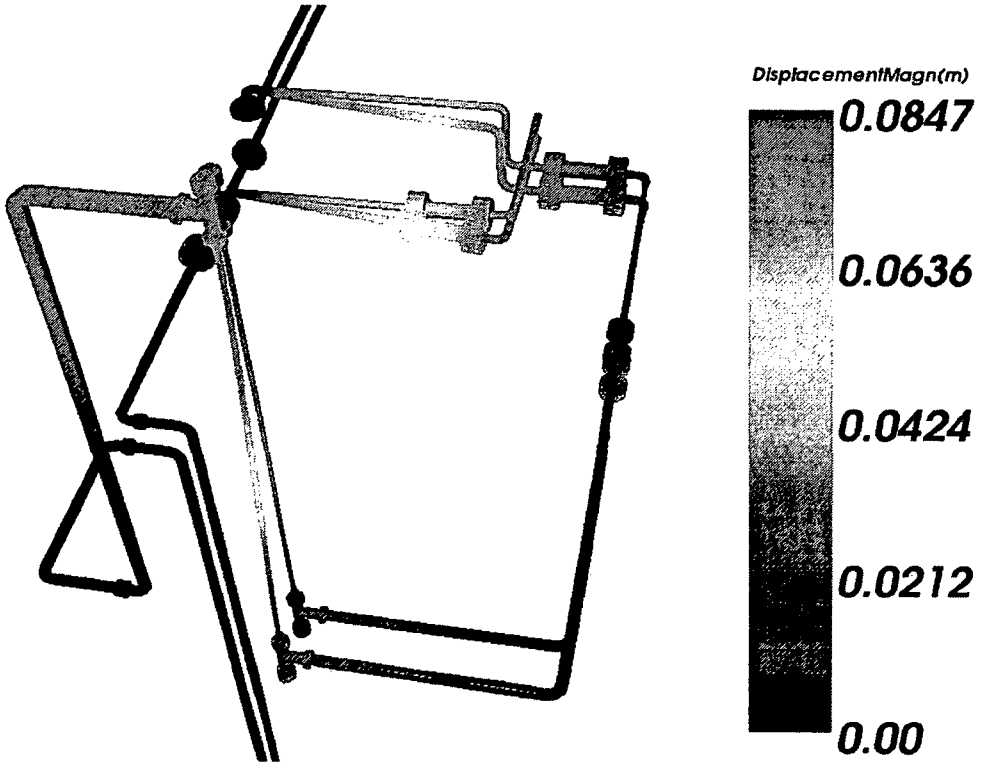

Figure 3.21 First pipe hanger layout; Displacement (x3 displacement magnification)

3.14.2.2 Second pipe hanger layout

As can be seen from the plot of effective stress, Figure 3.22, the effective stress values do not exceed 150MPa for the 300 sec., 1800 sec. and 3600 sec. power ramp up scenarios. It is seen that the maximum displacement (Figure 3.23) increases as the power ramp up scenario becomes more intensive. The Iso-surface plots of effective stress for 55 MPa (Figure 3.24) and the effective stress range 60...150 MPa (Figure 3.25) demonstrate the same trend (i.e. a more intensive heat input rate results in a higher stress level).

The Iso-surface plot of effective stress for the range 60...150 MPa is shown to demonstrate that there are very few zones with stress exceeding 60 MPa. It should be also noted that the yield stress for the INCONEL 617 (test section material) is about 210 MPa at the maximum allowable test section temperature (900K) that is higher than the yield stress for the loop parts made of 316SS. Taking into account the "geometry simplification" issue mentioned in the stress results for the first layout (i.e. effect of stress concentrators resulted from the simplified CAD model), it is expected that the actual maximum effective stresses do not exceed 50% of the yield stress.

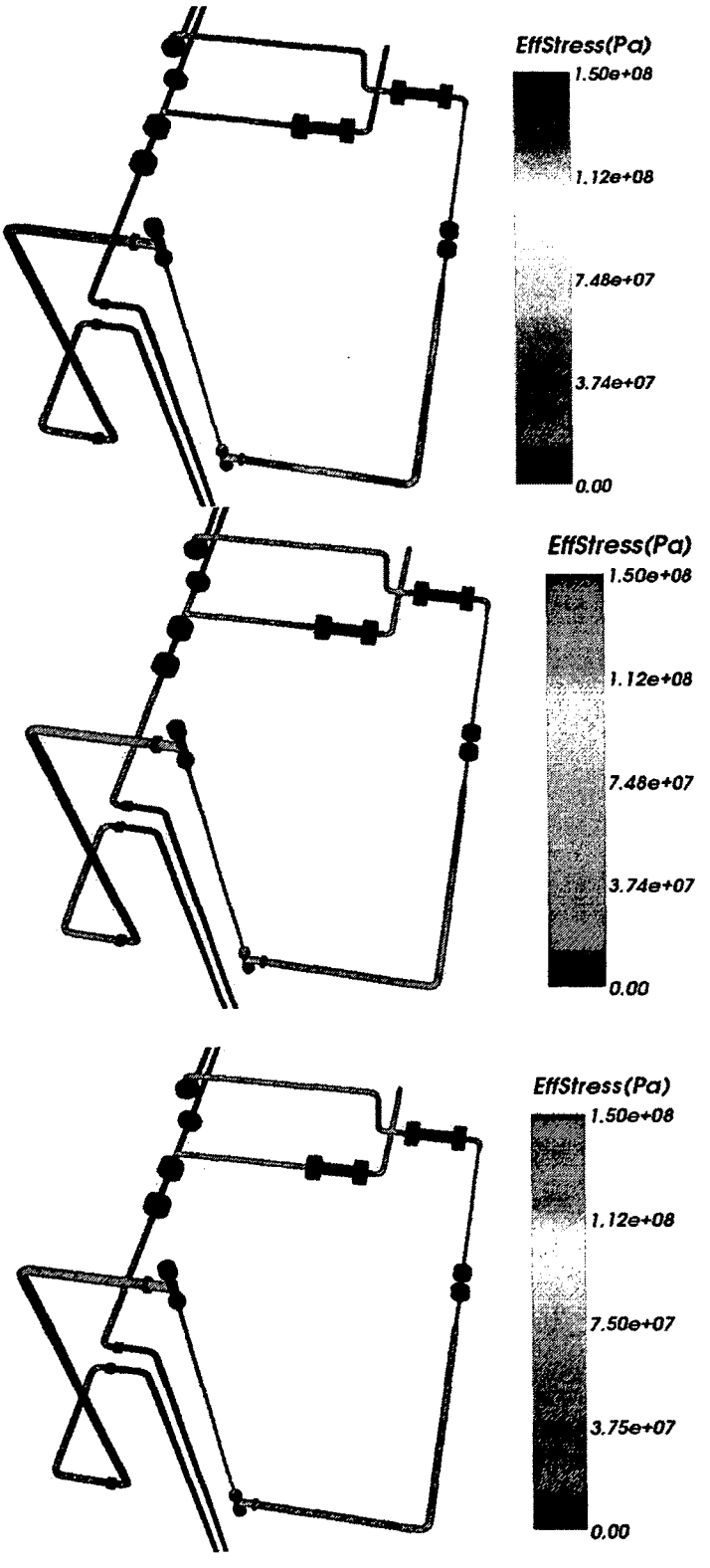

Figure 3.22 Second pipe hanger layout; Effective Stress; 300 sec., 1800 sec. and 3600 sec. power ramp up (top to bottom)

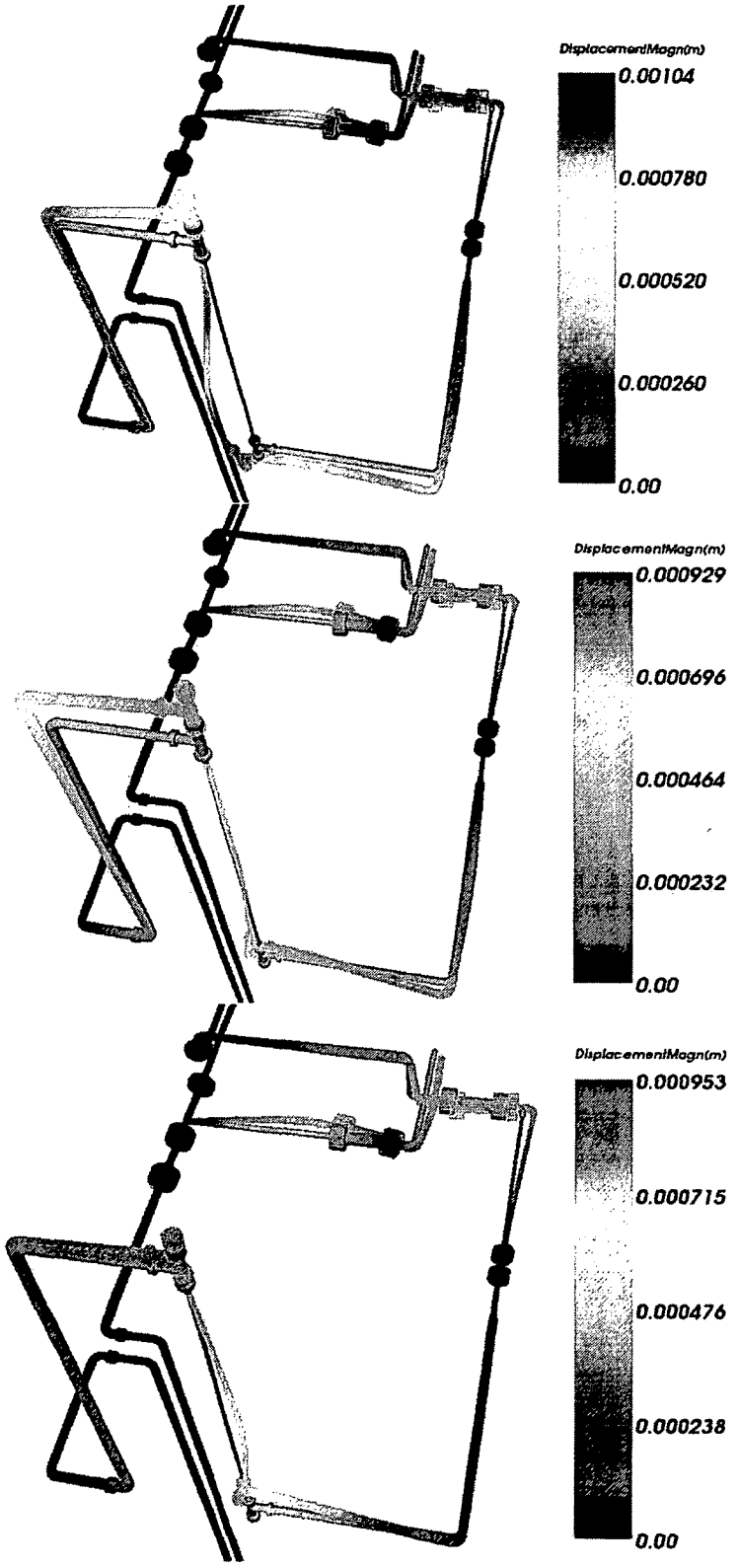

Figure 3.23 Second pipe hanger layout; Displacement; 300 sec., 1800 sec. and 3600 sec. power ramp up (top to bottom; x300 displacement magnification)

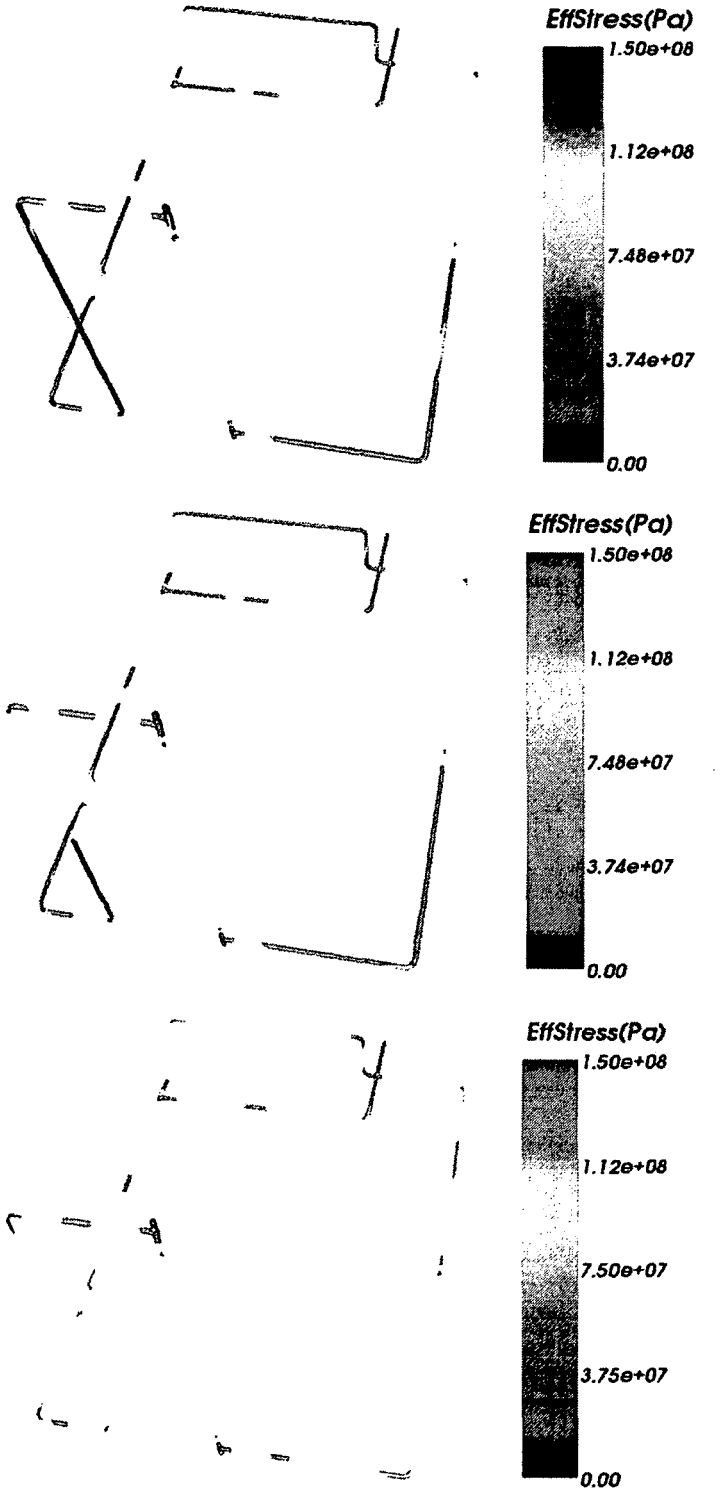

Figure 3.24 Second pipe hanger layout, Effective Stress, Iso-surfaces 55 MPa; 300 sec., 1800 sec. and 3600 sec. power ramp up (top to bottom)

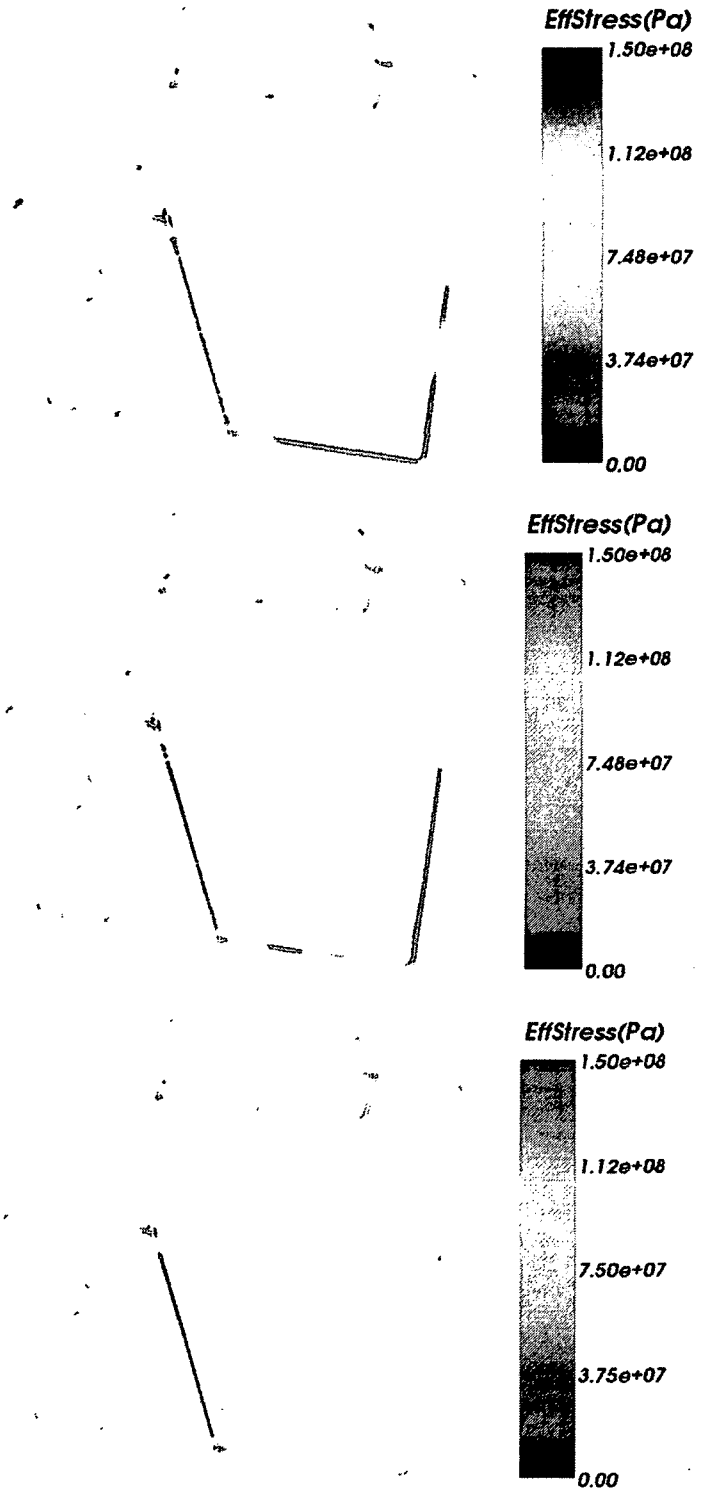

Figure 3.25 Second pipe hanger layout, Effective Stress, Iso-surfaces 60...150 MPa; 300 sec., 1800 sec. and 3600 sec. power ramp up (top to bottom)

Chapter 4: SCWL design modification

4.1 Shortcomings of the current design

At the early stage of the design process, utilization of CAE software, such as VrSuite, allows a designer to make better design solutions and can unveil or predict potential problems. This chapter demonstrates how the VrSuite can be used for the SCWL design verification.

Although the stress analysis of the SCWL done by R. G. Alena and the presented analysis suggest that the piping system of the SCWL is structurally sound, both analyses clearly show that there is a problem in the SCWL design (5.2 SCWL analysis conclusions).

The maximum effective stress in the "hot section" of the loop is supposed to be higher than in the "cold section" because in the "hot section" the high thermal gradients take place in addition to the mechanical stress caused by the pressurization. However, the maximum effective stress in the "cold section" of the piping system exceeds the maximum stress in the test section by more than 100%.

Since there is no objective cause for such high bending stresses in the "cold section" of the loop, it would be reasonable to assume that this high stress level can be mitigated through appropriate design solution.

After consideration of the given design in the light of the loop stress analysis results, it was concluded that the high stresses in the "cold" part are the result of the lack of thermal expansion compensation in this part of the SCWL. The author

believes that in the "cold section" there are at least two problems that relate to the thermal expansion of the piping system.

First, there are not sufficient mechanisms to compensate for the thermal expansion of the pipe section between the pump and heat exchanger, which are assumed to be rigidly attached to the floor while the thick-walled pipe connecting them is supposed to be heated from the room temperature up to 530-540K.

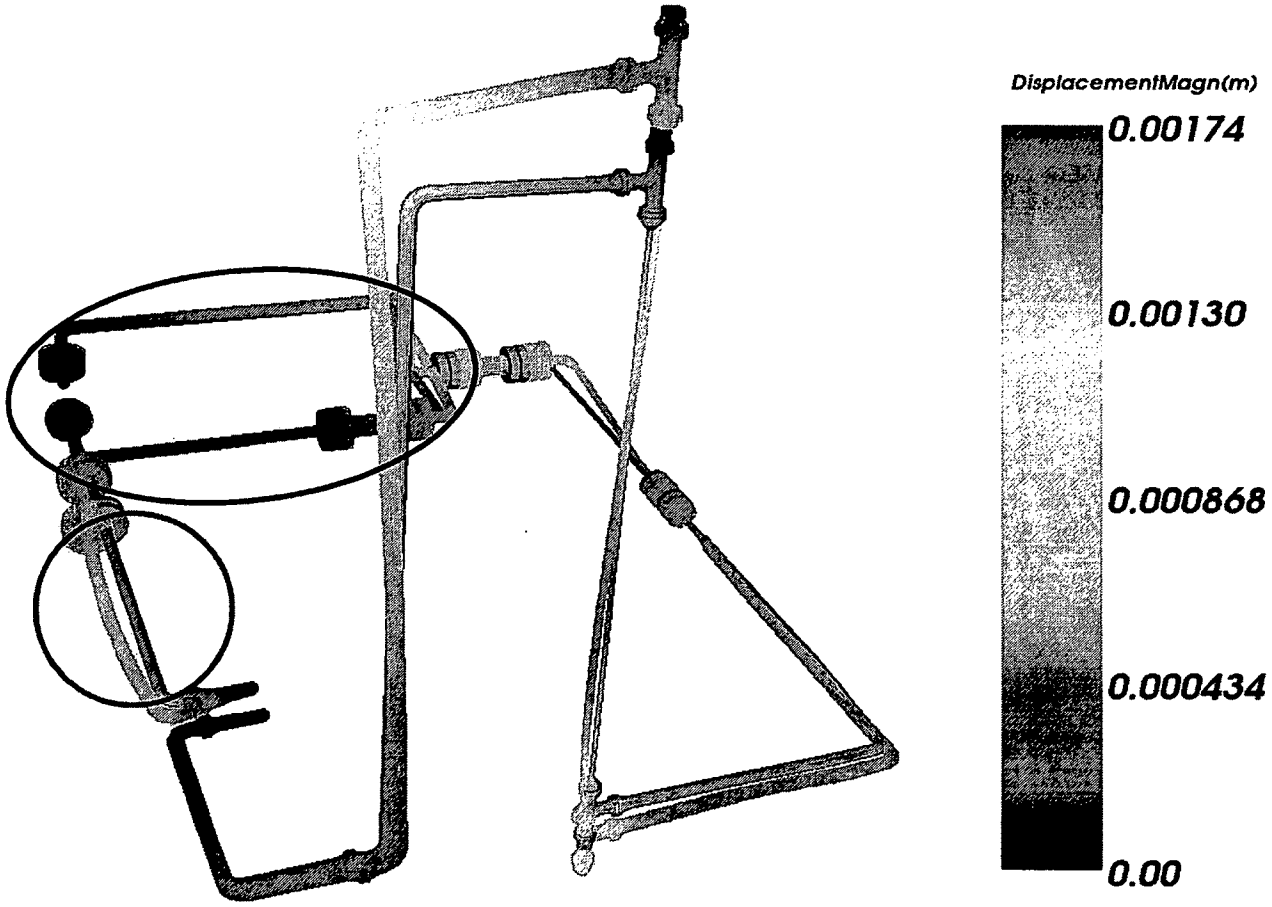

Figure 4.1 Displacement of the loop pipe system (x400 magnification factor)

Although the problem is not severe one, the results of the stress analysis suggest the noticeable thermal expansion of the pipe section between the heat exchanger and pump leading to the deflection of this part of the loop (zone highlighted in red), Figure 4.1.

Second, the rigid structure of the "small loop" (zone highlighted in black), created by two pipe branches going from the pump towards the global valves, results in significant thermal-mechanical stress and was the main reason for the high effective stress found by R. G. Alena [18].

4.2 Design modification

It was decided to propose one of the possible ways to mitigate the mentioned shortcomings.

One of the simplest ways to mitigate the thermal distortion of the pipe section that connects the rigidly fixed heat exchanger and pump is to let the pump move in axial direction. If, for any reason, this approach cannot be used and the pump must be fixed rigidly, then at least one acceptable measure for compensation of the thermal expansion (U-shape piping element, bellows, flexible hose, etc.) should be inserted into the pipe sections Position 3 or 4, Figure 4.2. Both locations for the thermal expansion compensation device may have certain advantages. For example, if the pipe Position 3 is replaced by a flexible hose, then along with elimination of the thermal stresses, the SCWL piping system will be better isolated from the mechanical vibrations caused by the pump. If a thermal compensator is used at the location of the pipe Position 4 (as shown in the Figure 4.2), it provides more space for the possible design solutions.

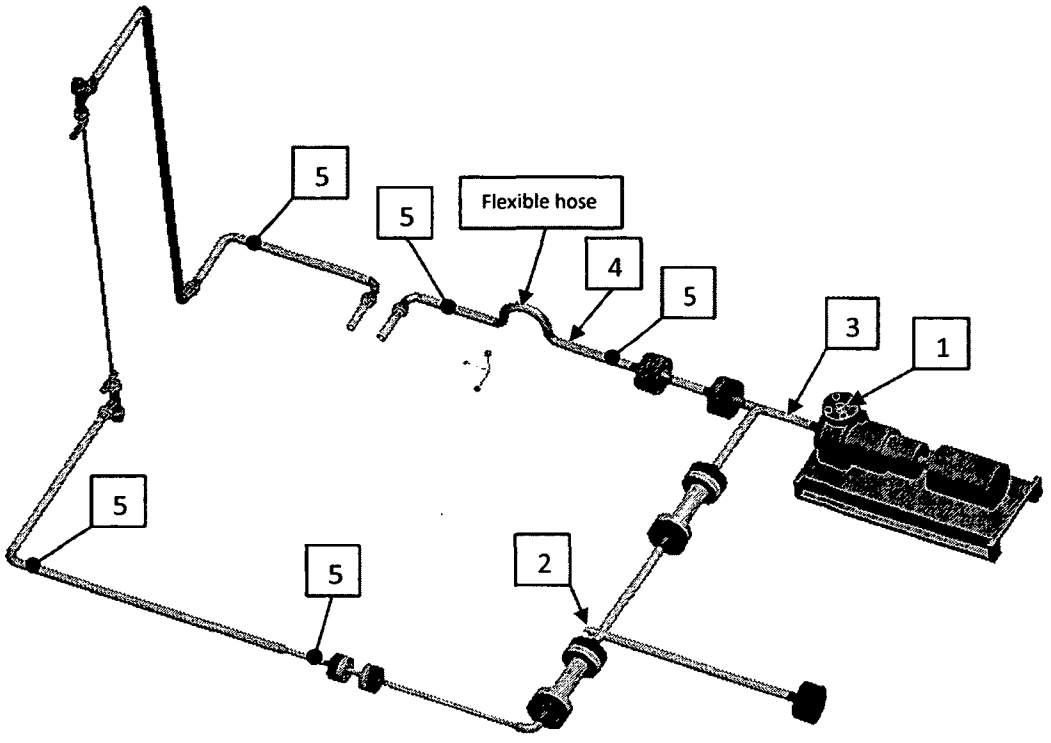

Figure 4.2 Proposed design modification scheme

The "small loop" mentioned above should also have at least one thermal compensator, or it should be eliminated as shown in the proposed design modification layout.

Note: the author's goal was to suggest possible design modification concepts, aimed to solve the concerns unveiled by the analysis, rather than to provide detailed design of the proposed modification. Therefore, all components of the modified loop are shown schematically.

In the proposed design, the pump outlet "1" is supposed to be connected with branch "2" of the cross by means of a flexible metal hose. Alternatively, as a possible way to decrease the required amount of the expensive flexible hose and

corresponding fittings, the outlet "1" and inlet "2" can be connected using a combination of the flexible hose and solid pipe.

The example of the acceptable hose, as well as possible design schemes, available fittings, and some other design details with respect to the proposed solution, can be found in Appendix 5.

In order to model the connection between outlet "1" and inlet "2" (Figure 4.2), taking into account the insignificant stiffness of the flexible hose in comparison with typical stainless steel pipes used in the SCWL, the Al-Soft material, available in the VrSuite material library, is chosen for the piping elements used for the connection. The material has Young's modulus 100 MPa and yield stress 1e14 MPa what makes the piping section used for the connection reasonably flexible.

4.3 Stress analysis of the proposed design scheme

The stress analysis of the loop version with modified design was done using an approach similar to the one used for the initial design version, including geometry simplifications, heat exchanger and pump thermodynamic models, meshing strategy, and computational sequence.

All parameters for advection-diffusion, fluid-flow, energy, and stress solvers are the same.

Due to the geometry modifications, there are some differences in the number of elements in the solid and fluid domains and in the voltage boundary conditions for the voltage-current solver, which are specified below.

The number of 8-node hexahedral elements in the solid and fluid domains are 11,715 and 15,120, correspondingly.

Table 4.1: Boundary conditions: Voltage-Current problem (modified design)

	300 sec. power ramp up scenario
Test section	0 and $5.1 * \sqrt{(t/3)}$ [V]
Preheater 1	0 and $7.1 * \sqrt{(t/3)}$ [V]
Preheater 2	0 and $4.0 * \sqrt{(t/3)}$ [V]

4.3.1 Results

4.3.1.1 Temperature fields in the solid and fluid domains

As was explained in the analysis of the "base design" version, it is essential to maintain the temperature of the solid and fluid domains at the levels that meet the loop design limitations and correspond to the loop operational parameters.

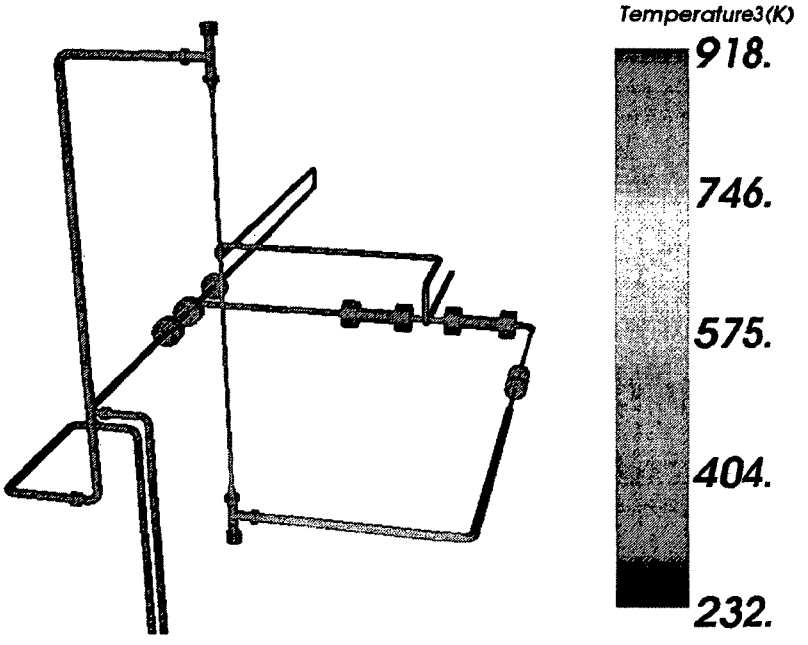

Figure 4.3 Solid domain temperature for the 300 sec. power ramp up scenario at the last time step (modified design)

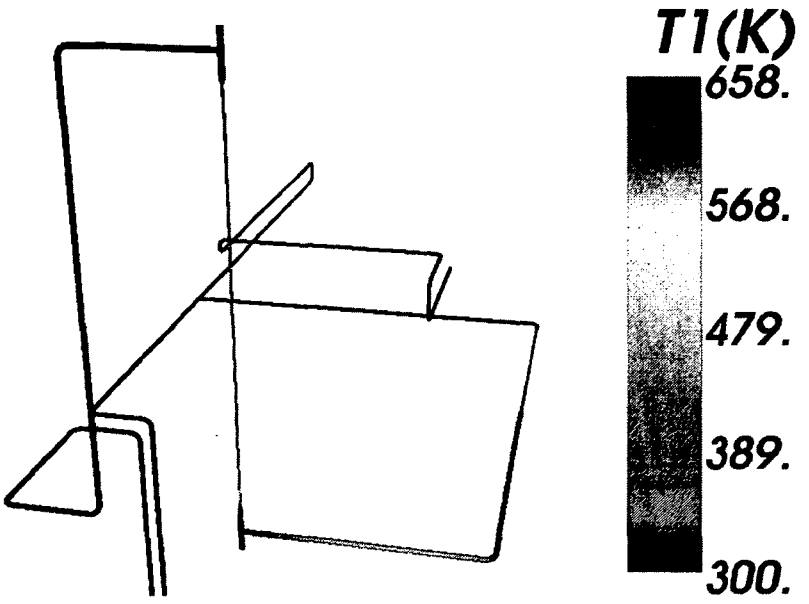

Figure 4.4 Fluid domain temperature for the 300 sec. power ramp up scenario at the last time step (modified design)

As can be seen in Figure 4.3 and Figure 4.4, the temperature of the loop components is below 900K, and the maximum temperature of the working fluid corresponds to the pseudo-critical water temperature at pressure P=25 MPa.

4.3.1.2 Stress; 300 sec. power ramp up

The maximum effective stress is relatively constant throughout the analysis time (150.8 MPa...151.1 MPa). It was assumed that the stress levels were mostly constant during the analyses, and it was decided to detail only the last time step for each case, where a slight increase in the maximum effective stress (151.1 MPa) takes place.

As can be seen from the plot of effective stress, Figure 4.6, the effective stress values do not exceed 151 MPa. Furthermore, it is seen that the proposed design does not have any bending stresses except the bending stresses caused by the thermal expansion of the test section.

Taking into account the "geometry simplification" issue mentioned in the stress results for the first layout (i.e. effect of stress concentrators resulted from the simplified CAD model), it is expected that the actual maximum effective stresses do not exceed 50% of the yield stress.

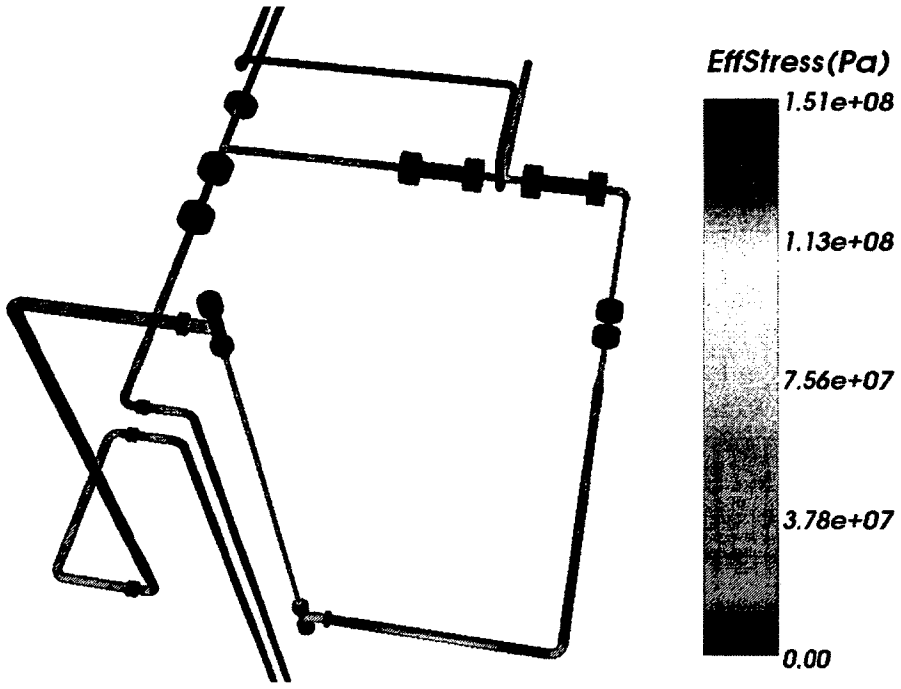

Figure 4.6 Third pipe hanger layout; Effective Stress

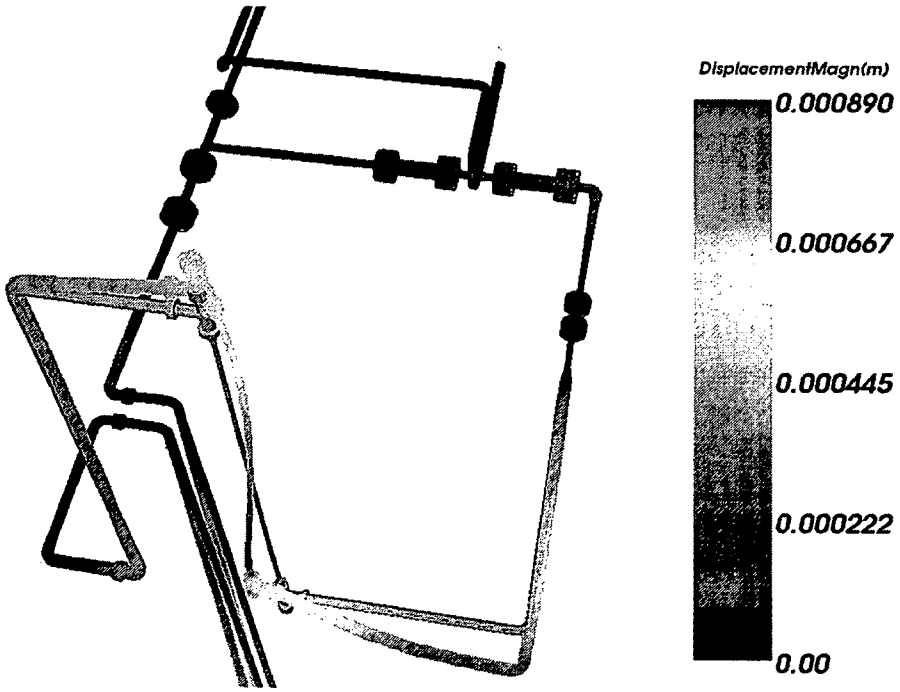

Figure 4.7 Third pipe hanger layout; Displacement (x300 displacement magnification)

Chapter 5: Conclusions and possible future work

5.1 Overall analysis conclusion

This work successfully demonstrated the capability of the chosen approach to analyze a 3D transient nonlinear coupled holistic macroscopic model of the piping system of the Carleton SCWL. This approach allows computing the 3D transient voltage, current, thermal, stress, and strain fields in the solid parts and thermal field of the fluid domain in only 1.5 hours of CPU time to compute one hour physical time (Intel® Xeon® Processor X5470) with time steps for the energy and advection-diffusion solvers as short as 10 and 5 seconds (see chapter 3.13 for details), computing local convection heat-transfer coefficients according to the Dittus-Boelter correlation. The maximum Courant number for the advection-diffusion solver in this analysis is about 10; the Fourier number for the energy solver is slightly bigger than unity.

Using this model, it is possible to do fast and precise optimization of a prototype or to design the corresponding test program, quickly changing the model parameters, such as the pipe hanger layout, electrical heat input, working fluid parameters, loop design or material properties.

If all necessary software capabilities used for the analysis methodology were available a priori, the thermal-stress analysis of the system comparable to the Carleton SCWL could be executed in less than one month by only one designer.

Comparing the demonstrated analysis approach with the traditional analysis methods (i.e., analysis by rule), it should be said that, in general, FEA usually takes more time than the similar analysis done using "design by rule approach".

However, while the design by rule allows only rough estimate of thermal and structural characteristics of the design of interest, a numerical FE model can allow resolving thermal and structural properties of the design with virtually any desired spatial and temporal resolution, depending on the available CPU resources and time for the analysis.

The choice of particular analysis method/methods may depend on many factors, including type of analyzed design, involved risks, cost of materials, level of technology/equipment, experience of an analyst, etc.

The main limitations of the current holistic microscopic model, which could noticeably affect the results of the proposed approach, are the absence of a turbulent model and use of incompressible fluid (water).

5.2 SCWL analysis conclusions

According to the results of the analysis, it is seen that the first pipe hanger layout considered in this analysis is unacceptable because it results in the excessively high effective stress level in the loop structure. Although, the second pipe hanger layout noticeably reduces the effective stress level, it is still in the vicinity of the maximum stress limit allowed by ASME 31.1 pressure vessel code (note: it is assumed that the maximum allowable stress in the ASME code is defined as the second invariant of deviatoric stress, Appendix 7). According to the code, the maximum allowable stress must be lower than the tensile strength of material at the design temperature divided by 3.5 (i.e. 28.6% of yield stress). As was shown in section 3.14.2.2, Figure 3.24, in the effective stress field for the second layout,

there are vast regions with the stress up to 55 MPa (i.e. around 25...30% of yield stress).

Even though the proposed second pipe hanger layout (described in chapter 3.7) mostly has the stress level comparable to the loop with the modified design (Chapter 4), the modified design completely eliminates bending stresses in the "cold" section of the loop and does not have any factors causing deflection of the piping section between the heat exchanger and pump, which can decrease the sealing capability of the filter bolted connections. In addition, in case of the unexpected working fluid temperature increase at the outlet of the heat exchanger, the deflection of this pipe section increases proportionally, aggravating the mentioned issue (the sealing capability). For example, the maximum displacement of this pipe section is about 0.5 mm at 533K (the heat exchanger outlet temperature at a steady state in accordance with the manufacturer specification) and is almost 0.9 mm at 600K.

It also should be noticed that the maximum effective stress in the loop is independent of the power ramp up rates considered in this analysis (Figure 3.22). There is no doubt that more intensive heating rates should cause higher thermal stresses in the structure and particularly in the loop hot section. Although the decrease of displacement and the corresponding decrease of the stress level (Figs. 3.23-3.25) support this statement, in order to have the detailed insight into the effect of the proposed power ramp up rules, the analysis of the stress history of the loop components is required.

Even though, comparing with the previous model and analysis done by R. G. Alena, the significant progress in the modeling of the SCWL was achieved, the presented model still needs to be improved according to the future work suggestions and validated when the experimental data from the real SCWL is available.

The maximum stress for ramping power in 300, 1800, and 3600 seconds was 150 MPa, which is fraction of yield stress.

The question of whether the stress compute by this model would satisfy ASME Pressure Vessel Code requirements is outside the scope of this thesis.

5.3 Future work:

1. Further development and validation of the proposed thermodynamic models for the SCWL pump and Heat Exchanger when the experimental data becomes available;
2. Implementation of the range of available convection coefficient correlations in the VrSuite software and selection of the most appropriate correlation/correlations for the specific loop elements and test regimes when the test data is available;
3. Simulation of the SCWL with partially or fully opened valve of the bypass piping branch for further investigation on the loop behaviour and development of the loop operation program;
4. Validation of the proposed model and development of the detailed test program;

5. Check of the sealing capability of the Grayloc and flanged joints in the context of overall loop analysis;
6. Continuation of the analysis of the SCWL using compressible working fluid and/or non-slip boundary conditions;
7. Simulation of the piping system rupture (water hammer effect) and Loss-of-Coolant Accident (LOCA) (i.e. shock waves in compressible fluid);
8. Simulation of the SCWL involving the Annular and Bundle test sections;
9. Simulation of the horizontal and downward flow directions in the test section with the corresponding modification of the SCWL preheating system;
10. Detailed study on the effects of the proposed power ramp up regimes on the stress levels generated in the SCWL components;
11. Studies directed on the validation of the equivalent thermal conduction coefficient in the fluid, which is intended to model the effect of radial heat flux facilitated by turbulence.
12. Accounting for the energy input into the water going through the pump (i.e. heating of the water in the pump due to the viscous dissipation).
13. Perform a power balance of the whole loop to make sure that there are no unintended heat sinks or sources that are introduced in the model

References

1. **Frank P. Incropera, David P. DeWitt** "Fundamentals of Heat and Mass Transfer", 2nd edition, School of Mechanical Engineering, John Wiley&Sons, 1985, pp. 202-204.;ISBN0471801267
2. **A. R. Shahani, S. M. Nabavi**, "Analytical solution of the quasi-static thermoelasticity problem in a pressurized thick-walled cylinder subjected to transient thermal loading". University of Technology, Tehran, Iran, 2006; http://cat.inist.fr/?aModele=afficheN&cpsidt=18772741; viewed online – December 2012;
3. **A, E. Segall**, "Transient analysis of thick-walled piping under polynominal thermal loading", Pennsylvania State University, 2003 http://www.ingentaconnect.com/content/els/00295493/2003/00000226/00000003/art00138; viewed online – December 2012;
4. **X. L. Gao**, "Elasto-plastic analysis of an internally pressurized thick-walled cylinder using a strain gradient plasticity theory", Michigan Technological University, 2003 http://www.ewp.rpi.edu/hartford/users/papers/engr/ernesto/poworp/Project/4.%20Supporting_Material/References/Gao.pdf; viewed online – December 2012;
5. **X. L. Gao**, "An Exact Elasto-Plastic Solution for an Open-Ended Thick-Walled Cylinder of a Strain-Hardening Material", Gansu University of Technology, 1992; *Int. J. Pres. Ves. Piping, 52*

6. **V. Radu, E. Paffumi, N. Taylor**, "New analytical stress formulae for arbitrary time dependent thermal loads in pipes", European Commission Joint Research Centre Institute for Energy, 2007 http://publications.jrc.ec.europa.eu/repository/bitstream/111111111/6273/1/eur%2022802%20en.pdf; viewed online – December 2012;

7. **Sanjeev Sharma, Manoj Sahni** and **Ravindra Kumar**, "Thermo Elastic-Plastic Transition of Transversely Isotropic Thick-Walled Rotating Cylinder under internal Pressure", JIIT Universuty, Noida, India, 2009 http://www.m-hikari.com/atam/atam2009/atam1-4-2009/sahniATAM1-4-2009.pdf; viewed online – December 2012;

8. **P. J. Schneider**, "Conduction Heat Transfer", 1957, pp. 240, 254-255; ISBN12016325607

9. **S. Suresh**, "Fatigue of materials", 2nd edition, Massachusetts Institute of Technology, Cambridge University Press, 1998, pp. 256-258, 260-265; ISBN0521570468

10. **Ian N. Sneddon**, "Use of Integral Transforms", 1972. 0070594368

11. **M. Necati Ozisik** "Boundary Value Problems of Heat Conduction", International Textbook Company, 1968, pp. 135-137; ISBN103438950133

12. **W. Kays, M. Crawford, B. Weigand.** Convective Heat and Mass Transfer 4th ed. New York : McGraw-Hill, 2005; ISBN9783642007187364200718X

13. **I. L. Pioro** and **R. B. Duffey**, "Literature Survey of Heat Transfer and Hydraulic Resistance of Water, Carbon Dioxide, Helium and Other Fluids at Supercritical and Near-Critical Pressures", AECL, 2003, pp.

http://www.iaea.org/inis/collection/nclcollectionstore/_public/35/087/35087435.pdf; viewed online – December 2012;

14. **I. L. Pioro, H. F. Khartabil, R. B. Duffey**, "Heat transfer to supercritical fluids flowing in channels – empirical correlations (survey)", AECL, 2003, pp. http://www.sciencedirect.com/science/article/pii/S0029549303003856; viewed online – December 2012;

15. **K. Yamagata, K. Nishikawa, S. Hasegawa**, and **S. Yoshida**, "Forced Convective Heat Transfer to Supercritical Water Flowing in Tubes", Kyushu University, Japan, 1971; INT J HEAT MASS TRANSFER , vol. 15, no. 12, pp. 2575-2593, 1972

16. **Alena R. Garsia**, "Carleton Supercritical Water Loop: Design-Driven Structural Analysis", Master's thesis. Carleton University, 2010.

21. **O.C. Zienkiewicz**, "The Finite Element Method", University of Wales, McGRAW-HILL Book Company (UC) Limited, 1977; ISBN0070840725

17. **S. Jahanian**, "Thermoelastoplastic Stree Analysis of Thick-Walled Tube of Nonlinear Strain Hardening", ASME, 1996; viewed online – December 2012; http://www.ewp.rpi.edu/hartford/users/papers/engr/ernesto/poworp/Project/4.%20Supporting_Material/References/Jahanian.pdf;

22. **Washington, University of.** UW Courses Web Server. *UW Courses Web Server.* [Online] 2010. courses.washington.edu/me354a/chap12.pdf

23. **Masih N. Balouch**, "Supercritical Water Loop Heat Exchanger Design Report", Carleton University, 2010

24. **Masih N. Balouch,** "Design of Test Sections for Use on the Carleton Supercritical Water and R-134a Loops", Carleton University, 2010

25. **Masih N. Balouch,** "Design of Test Loops for Forced Convection Heat Transfer Studies at Supercritical State". Master's thesis, Carleton University 2011
26. **Daniel McGuire**, Numerical Modeling of a Thermal-hydraulic Loop and Test Section Design for Heat Transfer Studies in Supercritical Fluids. Master's thesis, Carleton University 2011
27. **Anne Patricia Mason**, "Development and Thermohydraulic Modeling of a Supercritical Fluid Test Facility". Master's thesis, Carleton University 2011
28. Special Metals, Inc. Inconel Alloy 625. viewed Online; June 2012. http://www.specialmetals.com/documents/Inconel%20alloy%20625.pdf
29. Special Metals, Inc. Inconel Alloy 617. viewed Online; June 2012. http://www.specialmetals.com/documents/Inconel%20alloy%20617.pdf
30. **I. Pioro, S. Mokry**, "Heat Transfer to Fluids at Supercritical Pressures". University of Ontario Institute of Technology; http://cdn.intechopen.com/pdfs/13201/InTech-Heat_transfer_to_supercritical_fluids.pdf; viewed online – December 2012;
31. **Yanhua Yang, Xu Cheng, Shafang Huang**, "A new heat transfer correlation for supercritical fluids", 2009; viewed online – December 2012; http://link.springer.com/content/pdf/10.1007%2Fs11708-009-0022-0;

Appendix 1: VrSuite software verification

A1.1 Three classical problems for a semi-infinite solid with Dirichlet temperature, or convection, or constant flux BCs applied to the surface of the semi-infinite solid.

FEM solution

1. Mesh

The problems are approximated by 1.0 m x 0.1 m x 0.1 m rectangular domain that is discretized with uniform 8-node brick mesh. For comparison purposes two brick sizes 0.1 m x 0.1 m x 0.04 m – 25 elements and 0.1 m x 0.1 m x 0.01 m – 100 elements (Figure A1.1) were used

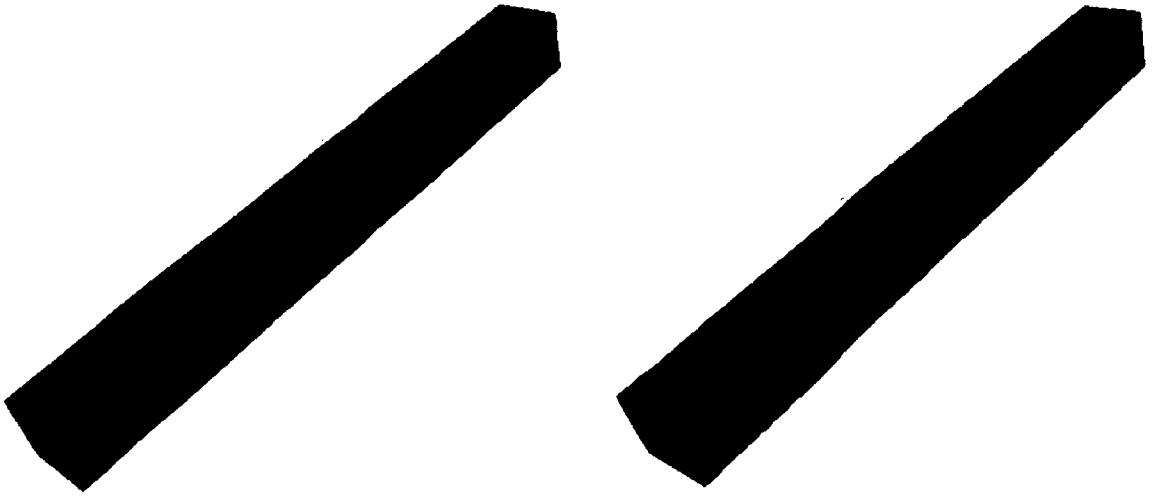

Figure A1.1 Mesh (from left to right) with 25 and 100 8-node elements

2. Governing equation

$$C_p \frac{DT}{Dt} - \nabla \cdot q + Q = 0; \;\; q = -k\nabla T$$

h is the enthalpy [J/m^3], t is the time [sec], q is the heat flux [W/m^2], Q is the heat generation [W/m^3], k is the thermal conductivity [W/(mK)], and T is the temperature [K].

3. Material properties

The properties of AISI316_at 573K, which are properties of AISI316L Steel at constant temperature T=573K (the average analyses temperature), from the VrSuite material library are used. The chosen properties are shown in Table A1.1.

Table A1.1: Mechanical and Thermal Properties of AISI316 at 573°K

Property	Thermal Conductivity	Specific Heat Capacity	Density
Dimension	W/(mK)	J/(kgK)	Kg/m^3
Value	18.19	535.6	7754.4

4. Initial Conditions

Initial temperature is 300K for all three problems.

5. Boundary conditions

The Dirichlet temperature/Convection/Constant Flux BCs boundary condition is applied to one end of the domain (Figure A1.2, Table A1.2). The rest of the surfaces are insulated in order to simulate 1D heat transfer, which takes place in case of the semi-infinite solid that extends to infinity in all but one direction and has only one identifiable surface.

Problem 1	**Problem 2**	**Problem3**
Constant Surface Temperature	**Constant Surface Heat Flux**	**Surface Convection**

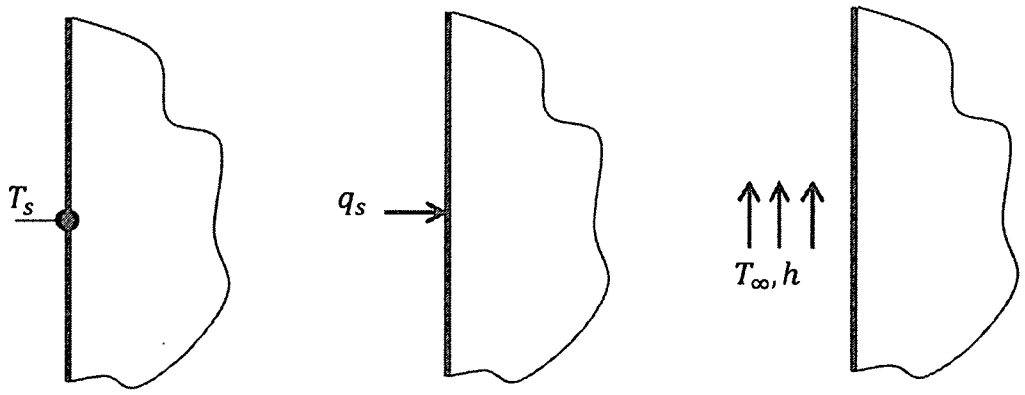

Figure A1.2 Boundary conditions (semi-infinite solid with Dirichlet temperature, or Convection, or Constant flux BCs)

Table A1.2: Boundary Conditions (semi-infinite solid with Dirichlet temperature, or Convection, or Constant flux BCs)

Test Problem	Boundary Conditions	
1	Dirichlet Temperature	700K
2	Constant Flux	120 kW/(m^2)
3	Convection	convection coefficient 1000 W/(m^{2}K) ambient temperature 700K

Time steps for the problems are chosen from the condition:

$$Fo = \frac{Dt}{l^2} \geq 1 \;\rightarrow\; \Delta t \geq \frac{l^2}{D}$$

Where Fo is the Fourier number, l is the characteristic length (mesh size in longitudinal direction), and D is the material thermal diffusivity. For the chosen material properties D=4.379e-6 [m^2/J].

For the chosen mesh sizes the corresponding time steps sizes are:

$$\Delta t_{coarse\ mesh} = 365.38\ sec; \qquad \Delta t_{fine\ mesh} = 22.84\ sec$$

The chosen time steps are $\Delta t_{coarse\ mesh} = 400.0\ sec\ \ and\ \ \Delta t_{fine\ mesh} = 25.0\ sec$

Analytic solutions

Problem 1 – Constant surface temperature

$$\frac{T(x,t)-T_S}{T_i-T_S}=erf\left(\frac{x}{2\sqrt{Dt}}\right)$$

$T(x,t)$ [K] is the transient temperature at distance x [m] from the surface towards the material of the semi-infinite solid, at time t [sec]; T_S [K] the constant temperature at the surface of the solid; T_i [K] is the initial body temperature; D [m^2/J] is the thermal diffusivity.

Problem 2 – Constant surface heat flux

$$T(x,t)-T_i=\frac{2q_S(Dt/\pi)^{1/2}}{k}exp\left(\frac{-x^2}{4Dt}\right)-\frac{q_S x}{k}erfc\left(\frac{x}{2\sqrt{Dt}}\right)$$

$T(x,t)$ [K] is the transient temperature at distance x [m] from the surface towards the material of the semi-infinite solid, at time t [sec]; T_i [K] is the initial body temperature; q_S [J/(m^2)] is the constant surface flux; D [m^2/J] is the thermal diffusivity, k [W/(mK)] is the thermal conductivity.

Problem 3 – Surface convection

$$\frac{T(x,t)-T_i}{T_\infty-T_i}=erfc\left(\frac{x}{2\sqrt{Dt}}\right)-\left[exp\left(\frac{hx}{k}+\frac{h^2Dt}{k^2}\right)\right]\left[erfc\left(\frac{x}{2\sqrt{Dt}}+\frac{h\sqrt{Dt}}{k}\right)\right]$$

$T(x,t)$ [K] is the transient temperature at distance x from the surface towards the material of the semi-infinite solid, at time t; T_i [K] is the initial body temperature; T_∞ [K] ambient temperature; D [m^2/J] is the thermal diffusivity, k [W/(mK)] is the thermal conductivity; h [W/((m^2)K)] is the convection coefficient.

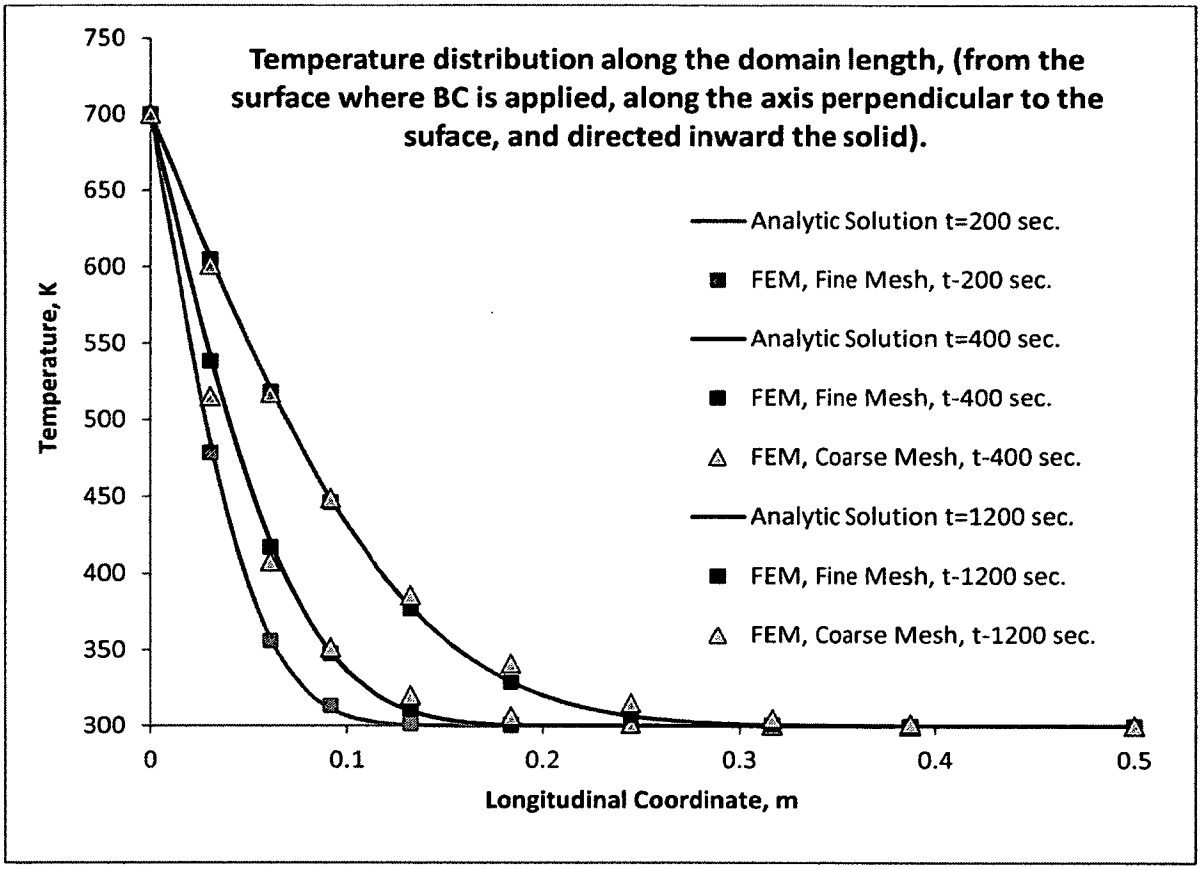

Figure A1.3 Dirichlet Temperature BC; Comparison of analytic and numerical solutions

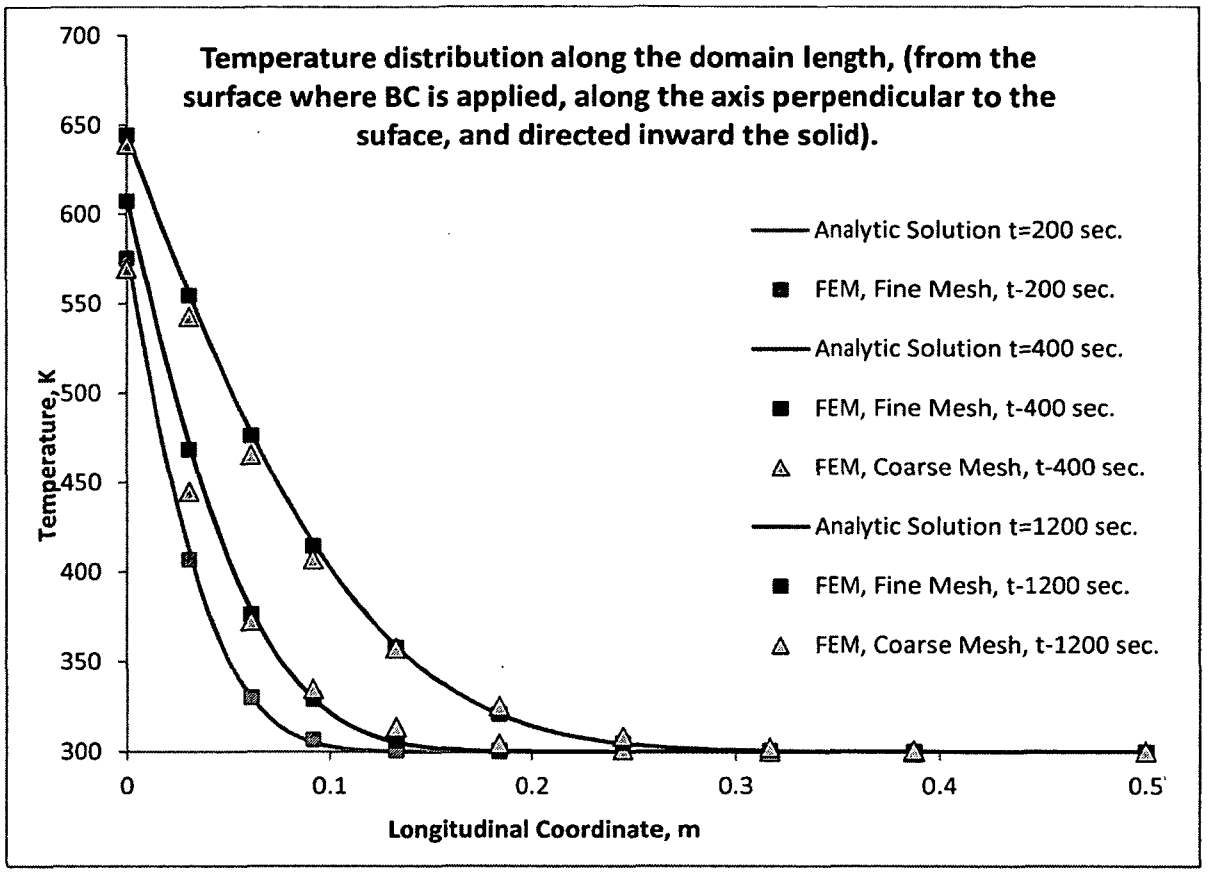

Figure A1.4 Convection BC; Comparison of analytic and numerical solutions

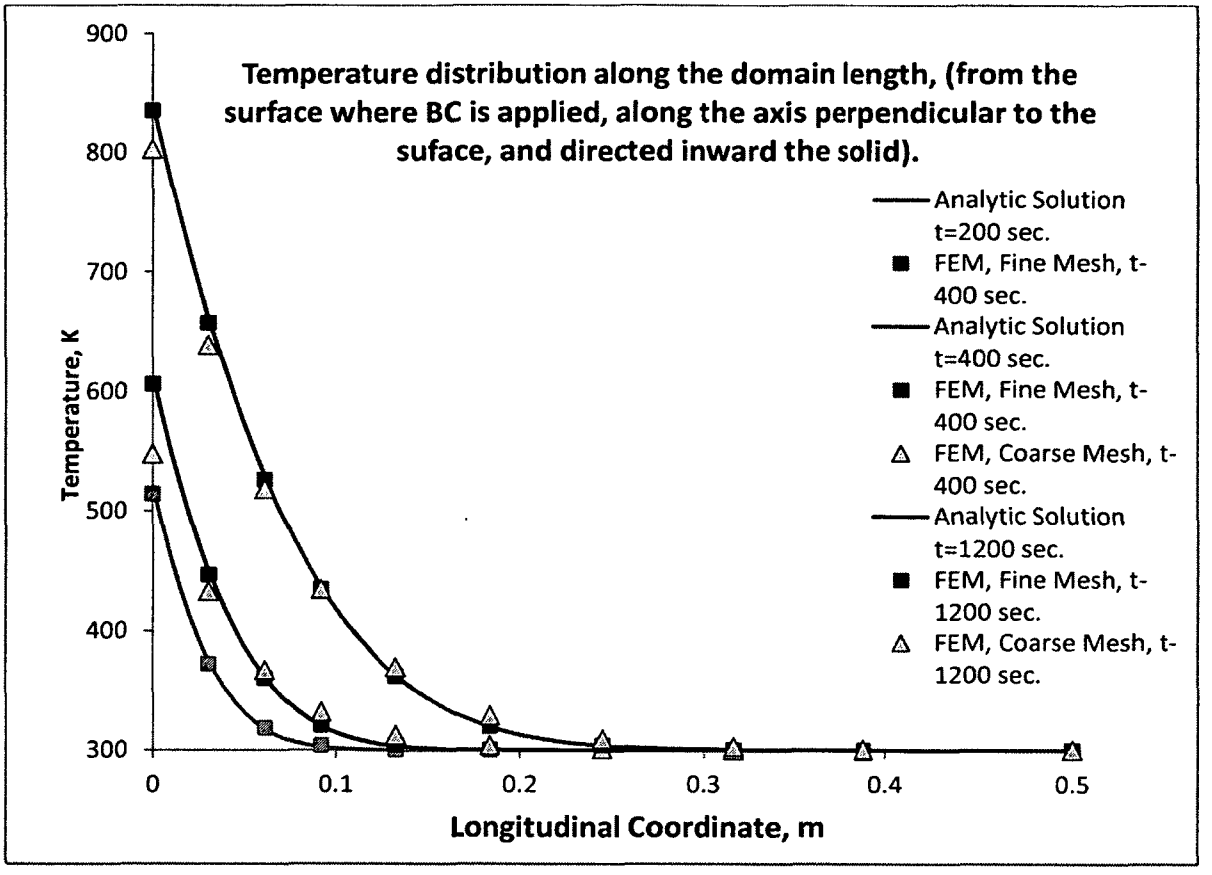

Figure A1.5 Constant Flux BC; Comparison of analytic and numerical solutions

A1.2 One-dimensional transient temperature distribution in an infinite cylinder with the uniform initial temperature and convective boundary condition.

FEM solutions

1. Mesh

Cylindrical domain $\emptyset 0.1m \times 0.01m$ discretized with 8-node brick mesh. For comparison purposes two mesh sizes (later referred as "fine mesh" and "coarse mesh"), were used, Table A1.3, Figure A1.6.

Table A1.3: Mesh properties (One-dimensional transient temperature distribution in an infinite cylinder)

Mesh	Number of elements in radial direction	Number of elements in circumferential direction	Number of elements in axial direction
Coarse mesh	20	70	4
Fine mesh	5	16	1

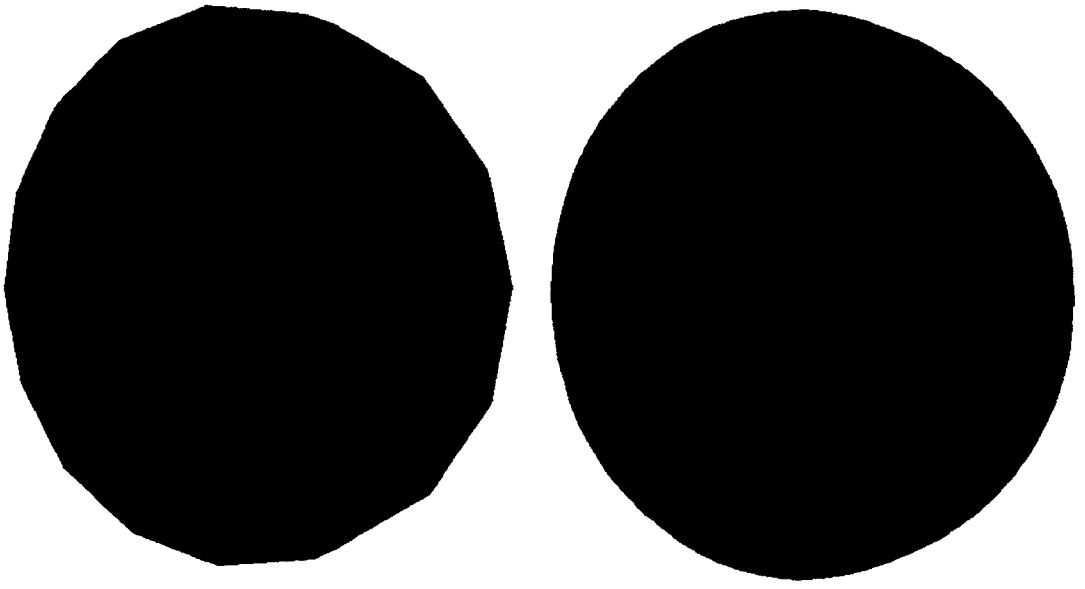

Figure A1.6 Used meshes (from left to right): Coarse mesh and Fine mesh

2. Governing equation

$$C_p \frac{DT}{Dt} - \nabla \cdot q + Q = 0; \;\; q = -k\nabla T$$

h is the enthalpy [J/m^3], t is the time [sec], q is the heat flux [W/m^2], Q is the heat generation [W/m^3], k is the thermal conductivity [W/(m*K)], and T is the temperature [K].

3. Material properties

The properties of BABAndersson Steel_at473K (473K is the average analysis temperature) from the VrSuite material library are used. The chosen properties are shown in Table A1.4.

Table A1.4: Mechanical and Thermal Properties of BABAndersson Steel_at 473K

Property	Thermal Conductivity	Specific Heat Capacity	Density
Dimension	W/(mK)	J/(kgK)	Kg/m^3
Value	40	484.7	7820

4. Initial Conditions

Initial temperature is 300K.

5. Boundary conditions

Convection BCs are applied to the outside radiuses of the domains. The convection coefficient h=1000 W/((m^2)K) and ambient temperature T=700K. The rest of the surfaces are insulated in order to simulate 1D heat transfer, which takes place in case of infinite cylinder.

Time steps for the problems with fine and coarse meshes are chosen to satisfy the condition:

$$Fo = \frac{Dt}{l^2} \geq 1 \;\rightarrow\; \Delta t \geq \frac{l^2}{D}$$

Where Fo is the Fourier number, l is the characteristic length (mesh size in radial direction), and D is the thermal diffusivity. For the chosen material properties D=10.533e-6 [m^2/J].

For the chosen mesh sizes the corresponding time steps sizes are:

$$\Delta t_{coarse\ mesh} = 9.476\ sec,\ \Delta t_{fine\ mesh} = 0.592\ sec$$

The chosen time steps are $\Delta t_{coarse\,mesh} = 10.0\,sec,\ \ \Delta t_{fine\,mesh} = 1.0\,sec$

Analytic solution

The exact solutions for the temperature distribution in an infinite cylinder with convection boundary condition in dimensionless form is

$$\theta^* = \sum_{n=1}^{\infty} C_n \exp(-\varphi_n^2 F_0) J_0(\varphi_n r^*)$$

Where, dimensionless temperature θ^* is

$$\theta^* = \frac{T - T_\infty}{T_i - T_\infty}$$

T is the time and coordinate dependent temperature of the cylinder, T_i is the initial domain temperature, and T_∞ is the ambient temperature.

$$C_n = \frac{2}{\varphi_n} \frac{J_1(\varphi_n)}{J_0^2(\varphi_n) + J_1^2(\varphi_n)}$$

The discrete values of φ_n are positive roots of the transcendental equation

$$\varphi_n \frac{J_1(\varphi_n)}{J_0(\varphi_n)} = \frac{1}{Bi}$$

The quantities J_0 and J_1 are Bessel functions of the first kind and zero and first order and r^* is the dimensionless radius.

The analytic solution is obtained using first 10 roots of the transcendental equation.

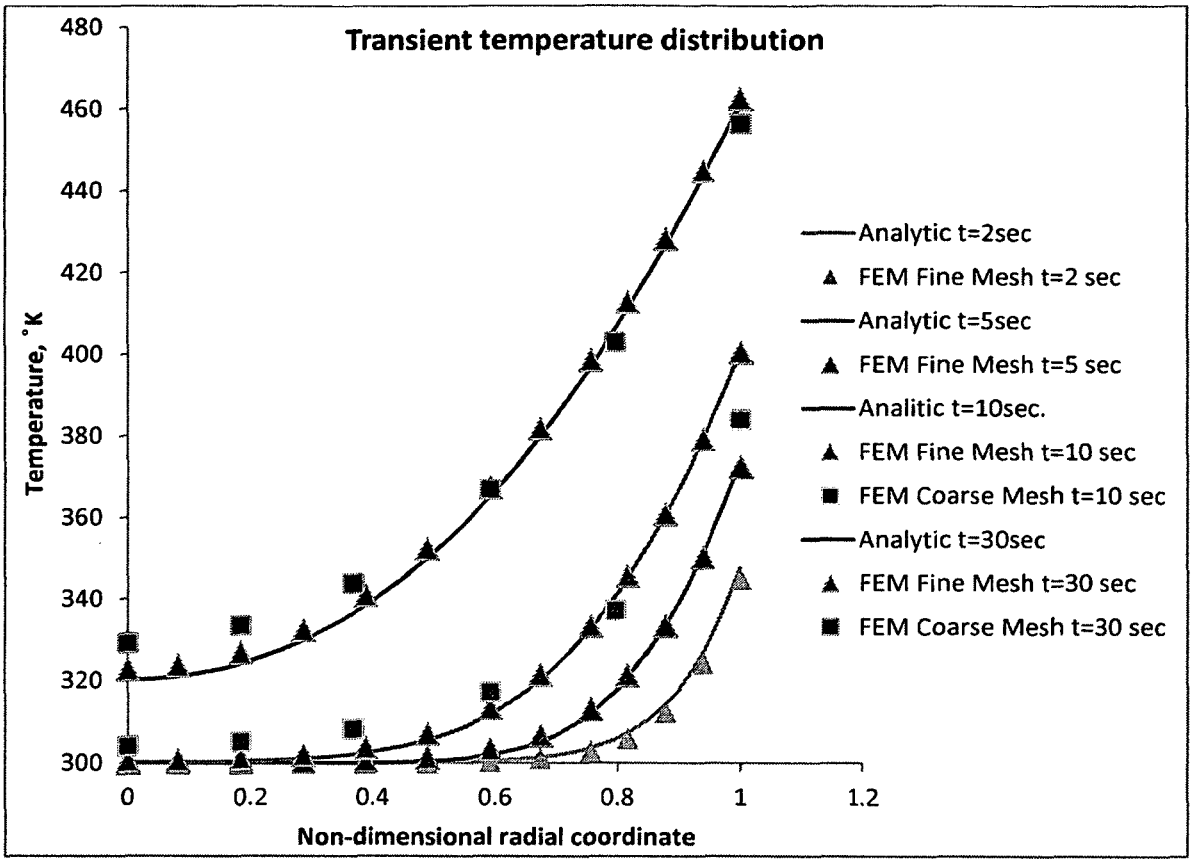

Figure A1.7 Comparison of analytic and numerical solutions

A1.3 One-dimensional transient temperature distribution in a solid sphere with the uniform initial temperature and Dirichlet thermal boundary condition at the sphere surface.

FEM solutions

1. Mesh

The solid spherical domains with the radius $R0.025\ m$ discretized with 8-node brick mesh. For comparison purposes, two mesh sizes (later referred as "fine mesh" and "coarse mesh") were used, Table 1.5, Figure 1.8, and Figure 1.9.

Table A1.5: Mesh properties (One-dimensional transient temperature distribution in a solid sphere)

Mesh	Number of elements in radial direction	Size of elements in radial direction
Coarse mesh	7	0.0036 [m]
Fine mesh	29	0.00086 [m]

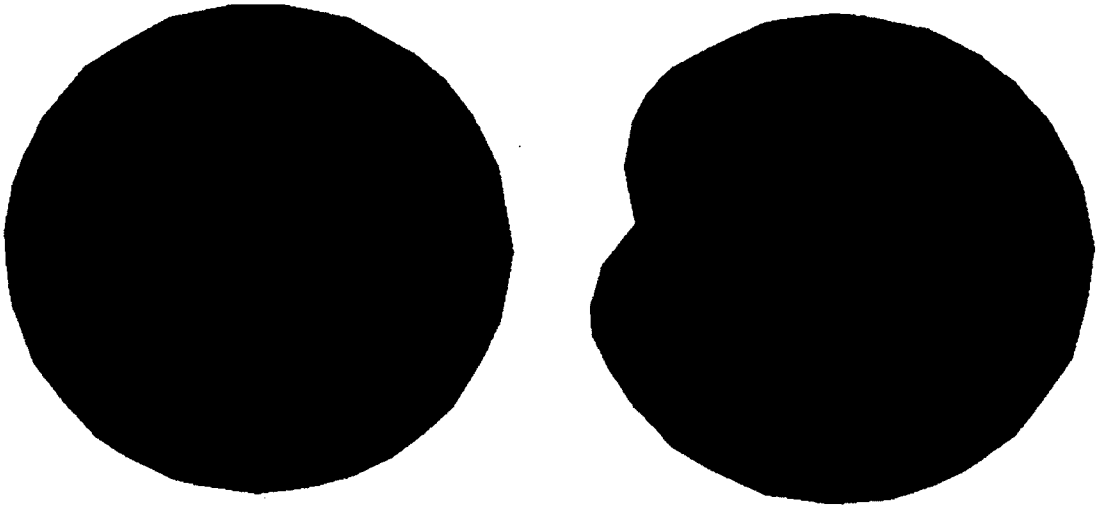

Figure A1.8 Coarse mesh (One-dimensional transient temperature distribution in a solid sphere)

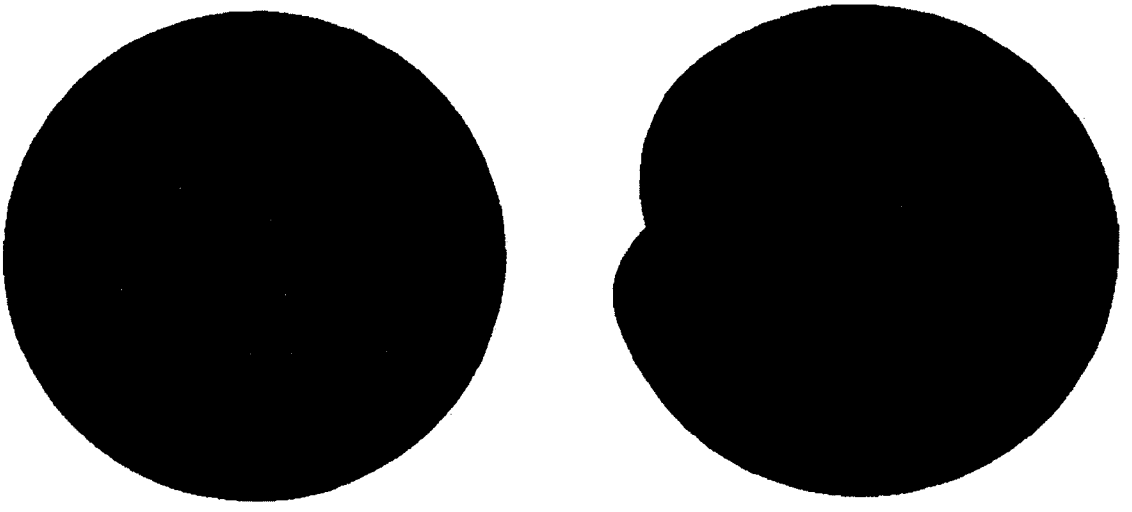

Figure A1.9 Fine mesh (One-dimensional transient temperature distribution in a solid sphere)

2. Governing equation

$$C_p \frac{DT}{Dt} - \nabla \cdot q + Q = 0; \;\; q = -k\nabla T$$

h is the enthalpy [J/m^3], t is the time [sec], q is the heat flux [W/m^2], Q is the heat generation [W/m^3], k is the thermal conductivity [W/(m*K)], and T is the temperature [K].

3. Material properties

The properties of BABAndersson Steel_at473K (473K is the average analyses temperature) from the VrSuite material library are used. The chosen properties are shown in Table A1.6.

Table A1.6 Mechanical and Thermal Properties of BABAndersson Steel_at473K

Property	Thermal Conductivity	Specific Heat Capacity	Density
Dimension	W/(mK)	J/(kgK)	Kg/m^3
Value	40	484.7	7865.47

4. Initial Conditions

Initial temperature is 300K.

5. Boundary conditions

Dirichlet temperature T=700K is applied to the surfaces of the domains.

Time steps for the problems with fine and coarse meshes are chosen to satisfy the condition:

$$Fo = \frac{Dt}{l^2} \geq 1 \quad \rightarrow \quad \Delta t \geq \frac{l^2}{D}$$

Where Fo is the Fourier number, l is the characteristic length (mesh size in radial direction), and D is the thermal diffusivity. For the chosen material properties D=10.533e-6 [m^2/J].

For the chosen mesh sizes the corresponding time steps sizes are:

$$\Delta t_{coarse\ mesh} = 1.21\ sec,\ \Delta t_{fine\ mesh} = 0.07\ sec$$

The chosen time steps are $\Delta t_{coarse\ mesh} = 2{,}5\ sec,\ \Delta t_{fine\ mesh} = 0.2\ sec$

Analytic solution

The exact solutions for the temperature distribution in a solid sphere with the Dirichlet temperature boundary condition in dimensionless form is

$$\frac{T - T_{out}}{T_i - T_{out}} = \frac{2r_{out}}{\pi r} \sum_{n=1}^{\infty} \frac{(-1)^{n+1}}{n} \exp(-(\pi n)^2 F_0) \sin(\pi n \frac{r}{r_{out}})$$

Where, T is the time and coordinate dependent temperature of the domain, T_i is the initial domain temperature, r_{out} is the outside radius and T_{out} is the Dirichlet temperature at the domain surface.

First 10 terms of the given solution are used for the analytic solution.

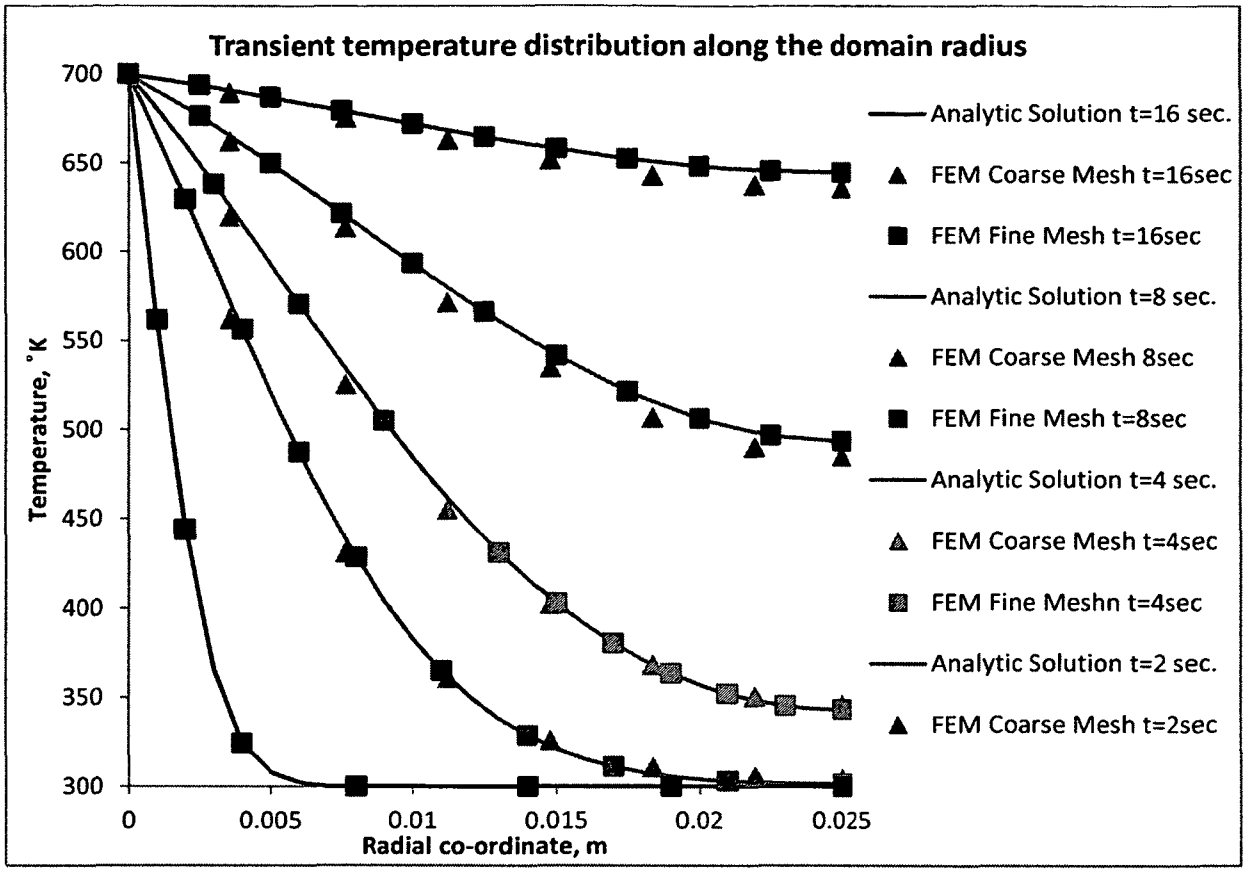

Figure A1.10 Comparison of analytic and numerical solutions

A1.4 Stress in an internally pressurized thick-walled cylinder made of elastic-strain-hardening plastic material [5].

FEM solutions

1. Mesh

The domain of the problem is a hollow cylinder with outside and inside diameters equal to the typical outside and inside diameters a=0.02794 m and b=0.04826 m of the SCWL piping system. The domain length is l=0.0025 m. The domain is discretized with 8-node brick mesh with eight elements in radial, two elements in axial, and 75 elements in circumferential directions, FigureA1.11.

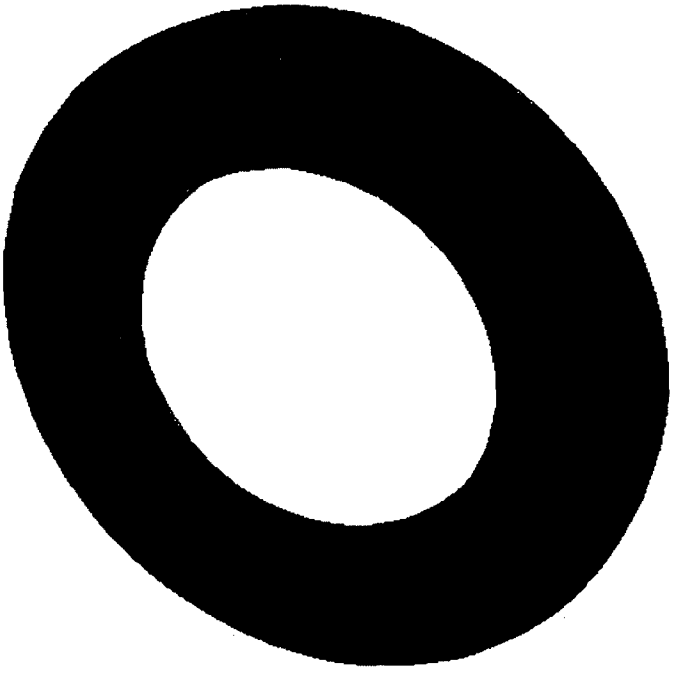

Figure A1.11 Mesh (Stress in an internally pressurized thick-walled cylinder)

2. Governing equation

$$\nabla \cdot \sigma + b = 0, \qquad \sigma = E\varepsilon, \qquad \varepsilon = (\nabla u + (\nabla u)^T + (\nabla u)^T \nabla u)/2$$

The first equation above is the conservation of momentum equation where inertial term "$\rho(\frac{\partial V}{\partial t} + V \cdot \nabla V)$", with the density field ρ and the velocity field V, is ignored. In the governing equations above, σ is the Cauchy stress tensor, E is the 6x6 elasticity tensor, ε is the Green-Lagrange strain tensor, and b is the body force.

3. Material properties

The properties of BABAndersson Steel from the VrSuite material library are used. The chosen properties are shown in Table A1.7.

Table A1.7: Mechanical and Thermal Properties of BABAndersson Steel_at473K

Property	Poisson ratio	Young's modulus	Density	Yield stress
Dimension		GPa	Kg/m^3	MPa
Value	0.3	210,000	7865.47	340

4. Initial Conditions

Initial temperature of the domain is 300K.

5. Boundary conditions

Neumann pressure boundary condition P=140 MPa is applied to the inside diameter of the domain. All rigid body modes are restrained.

Analytic solution

The chosen analytic solution splits the solution into solutions for elastic and plastic regions. The radius of elasto-plastic interface is r_c.

Solution in the elastic region

$$\sigma_{rr} = \frac{p_c r_c^2}{b^2 - r_c^2}\left(1 - \frac{b^2}{r^2}\right);\ \sigma_{\theta\theta} = \frac{p_c r_c^2}{b^2 - r_c^2}\left(1 - \frac{b^2}{r^2}\right);\ \sigma_{zz} = 2\nu\frac{p_c r_c^2}{b^2 - r_c^2};$$

where σ_{rr}, $\sigma_{\theta\theta}$, and σ_{zz} are radial, hoop, and axial stress components; p_c, r_c, ν, b, a, and r are the pressure at the elasto-plastic interface, radius of elasto-plastic interface, Poisson's ratio, domain outside and inside radiuses, and current radius.

Solution in the plastic region

The power-law hardening model in the classical plasticity theory has the form:

$$\sigma_{effective} = k\varepsilon_{effective}^{m}$$

Since the coefficients k and m from the hardening model are used in the solution for the plastic region, several virtual tensile tests for the chosen material were performed to obtain the values of the effective plastic strains and the corresponding effective plastic stresses for the expected range of effective plastic strains. The corresponding constants are m=0.0001924 and k=3.3549E+08.

The stress component in the plastic region is:

$$\sigma_{rr} = -\frac{\sigma_y}{\sqrt{3}}\left(1 - \frac{r_c^2}{b^2}\right) + \frac{2}{\sqrt{3}}\left[\frac{k}{2m}\left(\frac{\sigma_y}{E}\right)^m\left(1 - \frac{r_c^{2m}}{r^{2m}}\right) - \frac{\sigma_y c}{E}\frac{r_c^2}{a^4}\left(\frac{a^4}{r_c^4} - \frac{a^4}{r^4}\right)\right]$$

$$\sigma_{\theta\theta} = -\frac{\sigma_y}{\sqrt{3}}\left(1-\frac{r_c^2}{b^2}\right)+\frac{2}{\sqrt{3}}\left[\frac{k}{2m}\left(\frac{\sigma_y}{E}\right)^m\left(1+(2m-1)\frac{r_c^{2m}}{r^{2m}}\right)-\frac{\sigma_y c}{E}\frac{r_c^2}{a^4}\left(\frac{a^4}{r_c^4}-\frac{3a^4}{r^4}\right)\right]$$

$$\sigma_{rr} = 0.5(\sigma_{rr}+\sigma_{\theta\theta})$$

where the value of r_c can be found, using iterative procedure, from the following expression

$$P_i = -\frac{\sigma_y}{\sqrt{3}}\left(1-\frac{r_c^2}{b^2}\right)+\frac{2}{\sqrt{3}}\left[\frac{k}{2m}\left(\frac{\sigma_y}{E}\right)^m\left(\frac{r_c^{2m}}{r^{2m}}-1\right)-\frac{\sigma_y c}{E}\frac{r_c^2}{a^4}\left(1-\frac{a^4}{r_c^4}\right)\right]$$

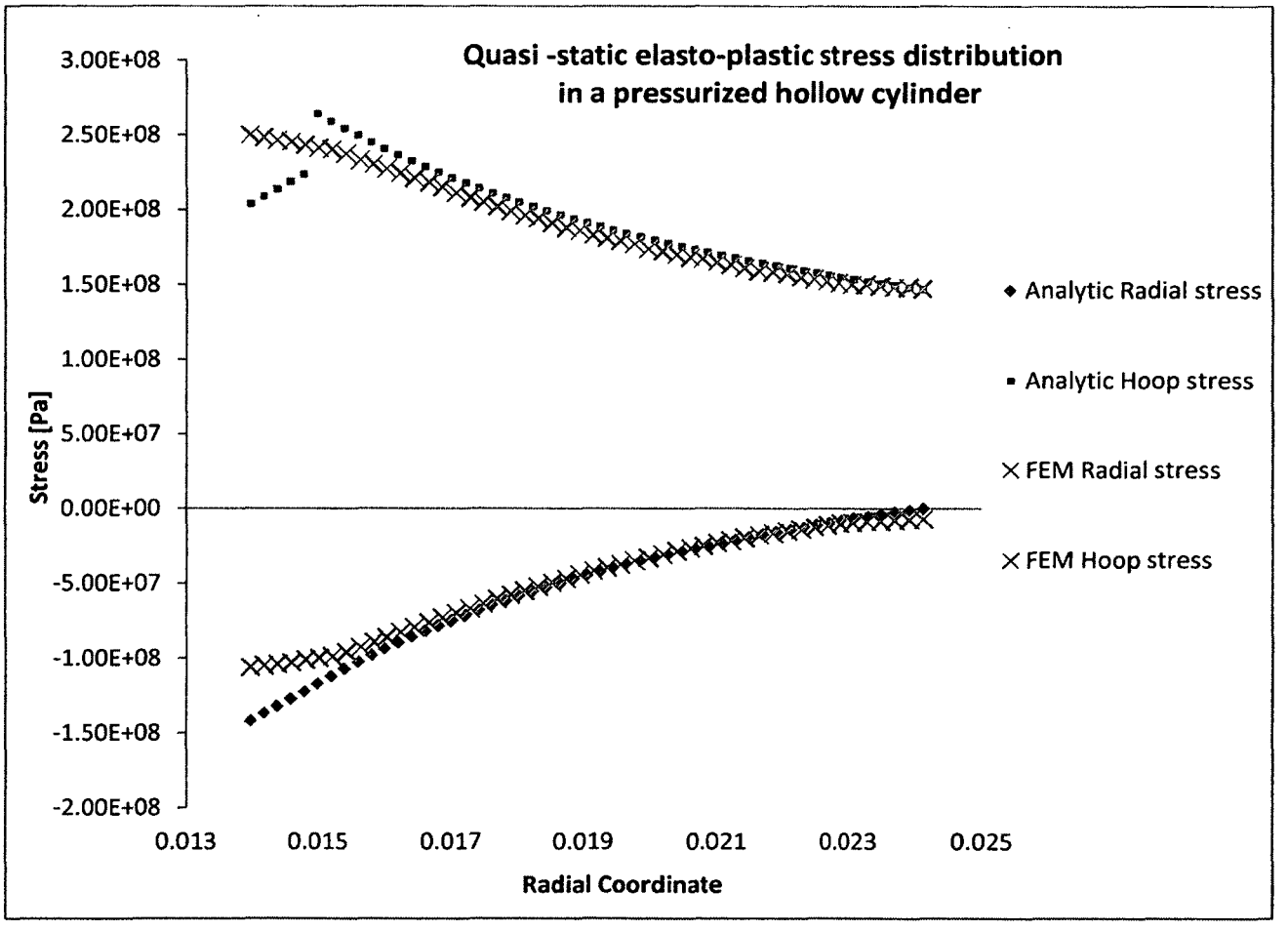

Figure A1.12 Comparison of analytic and numerical solutions (Stress in an internally pressurized thick-walled cylinder)

A1.5 Discussion

It is seen that in most cases the VrSuite solutions provide reasonable prediction of the exact solutions for the considered problems, converging to exact solutions with the mesh refinement.

The possible explanation for the deviations seen in the problems for semi-infinite solid (A1.1) can be the backward difference computational scheme used for the analysis. Although the scheme does not provide the greatest accuracy [21], it is often preferred for practical applications due to its numerical stability.

Even though in the last test problem (A1.4) the FEM solution corresponds to the chosen analytic solution in the elastic zone very well and it generally follows the trend of the analytic solution for the plastic region, there are obvious deviations of numerically obtained nodal stress components in the plastic zone from the proposed analytic solution. One of the possible explanations is that the author of the analytic solution allowed "sliding" at the elasto-plastic interface. The FEM problem reformulated to two "sliding" (i.e. no shear stress allowed in any direction tangent to the interface) coaxial cylinders, corresponding to the plastic and elastic zones, demonstrated a trend similar to the considered analytic solution. The "Contact element" VrSuite feature was used to model the desired interface properties. However, time limitations did not allow the author to refine the considered FE problem in order to closely match its analytic counterpart.

Appendix 2: List of coded convection coefficient correlations for water flowing upward inside circular tubes [14, 15, 16, 32, and 34]:

- The Dittus-Boelter correlation (hot wall/cold fluid case)

$$Nu = 0.023 Re_b^{0.8} Pr_b^{0.4}$$

This is the most commonly used correlation for predicting fully developed turbulent flow heat transfer coefficients inside smooth round tubes. It usually claimed that the correlation predicts the experimental data within ±25% for a flow in circular pipes with $0.7 < Pr < 120$ and $10{,}000 < Re_D < 120{,}000$, where the Reynolds number is based on the pipe diameter. This correlation is usually referred as a single-phase correlation and should be used with caution when a phase change takes place.

- The correlation of Bringer and Smith (1957):

$$Nu_x = 0.0266 Re_x^{0.77} Pr_w^{0.55}$$

Where Nu_x and Re_x are evaluated at t_x. The t_x is defined as t_b if $\frac{t_{pc}-t_b}{t_w-t_b} < 0$

as t_{pc} if $\frac{t_{pc}-t_b}{t_w-t_b} = 0 \ldots 1.0$, and as t_w if $\frac{t_{pc}-t_b}{t_w-t_b} > 1.0$.

This correlation does not take into account the peak in thermal conductivity near the pseudo-critical temperature.

- Bishop's correlation (1964):

$$Nu_x = 0.0069 Re_x^{0.9} \overline{Pr}_x^{0.66} \left(\frac{\rho_w}{\rho_b}\right)_x^{0.43} \left(1 + 2.4\frac{D}{x}\right)$$

The correlation was derived from the experimental data within the following range of flow and operating parameters: pressure 22.8...27.6 MPa, bulk

temperature 282...527C, mass flux 651...3662 kg/(s*m^2), and heat flux 0.31...3.46 MW/m^2. The term (1+2.4 *D/x*) accounts for the entrance-region effect. The x in this correlation is the axial location along a tube axis. The data was generalized using the given correlation with a fit of ±15%.

- Swenson's correlation (1965):

$$\frac{hD}{k_w} = 0.00459\left(\frac{DG}{\mu_w}\right)^{0.923}\left(\frac{H_w - H_b}{T_w - T_b}\frac{\mu_w}{k_w}\right)^{0.613}\left(\frac{\rho_w}{\rho_b}\right)^{0.213}$$

The majority of thermophysical properties in the Swenson's correlation are based on the wall temperature rather than on the bulk-fluid temperature. This correlation was obtained for the following range of operating parameters: pressure 22.8...41.4 MPa, bulk temperature 75...576C, mass flux 542...2150 kg/(s*m^2), t_w=93..649C, and t_b=75....576C. According to the obtained experimental data, the thermodynamic properties of fluid were strongly affected by a corresponding heat flux in the near-critical region. The heat transfer coefficient had a sharp peak at low heat fluxes and decreased together with the heat flux increase. The correlation predicts the experimental data within ±15%.

- Krasnoshchekov's correlation (1967):

$$Nu = Nu_0\left(\frac{\rho_w}{\rho_b}\right)^m\left(\frac{\bar{c}_p}{c_{pb}}\right)^n$$

where

$$Nu_0 = \frac{\left(\frac{\xi}{8}\right)Re_b\overline{Pr}}{12.7\sqrt{\frac{\xi}{8}}\left(\overline{Pr}^{2/3} - 1\right) + 1.07}$$

and

$$\xi = \frac{1}{(1.82lg(Re_b) - 1.64)^2}$$

Exponent $m = 0.3$ at $1.02 \leq p/p_{cr} \leq 1.45$. Exponent n can be found graphically (34).

- Jackson's correlation (1975):

$$Nu = 0.0183 Re_b^{0.82} \overline{Pr}^{0.5} \left(\frac{\rho_w}{\rho_b}\right)^n$$

The correlation is a modification of the original correlation of Krasnoshchekov and Protopopov (1959, 1960) to transform it to the Dittus-Boelter-type form. In the correlation the exponent $n = 0.4$ for $T_b < T_w < T_{pc}$ and for $1.2T_{pc} < T_b < T_w$; $n = 0.4 + 0.2\left(\frac{T_w}{T_{pc}} - 1\right)$ for $T_b < T_{pc} < T_w$; and $n = 0.4 + 0.2\left(\frac{T_w}{T_{pc}} - 1\right)\left[1 - 5\left(\frac{T_b}{T_{pc}} - 1\right)\right]$ for $T_{pc} < T_b < 1.2T_{pc}$ and $T_b < T_w$.

- Mokry's correlation (2009):

$$Nu_b = 0.0061 Re_b^{0.904} \overline{Pr}_b^{0.684} \left(\frac{\rho_w}{\rho_b}\right)^{0.564}$$

Appendix 3: Accounting for the effects of turbulence in the SCWL fluid domain (test problems)

In order to determine the appropriate scaling coefficient for the fluid thermal conductivity, which can model the heat transfer rate in a corresponding turbulent flow, the comparative analysis of test problems computed in ANSYS CFX and VrSuite was done.

Since the test section is the most critical part of the SCWL in terms of the temperature magnitude and thermal stresses, it was decided to do the test problems for the fluid domain with the size identical to the size of the tubular test sections interior, which is supposed to be filled with the water (i.e. cylindrical fluid domain with d=12.5 mm, L=2048 mm). It also should be noticed that the mesh for the "Test problem 1" was done using extrusion of a 2D mesh. The 2D region was meshed to have the topology that is possibly close to the topology of the mesh used in the "Test problem 2" presented in this appendix.

A3.1 Test problem 1

Problem statement

The domain is descritized with 12540 8-node hexahedron elements, Figure A3.1. Three test problems were set with the parameters shown in Table 3.1.

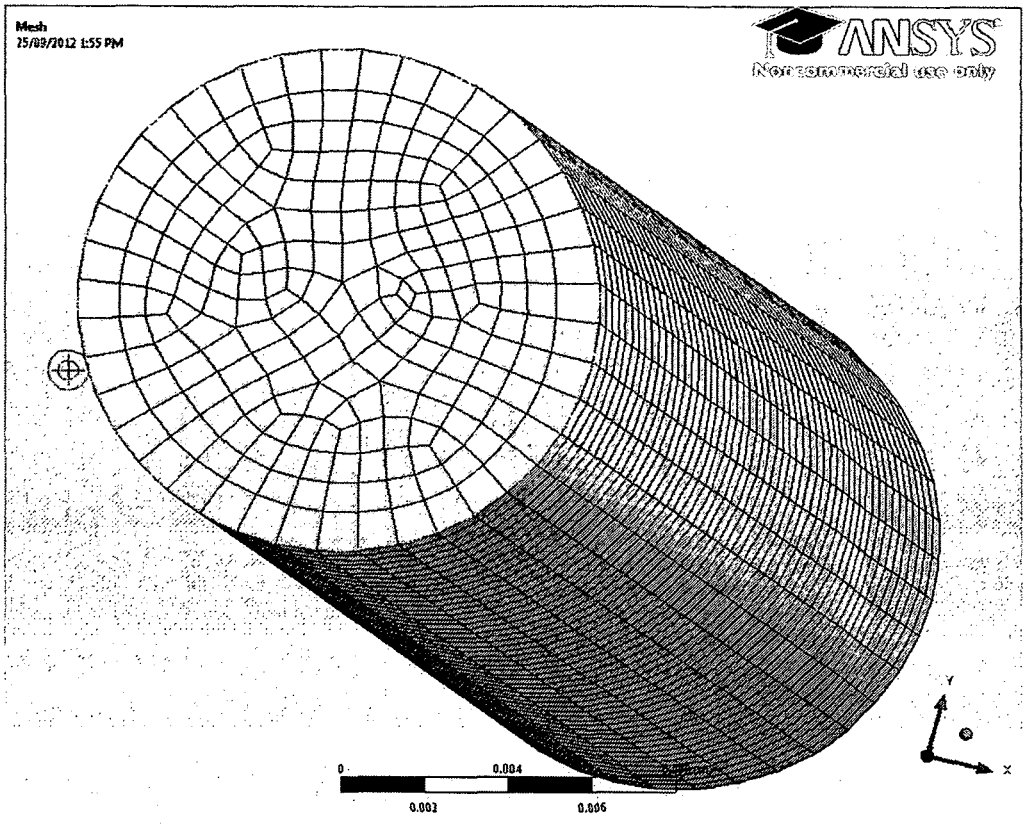

Figure A3.1 Domain; Ansys CFX (thermal conductivity multiplier test problem)

Table A3.1: Parameters used in the analysis (thermal conductivity multiplier test problem; test problem 1)

Test problem	1	2	3
Type	Transient		
Turbulence model	Laminar flow	SST	K-Epsilon
Problem type	Single phase		
Material	Water		
Heat transfer	Total Energy		
Total time/time step size, sec	42/0.05		

Initial domain temperature, K		300	
Inlet BC	Flow regime	Subsonic	
	Inlet normal speed, m/sec	0.05	
	Turbulence/medium intensity,	n/a	5%
	Heat transfer; static temperature, K	300	
Outlet BC	Flow regime	Subsonic	
	Mass and momentum/average static pressure	25 MPa	
	Pres. Profile blend	0.05	
	Pressure averaging	Average over whole outlet	
Wall BC	mass and momentum	Free slip wall	
	Heat transfer: Heat transfer coefficient, W/(Km^2)	1000	
	Heat transfer: Ambient temperature, K	400	
Solver Control	Advection scheme	high resolution	
	Time step initialization	automatic	
	Turbulence numeric	first order	
	Convergence control: MinCoeffLoops/MaxCoeffLoops	1/20	
	Residual type	RMS	
	Residual target	1e-4	

Results

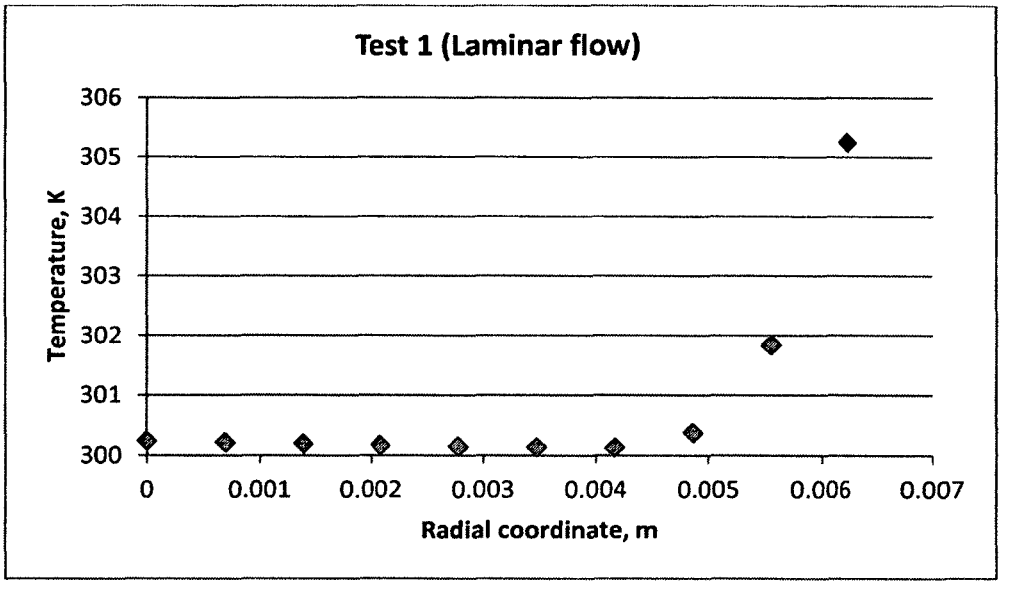

Figure A3.2 Temperature distribution across radius (Laminar flow)

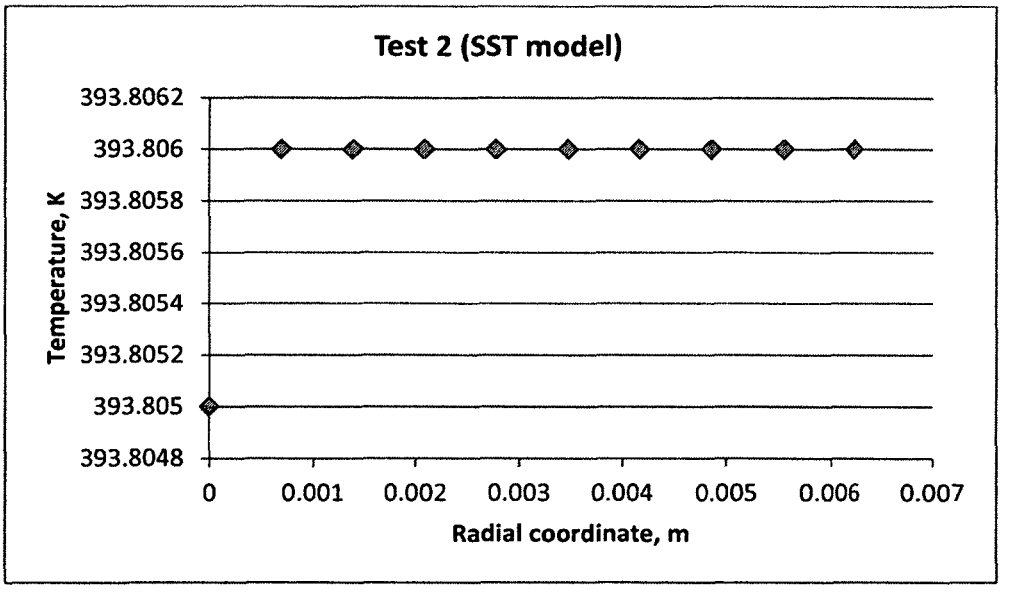

Figure A3.3 Temperature distribution across radius (SST turbulence model)

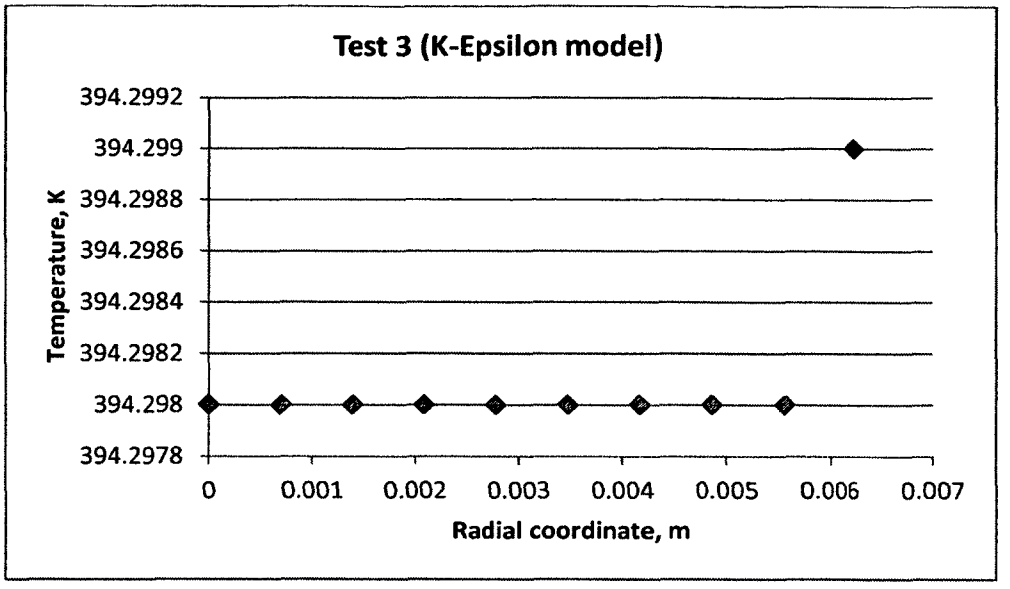

Figure A3.4 Temperature distribution across radius (K-Epsilon turbulence model)

As can be seen from the temperature distributions across the domain radius computed for different turbulence models (Figs. A3.2...A3.4), the temperature differences between the axial and outside locations in the domain are about 5, 0.001, and 0.001 degrees. In other words, in order to model the radial heat flux in a turbulent flow using increased thermal conductivity, the modified thermal conductivity should decrease the radial temperature difference by the factor "500".

Using the VrSuite software for the problem with similar test setup (i.e. identical BCs, fluid domain size, and similar mesh topology shown in Figure A3.5), it was found that if thermal conductivity is increased by factor "1000", the radial temperature difference is decreased by factor "500" (approx.).

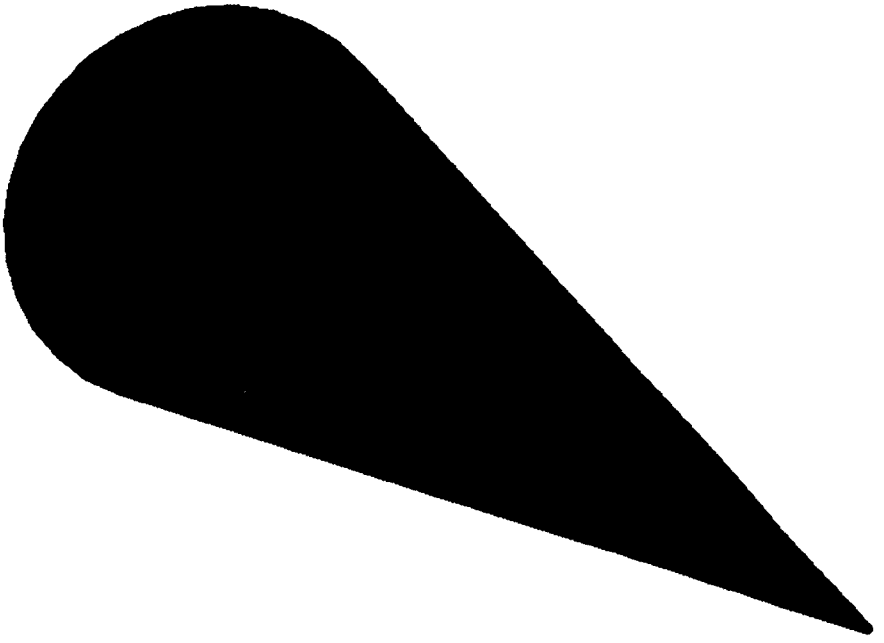

Figure A3.5 Domain; VrSuite (thermal conductivity multiplier test problem)

A3.2 Test problem 2

In order to make sure that the increase in thermal conductivity, using scaling factor defined in the previous test problem, is not going to cause the inacceptable increase of axial diffusion leading to an incorrect temperature field in the fluid domain, the additional tests were done using the VrSuite software.

Problem statement

The test problem is represented by a cylindrical fluid domain (d=12.5 mm, L=2048 mm), descritized with 8160 8-node hexahedron elements (Figure A3.5), with initial temperature T=300K, inlet Dirichlet temperature 300K, and convection boundary conditions applied to the outside radius with ambient temperature

T=400K and convection coefficient h=1000 W/(m^{2}K). Uniform inlet velocity V=0.05 m/sec with slip wall BC are used.

The water material properties (NIST web site) were modified for the 1st and 2nd tests as follows:

- 1st test: the isotropic coefficient of thermal conductivity was multiplied by one thousand
- 2nd test: only radial components of the coefficient of thermal conductivity were multiplied by one thousand

Results

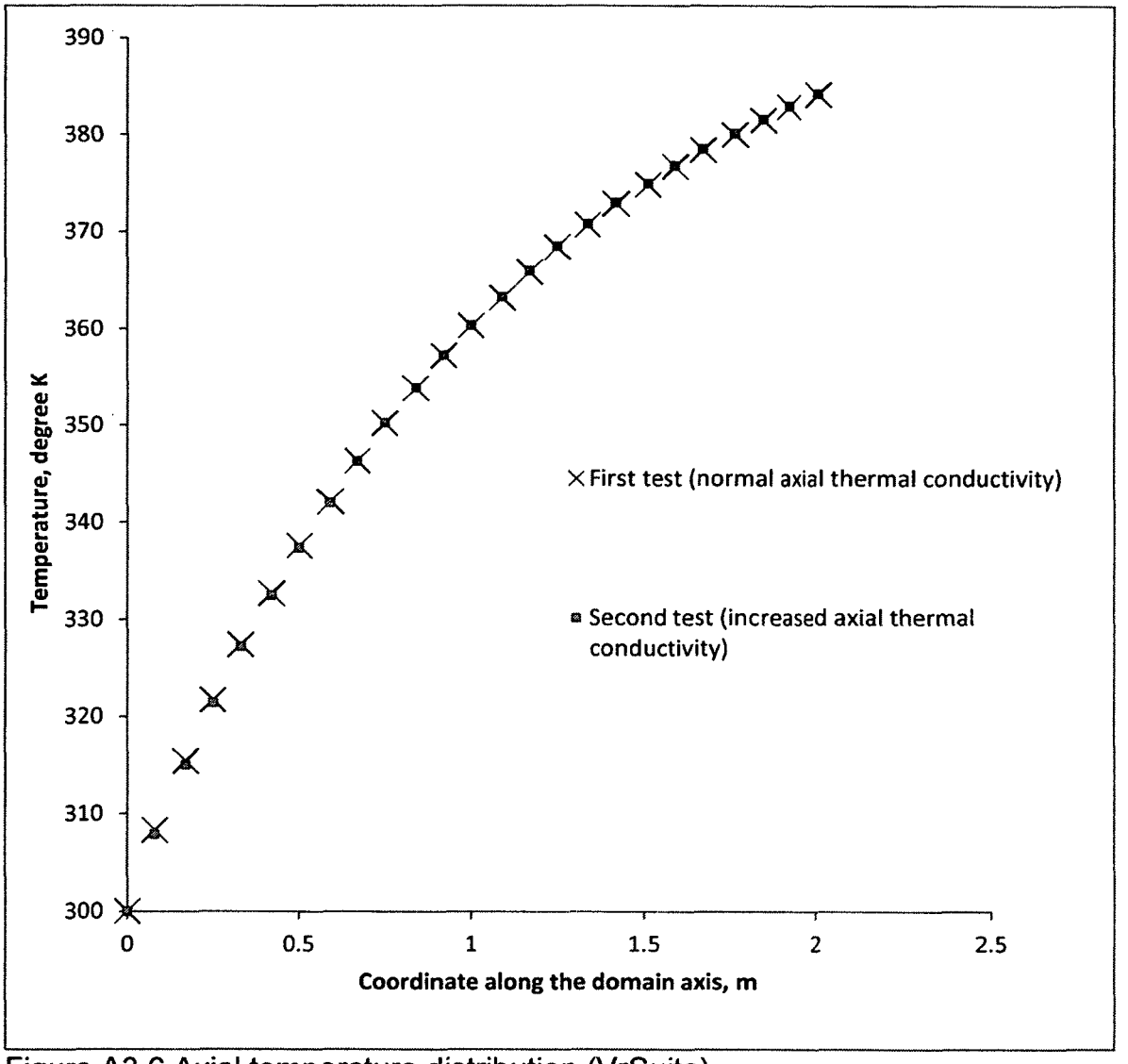

Figure A3.6 Axial temperature distribution (VrSuite)

As can be seen in Figure A3.6, the effect of axial diffusion caused by the increased thermal conductivity is insignificant and by far dominated by the radial heat flux.

Appendix 4: Meshing strategies used in VrSuite

Solid and fluid domains of the SCWL model are discretized with 8-node hexahedral elements. The domains were meshed solely by the tools developed specifically for the model and available in the VrSuite software. The meshing was done using automatic (predefined) and user-defined (user-made) strategies.

A4.1 Predefined meshing systems

The VrSuite software has a set of meshers intended for meshing some typical domain geometries. For example, "Pipe meshing system" can be used for meshing parts that are typically used in piping systems. This meshing system has standard set of options that can produce the mesh of a given pipe-like domain or alternatively the mesh of "fluid" inside the domain of interest. Figure A4.1 shows the meshes of the hollow cylinder, elbow, tee, cross, and reducer and corresponding "fluid" meshes. The options also allow defining the number of elements across the radius, number of circumferential elements, longitudinal mesh size, and other specific mesh characteristics.

It should be noticed that the corresponding solid and fluid domains have conforming meshes.

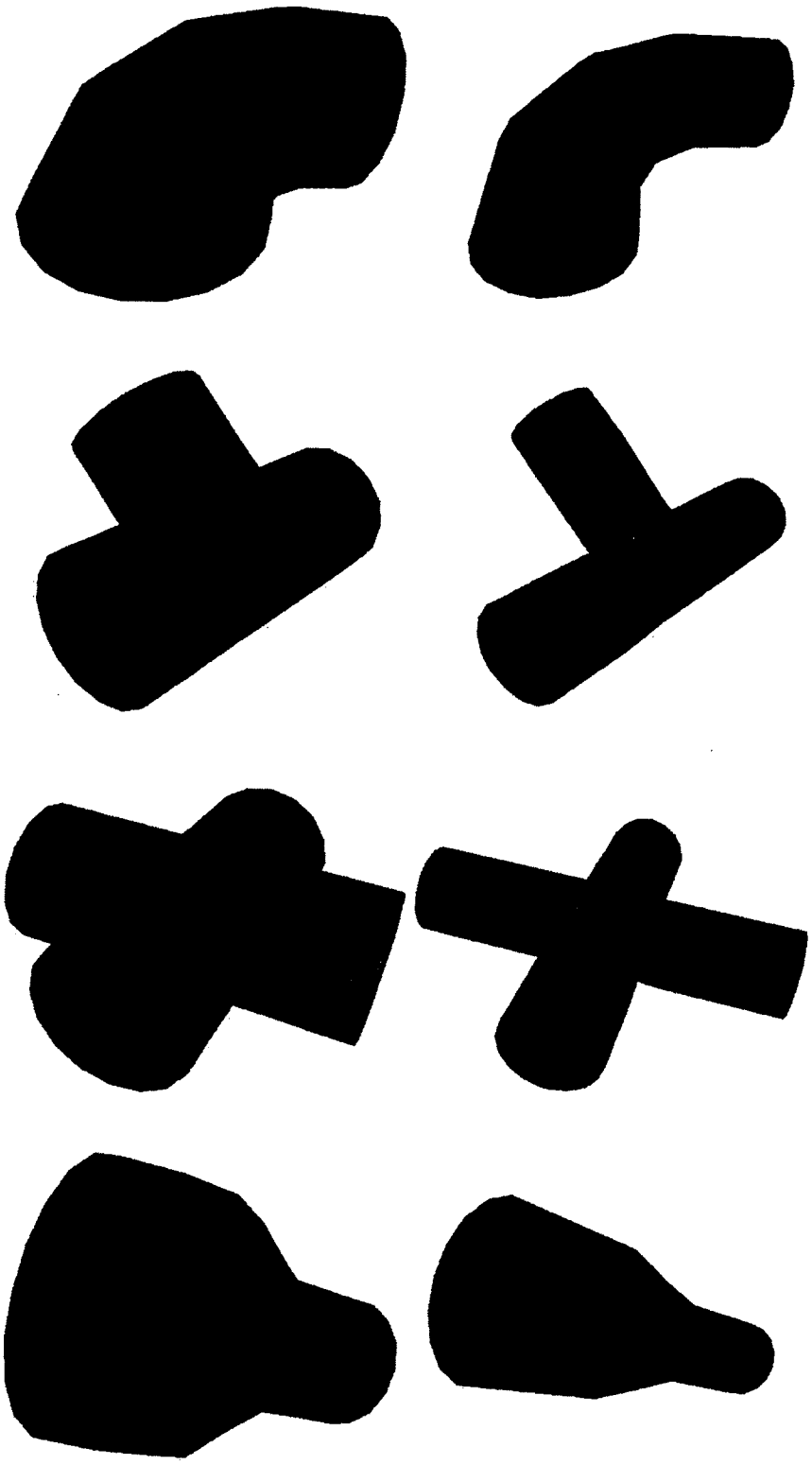

Figure A4.1 Examples of mesh done by automatic "Pipe meshing system"

Along with the Pipe meshing system, VrSuite has predefined meshers for more specific shapes, such as the tee joint with flanges, Figure A4.2, used in the loop. Depending on the particular geometry, such meshing systems have additional options. In case of the tee joint, a user has to define the outside diameters of the flanges, their thickness and some other parameters.

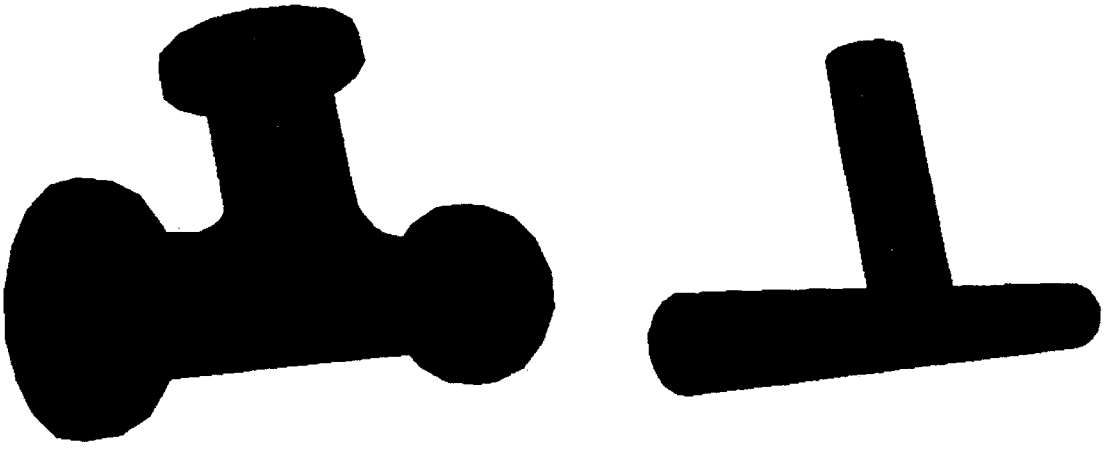

Figure A4.2 Tee joint with flanges - solid and "fluid" mesh examples

A4.2 User defined meshing systems

VrSuite offers extensive set of meshing tools for domains not covered by the predefined meshing systems. Since almost all parts of the model, which are meshed by the user defined meshing strategy, are axisymmetric, the meshing sequence is typical for all such elements and consists of the following steps:

1. Define the 2D cross section that is one half of the cross section defined by a part with a plane passing through the symmetry axis line of the part.
2. Mesh the 2D region.
3. Obtain the 3D mesh by rotation of the 2D meshed cross section around the part axis.

The meshing sequence for the parts that were meshed using extrusion rather than rotation has very similar meshing sequence. The only difference is that the 3D mesh is obtained by extrusion instead of rotation.

In some cases a combination of extrusion and rotation methods can be used to mesh more complex geometry. For example, the geometry of a typical SCWL bolted flange can be meshed using the simplifying assumption that the flanges are axis symmetrical (i.e., there are no holes). However, if one wants to mesh the flanges with the bolt holes, the geometry can be split into three parts, and an appropriate meshing approach (i.e., extrusion or rotation of 2D mesh) can be used for each mesh segment.

A4.3 Additional considerations

The primary purpose of the analysis is to obtain accurate transient thermal, displacement, and stress fields in the SCWL piping system rather than in the valves or elements of flanged and Grayloc connections. As a result, the mesh sizes of the piping system elements are chosen to be finer than the elements sizes of the mentioned/commercial components. In addition, the piping mesh size

is chosen taking into account the magnitudes of the expected thermal gradients, and therefore, the corresponding thermal stress fields.

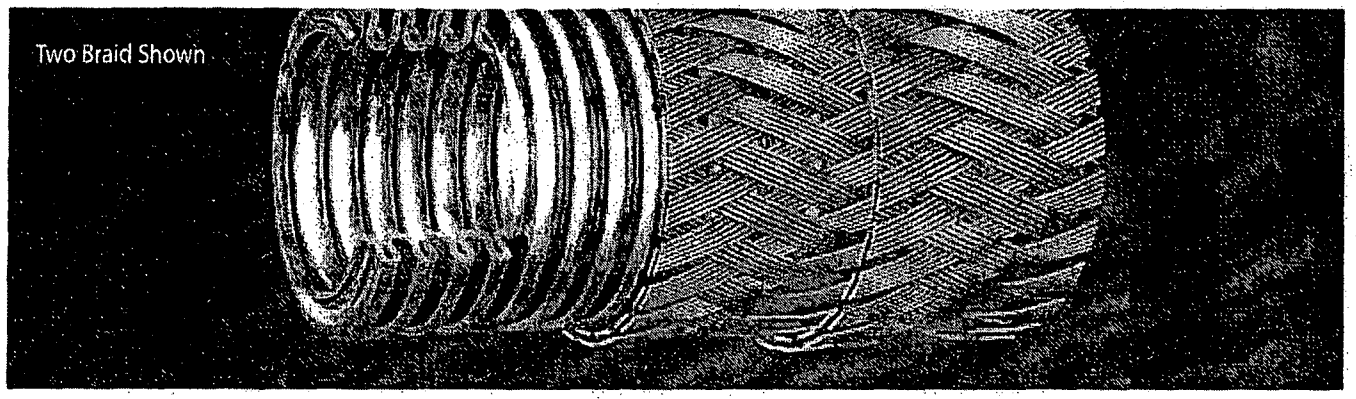

402X

Construction:

T316L stainless steel heavy weight hose
T321 direct double braid
Annular construction
For ultra high pressure and hydraulic applications

Sizes:

1/4" through 2"

Maximum Working Pressure:

Full vacuum up to 5300 psig depending on size

Temperature:

Cryogenic to 1500°F

NOMINAL HOSE I.D.	HOSE TYPE	HOSE O.D.	WEIGHT PER FT.	MIN.LIVE LENGTH FOR VIBRATION	MINIMUM BEND RADIUS STATIC BEND	MINIMUM BEND RADIUS DYNAMIC FLEXING	MAXIMUM WORKING PRESSURE	MAXIMUM TEST PRESSURE	NORMAL BURST PRESSURE
1/4"	402X	0.63	0.39	4.25	2.00	8.250	5300	7950	21200
3/8"	402X	0.81	0.53	5.00	2.50	9.000	3900	5850	15600
1/2"	402X	1.05	0.75	6.00	3.00	10.500	3600	5400	14400
3/4"	402X	1.43	1.63	7.00	4.00	12.750	3550	5325	14200
1"	402X	1.75	2.07	8.25	5.25	15.000	2800	4200	11200
1 1/4"	402X	2.08	2.93	9.00	6.50	17.250	2480	3720	9920
1 1/2"	402X	2.41	3.62	10.00	8.00	19.500	2200	3300	8800
2"	402X	3.05	4.63	12.00	11.50	24.000	1675	2512	6700

403XM – T321 Ultra Heavy Hose with Special Tri Stainless Steel Braids

NOMINAL HOSE I.D.	HOSE TYPE	HOSE O.D.	WEIGHT PER FT.	MIN.LIVE LENGTH FOR VIBRATION	MINIMUM BEND RADIUS STATIC BEND	MINIMUM BEND RADIUS DYNAMIC FLEXING	MAXIMUM WORKING PRESSURE	MAXIMUM TEST PRESSURE	NORMAL BURST PRESSURE
3"	403XM	3.94	5.47	15.00	25.00	86.000	1200	1800	4800

Welded Pipe End with 37-1/2 degree bevel

Size Availability: 1/8" diameter to 12" diameter

Material Availability: Carbon Steel, T304 Stainless Steel, T304L Stainless Steel, T321 Stainless Steel, T316 Stainless Steel, T316L Stainless Steel

Schedule Availability: 5, 10, 40, 80, 160, XX

Note: Not all sizes and schedules are available in combination - consult factory for details

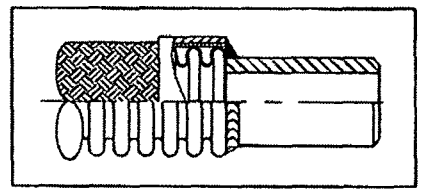

Welded Concentric Reducer

Size Availability: 1/2" diameter to 12" diameter and combinations thereof

Material Availability: Carbon Steel, T304 Stainless Steel, T304L Stainless Steel, T321 Stainless Steel, T316 Stainless Steel, T316L Stainless Steel, Monel 400, Hastalloy, Incoloy, Inconel

Schedule Availability: 5, 10, 40, 80, 160, XX

Note: Not all sizes and schedules are available in combination - consult factory for details

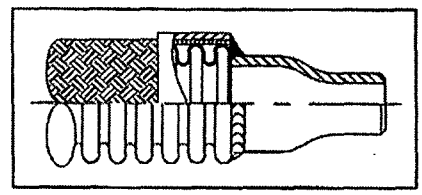

Welded Long Radius 90 Degree Elbow

Size Availability: 1/2" diameter to 12" diameter

Material Availability: Carbon Steel, T304 Stainless Steel, T304L Stainless Steel, T321 Stainless Steel, T316 Stainless Steel, T316L Stainless Steel, Monel 400, Hastalloy, Incoloy, Inconel

Schedule Availability: 5, 10, 40, 80, 160, XX

Note: Not all sizes and schedules are available in combination. Short radius, 45's and other angles are available - consult factory for details

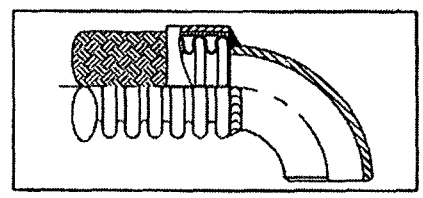

Welded NPT male nipple

Size Availability: 1/8" diameter to 8" diameter

Material Availability: Carbon Steel, T304 Stainless Steel, T304L Stainless Steel, T321 Stainless Steel, T316 Stainless Steel, T316L Stainless Steel

Schedule Availability: 5, 10, 40, 80, 160, XX

Note: Not all sizes and schedules are available in combination - consult factory for details

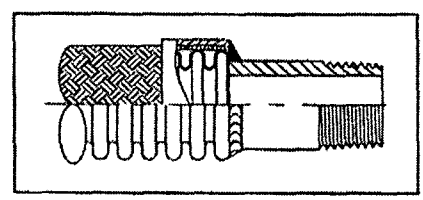

NPT Male Nipple with Integral Hex Nut

Size Availability: 1/4" diameter to 2" diameter

Material Availability: Carbon Steel, T304 Stainless Steel, T304L Stainless Steel, T321 Stainless Steel, T316 Stainless Steel, T316L Stainless Steel, Monel 400, Hastalloy, Incoloy, Inconel

Schedule Availability: 5, 10, 40, 80, 160, XX

Note: Not all sizes, schedules and materials are available in combination - consult factory for details

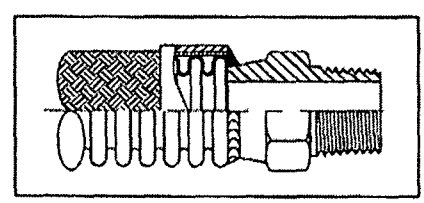

NPT male with welded on Hex Nut

Size Availability: 1/2" diameter to 4" diameter

Material Availability: Carbon Steel, T304 Stainless Steel, T304L Stainless Steel, T321 Stainless Steel, T316 Stainless Steel, T316L Stainless Steel, Monel 400, Hastalloy, Incoloy, Inconel

Manufactured from hexagon bar stock.

Note: Not all sizes, and materials are available in combination - consult factory for details

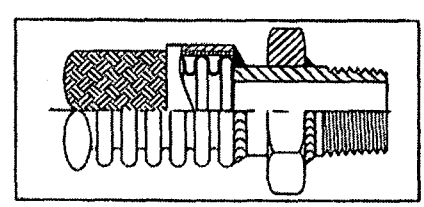

Welded Plate Flange ANSI Class 150 drilling

Size Availability: 1/2" diameter to 12" diameter

Material Availability: Carbon Steel and Stainless Steel

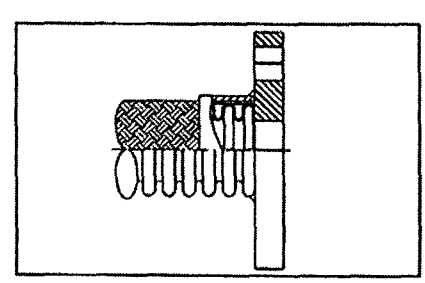

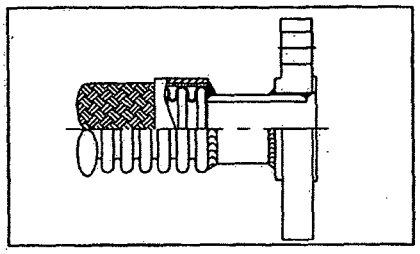

Raised Face Slip-On Flange on Pipe End

Size Availability: 1/2" diameter to 12" diameter
Material Availability: Carbon Steel, T304 Stainless Steel, T304L Stainless Steel, T321 Stainless T316 Stainless Steel, T316L Stainless Steel, Monel 400, Hastalloy, Incon
Schedule Availability: 5, 10, 40, 80, 160, XX
ANSI Class Ratings: 150, 300, 600, 900, 1500, 2500
RTJ flanges also available - consult factory for details
Note: Not all sizes and schedules are available in combination - consult factory for details

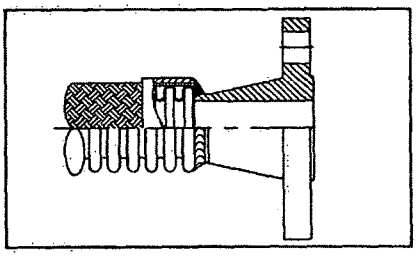

Welded Raised Face Weldneck Flange

Size Availability: 1/2" diameter to 12" diameter
Material Availability: Carbon Steel, T304 Stainless Steel, T304L Stainless Steel, T321 Stainless S T316 Stainless Steel, T316L Stainless Steel, Monel 400, Hastalloy, Incoloy
Schedule Availability: 5, 10, 40, 80, 160, XX
ANSI Class Ratings: 150, 300, 600, 900, 1500, 2500
RTJ flanges also available - consult factory for details
Note: Not all sizes and schedules are available in combination - consult factory for details

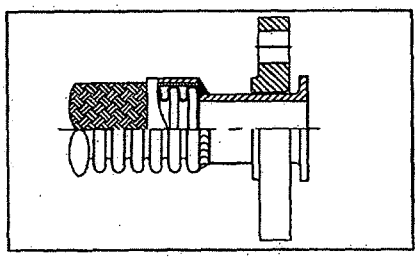

Lap Joint Floating Flange with Type "A" MSS stub end

Size Availability: 1/2" diameter to 12" diameter
Material Availability: Carbon Steel, T304 Stainless Steel, T304L Stainless Steel, T321 Stainless S T316 Stainless Steel, T316L Stainless Steel, Monel 400, Hastalloy, Incoloy
Schedule Availability: 5, 10, 40, 80, 160, XX
ANSI Class Ratings: 150, 300, 600, 900, 1500, 2500
Note: Not all sizes and schedules are available in combination.
Type "C" stub ends are also available - consult factory for details.

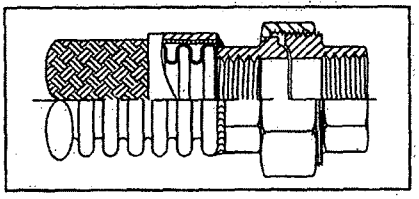

Welded Female Union

Size Availability: 1/2" diameter to 4" diameter
Material Availability: Carbon Steel, T304 Stainless Steel, T304L Stainless Steel, T316 Stainless S T316L Stainless Steel
Pressure: 150, 300, 3000, 6000 pound

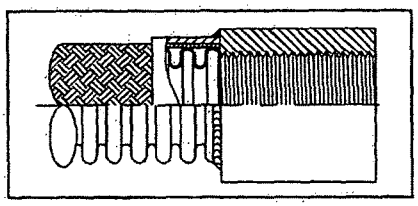

Welded Female NPT Half Pipe Coupling

Size Availability: 1/2" diameter to 4" diameter
Material Availability: Carbon Steel, T304 Stainless Steel, T304L Stainless Steel, T321 Stainless S T316 Stainless Steel, T316L Stainless Steel, Monel 400, Hastalloy, Incoloy,
Pressure: 150, 300, 3000, 6000 pounds
Note: Not all sizes and Pressures are available in combination.
Female NPT Full Pipe Coupling is also available - consult factory for details

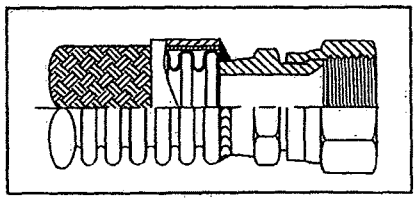

Welded JIC Swivel Female

Size Availability: 1/4" diameter to 2" diameter
Material Availability: Carbon Steel & T316 Stainless Steel

IV. MOTION

Most industrial applications can be reduced to one of five classes of motion: 1) **Angular**; 2) **Axial**; 3) **Offset**; 4) **Radial**; or 5) **Random.**

1. Angular Motion:
Motion that occurs when one end of a hose assembly is deflected in a simple bend with the ends not remaining parallel. Angular motion may be incorporated in an installation to accommodate misalignment and vibration only, but must not be used to accommodate expansion that would result in unloading the braid.

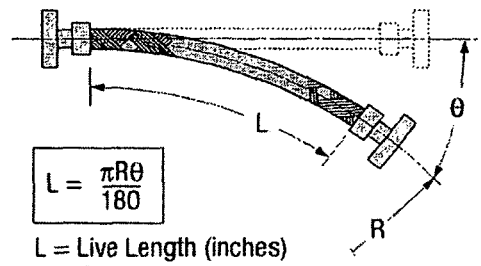

$$L = \frac{\pi R \theta}{180}$$

L = Live Length (inches)
R = ℄ Bend Radius (inches)
θ = Angle of Bend (degrees)
π = 3.1416

2. Axial Motion:
This type of motion occurs when one end of a hose assembly is deflected along its longitudinal axis. Axial motion is applicable to annular corrugated, unbraided flexible hose only. Neither helical hose nor braided hose should be used in axial motion applications.

3. Offset Motion:
Motion that occurs when one end of the hose assembly is deflected in a plane perpendicular to the longitudinal axis with the end remaining parallel. Offset is measured in inches of displacement of the free end center line from the fixed end center line. In offset motion applications, the offset should never be greater than one-fourth (25%) of the minimum center line bend radius.

OFFSET MOTION

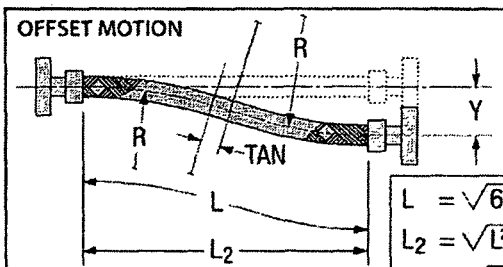

Please refer to chart for live length of hose in offset on page 25

$$L = \sqrt{6YR+Y^2}$$
$$L_2 = \sqrt{L^2-Y^2}$$
$$Y_M = \sqrt{9R^2+L^2-3R}$$

L = Hose Live Length (inches)
L_2 = Projected Linear Length At Offset (inches)
R = ℄ Bend Radius (inches)
Y = ℄ Offset, Motion (inches)
Y_M = ℄ Maximum offset for a given L and R (inches)

NOTE: Where Offset Motion "Y" occurs both sides of ℄ the Hose Live Length should be based on Total Travel or 2 times Y.

4. Radial Motion:
This type of motion occurs when the center line of a hose assembly is bent in a circular arc. In industrial applications, radial motion is most commonly found in traveling loops.

CLASS "A" TRAVELING LOOPS

...For Maximum Vertical Travel

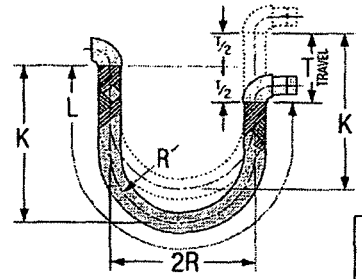

$$L = 4R+T/2$$
$$K = 1.43R+T/2$$

...For Maximum Horizontal Travel

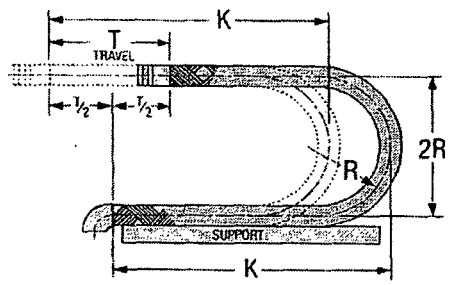

T = Total travel (in.)
R = Center line bend radius (in.)
L = Hose live length (in.)
K = Loop Length (in.)

CLASS "B" TRAVELING LOOPS

...For Short Horizontal Travel

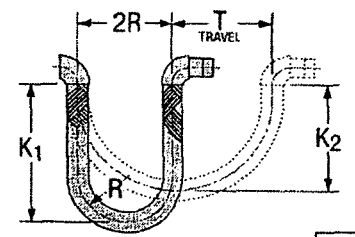

...For Short Vertical Travel

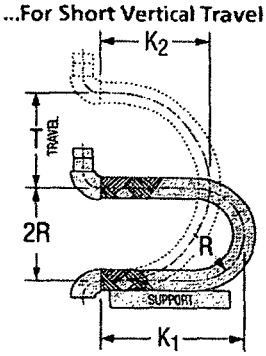

$$L = 4R+1.57T$$
$$K_1 = 1.43R+.785T$$
$$K_2 = 1.43R+T/2$$

NOTE:
In loop installations both connections and travel should be in same plane as bend.

5. **Random Motion:**
Non-predictable motion that occurs from manual handling of a assembly. Loading and unloading hose would generally fall into this category. Abusive handling of hose is an important factor to consider in applications involving random motions. The use of an interlocked (RT-6) guard over the corrugated hose is recommended to protect the hose assembly from rough handling and "over-bending" adjacent to the fittings.

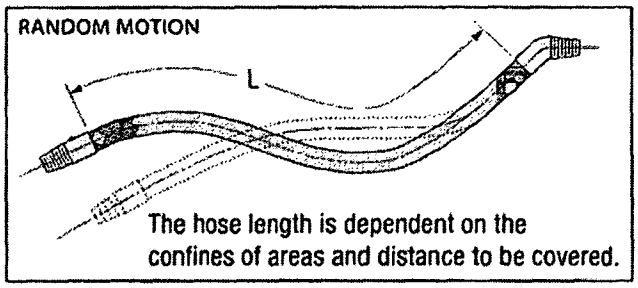

V. MOTION FREQUENCY

The frequency of a particular class of motion to which a flexible metal hose may be subjected by repeated flexing or bending. The frequency of motion may be divided into three basic categories: namely vibration, dynamic, and continuous. The minimum live length required for these motion categories may be selected as follows:

1. **Vibration:**
For the normal vibration encountered in industrial applications, such as pump and compressor discharge lines and engine exhaust installations, the hose live lengths should be taken from the Minimum Live Length For Vibration column on Technical Data Pages.

Normal vibration is shown as the unshaded area of the chart below. If the expected combination of double amplitude (total motion excursion) and frequency falls into the shaded area, consult US Hose Engineering Group.

Caution: Avoid hose resonance. If resonance is anticipated, consult US Hose Engineering Group.

2. **Dynamic Motion:**
Motion that occurs on a regular or irregular basis normally the result of thermal expansion and contraction or other noncontinuous actions.

The dynamic flexing bend radius shown on Hose Technical Data Pages shall be used in the formulas for angular, radial and offset motion when determining hose live length for dynamic motion.

3. **Continuous Motion:**
Motion that occurs on a regular cyclic basis normally at a slow cyclic rate and constant travel. For Continuous Lateral Offset Motion double the minimum centerline bend radius for Dynamic Flexing shown on Hose Technical Data Pages.

4. **Static Bend:**
The minimum center line bend radius to which a flexible metal hose may be bent for installation. No further motion is to be imposed other than normal vibration.

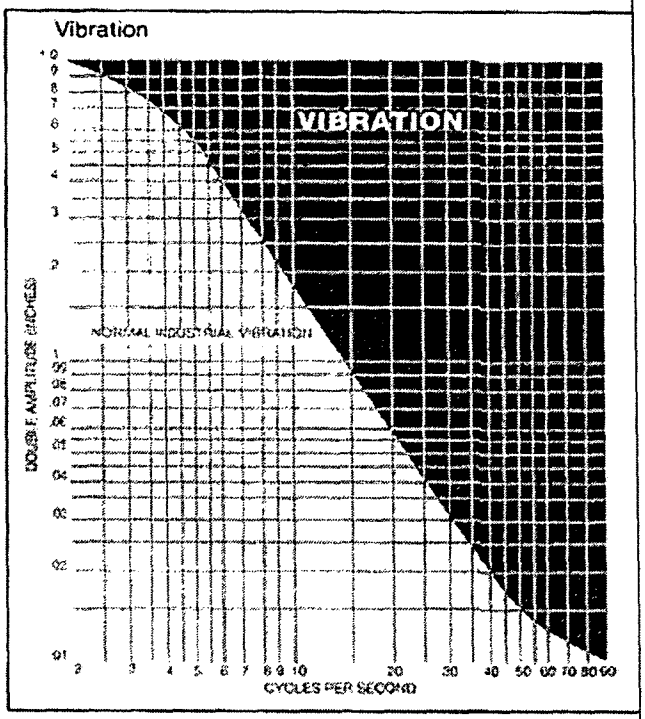

VI. CYCLE LIFE

The cycle life expectancy of a metal hose is affected by various factors such as: operating pressure, operating temperature, materials, bend radius (the movement per corrugation due to the flexure), the thickness of the corrugation. Any change in one of these factors will result in a change in the cycle life of a metal hose assembly.

The cycle life of a metal hose assembly is proportional to the sum of the pressure stress range and deflection stress range. The life expectancy can be defined as the total number of competed cycles which can be expected from the metal hose assembly based on S/N curves and data tabulated from tests performed under simulated operating conditions. A cycle is defined as one complete movement from the initial position in the system to some operating point and returning to the original position.

This information should be used as a guide only. We cannot predict every variable which might be encountered in every application nor any misapplication, mechanical damage, and/or any uncontrollable situation.

Appendix 6: Material properties

Properties of the employed materials

Table A6.1: Thermal-physical properties of INCONEL 617 (solution annealed) [30]

Young's modulus, Pa		Hardening modulus, Pa		Yield stress, Pa		Coefficient of thermal expansion, 1/K		Thermal conductivity, W/(m*K)		Electrical conductivity, S/m	
Temperature, K	Property	Temperature, K	Property	Temperature, K	Property	Temperature, K	Property	Temperature, K	Property	Temperature, K	Property
298	2.11 E+11	295	2.26 E+09	295	2.90 E+08	373	1.16 E-05	293	1.34 E+01	2.93 E+02	8.18 E+05
373	2.06 E+11	900	2.10 E+09	373	2.70 E+08	473	1.26 E-05	373	1.47 E+01	3.73 E+02	8.03 E+05
473	2.01 E+11	1000	1.40 E+09	473	2.60 E+08	573	1.31 E-05	473	1.63 E+01	4.73 E+02	7.95 E+05
573	1.94 E+11	1150	8.00 E+08	573	2.40 E+08	673	1.36 E-05	573	1.77 E+01	5.73 E+02	7.89 E+05
673	1.88 E+11	1250	4.00 E+08	673	2.30 E+08	773	1.39 E-05	673	1.93 E+01	6.73 E+02	7.82 E+05
773	1.81 E+11			773	2.30 E+08	873	1.40 E-05	773	2.09 E+01	7.73 E+02	7.75 E+05
873	1.73 E+11			873	2.10 E+08	973	1.48 E-05	873	2.25 E+01	8.73 E+02	7.65 E+05
973	1.66 E+11			973	2.00 E+08	1073	1.54 E-05	973	2.39 E+01	9.73 E+02	7.51 E+05
1073	1.57 E+11			1073	1.10 E+08	1173	1.58 E-05	1073	2.55 E+01	1.07 E+03	7.45 E+05
1173	1.49 E+11			1173	7.00 E+07	1273	1.63 E-05	1173	2.71 E+01	1.17 E+03	7.47 E+05
1273	1.39 E+11			1273	4.00 E+07			1273	2.87 E+01	1.27 E+03	7.26 E+05
1.37 E+03	1.29 E+11										

Table A6.2: Thermal-physical properties of INCONEL 625 (Annealed at 1925F (1052C)) [31]

Young's modulus, Pa		Hardening modulus, Pa		Yield stress, Pa		Coefficient of thermal expansion, 1/K		Thermal conductivity, W/(m*K)		Electrical conductivity, S/m	
Temperature, K	Property	Temperature, K	Property	Temperature, K	Property	Temperature, K	Property	Temperature, K	Property	Temperature, K	Property
295	2.14 E+11	295	2.26 E+09	300	4.96 E+08	123	1.09 E-05	116	7.2	294	7.75 E+05
373	2.10 E+11	900	2.10 E+09	473	4.64 E+08	173	1.17 E-05	144	7.5	311	7.69 E+05
473	2.05 E+11	1000	1.40 E+09	673	4.29 E+08	223	1.23 E-05	200	8.4	366	7,56 e+05
573	1.99 E+11	1150	8.00 E+08	873	4.10 E+08	293	1.04 E-05	259	9.2	477	7.46 E+05
673	1.93 E+11	1250	4.00 E+08	1073	4.08 E+08	373	1.33 E-05	294	9.8	589	7.41 E+05
773	1.87 E+11			1273	4.05 E+08	473	1.38 E-05	301	10.1	700	7.35 E+05
873	1.80 E+11			1473	3.93 E+08	573	1.42 E-05	366	10.8	811	7.25 E+05
973	1.72 E+11			1673	3.81 E+08	673	1.45 E-05	477	12.5	922	7.25 E+05
1073	1.64 E+11			1873	2.41 E+08	773	1.49 E-05	589	14.1	1033	7.30 E+05
1173	1.54 E+11			2073	7.50 E+07	873	1.53 E-05	700	15.7	1144	7.35 E+05
1273	1.43 E+11			2273	4.20 E+07	973	1.58 E-05	811	17.5		
						1073	1.61 E-05	922	19		
						1173	1.64 E-05	1033	20.8		
								1144	22.8		
								1255	25.2		

Table A6.3: Thermal-physical properties of AISI 316 stainless steel (VrSuite material library)

Young's modulus, Pa		Hardening modulus, Pa		Yield stress, Pa		Coefficient of thermal expansion, 1/K		Thermal conductivity, W/(m*K)	
Temperature, K	Property	Temperature, K	Property	Temperature, K	Property	Temperature, K	Property	Temperature, K	Property
4	2.08 E+11	0	2.20 E+09	20	5.20 E+08	4	1.02 E-05	4	2.8
73	2.09 E+11	273.15	2.16 E+09	273	2.70 E+08	73	0.00 0013	73	7.9
273	2 E+11	673.15	1.85 E+09	293	2.59 E+08	273	1.63 E-05	273	13.29
293	1.99 E+11	973.15	3.00 E+07	323	2.44 E+08	293	1.65 E-05	293	13.64
323	1.96 E+11	1500	3.00 E+07	373	2.22 E+08	323	1.67 E-05	323	14.15
373	1.92 E+11	2000	3.00 E+07	423	2.03 E+08	373	1.71 E-05	373	14.99
423	1.88 E+11			473	1.88 E+08	423	1.75 E-05	423	15.81
473	1.84 E+11			523	1.76 E+08	473	1.79 E-05	473	16.62
523	1.8 E+11			573	1.66 E+08	523	1.83 E-05	523	17.41
573	1.76 E+11			623	1.58 E+08	573	1.86 E-05	573	18.19
623	1.72 E+11			673	1.52 E+08	623	0.00 0019	623	18.96
673	1.68 E+11			723	1.47 E+08	673	1.94 E-05	673	19.73
723	1.64 E+11			773	1.43 E+08	723	1.98 E-05	723	20.49
773	1.6 E+11			823	1.39 E+08	773	2.02 E-05	773	21.26
823	1.56 E+11			873	1.35 E+08	823	2.05 E-05	823	22.03
873	1.52 E+11			923	1.30 E+08	873	2.09 E-05	873	22.81
923	1.48 E+11			973	1.25 E+08	923	2.13 E-05	923	23.61

973	1.44 E+11			1023	1.18 E+08	973	2.16 E-05	973	24.42
1023	1.39 E+11			1073	1.10 E+08	1023	0.00 0022	1023	25.24
1073	1.35 E+11			1123	9.89 E+07	1073	2.24 E-05	1073	26.09
1123	1.31 E+11			1173	8.56 E+07	1123	2.27 E-05	1123	26.96
1173	1.27 E+11			1223	5.00 E+07	1173	2.31 E-05	1173	27.86
1223	1.23 E+11			1273	1.00 E+07	1223	2.35 E-05	1223	28.8
1273	1.19 E+11			1373	1.00 E+06	1273	2.38 E-05	1273	29.76
1373	1.11 E+11			1473	1.00 E+06	1373	2.45 E-05	1323	30.77
1473	1.03 E+11			1573	5.00 E+05	1473	2.52 E-05	1373	31.81
1573	9.48 E+10			1673	1.00 E+05	1573	2.59 E-05	1423	36.81
1673	8 E+10			1773	5.00 E+04	1673	2.66 E-05	1473	41.81
1723	4 E+10			1873	1.00 E+04	1773	2.73 E-05	1523	46.81
1773	1 E+10			1973	5.00 E+03	1873	2.79 E-05	1573	51.81
3273	1 E+09			2073	1.00 E+03	1973	2.86 E-05	1623	56.81
				2173	5.00 E+02	2073	2.92 E-05	1673	61.81
				2273	1.00 E+02	2173	2.99 E-05	1723	71.81
				2373	9.00 E+01	2273	3.05 E-05	1773	81.81
						2373	3.11 E-05	1823	91.81
						2473	3.18 E-05	1873	101.81
						2573	3.24 E-05	1923	111.81
						2673	0.00 0033	1973	121.81
						2773	3.36 E-05	2023	131.81
						2873	3.42 E-05	2073	141.81
						2973	3.47 E-05	2973	141.81
						3073	3.53 E-05		

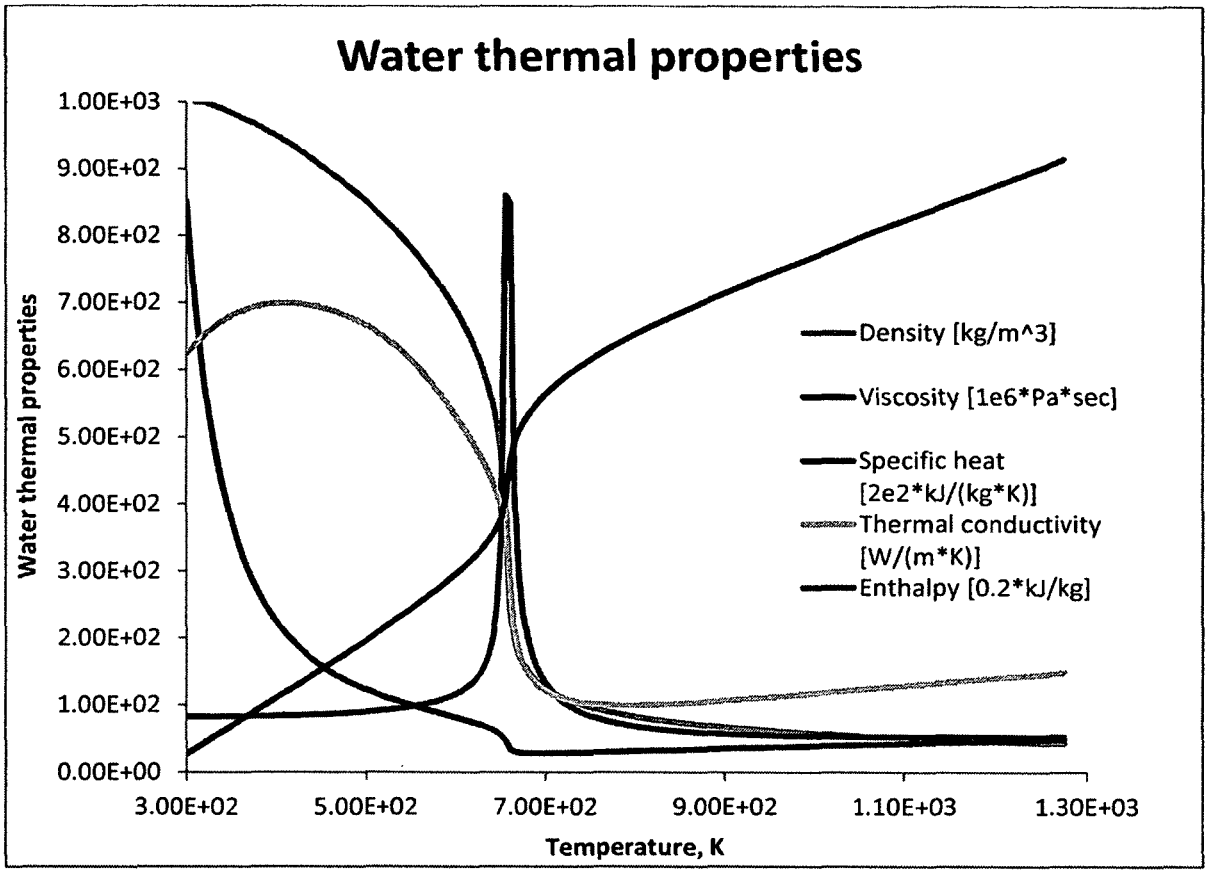

Figure A6.1 Thermal-physical properties of water at 25 MPa (NIST website)

Appendix 7: Definitions of the effective stress and yield criteria in the VrSuite software

The effective stress mentioned in this thesis is defined as the second invariant of deviatoric stress:

$$J_2 = \sqrt{0.5[(\sigma_{11} - \sigma_{22})^2 + (\sigma_{22} - \sigma_{33})^2 + (\sigma_{11} - \sigma_{33})^2 + 6(\sigma_{23}^2 + \sigma_{31}^2 + \sigma_{12}^2)]}$$

Where $\sigma_{11}, \sigma_{12}, \sigma_{31}, \sigma_{22}, \sigma_{23}, and\ \sigma_{33}$ are the components of the stress the tensor.

In the VrSuite code, the yield function is defined in terms of von Mises or effective stress.